RELATIONSHIP BETWEEN SAPROLITE-HOSTED GROUNDWATER GEOCHEMISTRY, BASEFLOW, AND WEATHERING DEPTH AT REDLAIR OBSERVATORY, A CRITICAL ZONE RESEARCH SITE ON THE NORTH CAROLINA PIEDMONT

by

Julianna S. Horgan

A thesis submitted to the faculty of
The University of North Carolina at Charlotte
in partial fulfillment of the requirements
for the degree of Master of Science in
Earth Science

Charlotte

2021

Approved by:

_____
Dr. David Vinson

_____
Dr. Martha Cary Eppes

_____
Dr. Craig Allan

ABSTRACT

JULIANNA S. HORGAN. Relationship Between Saprolite-Hosted Groundwater Geochemistry, Baseflow, and Weathering Depth at Redlair Observatory, a Critical Zone Research Site in the North Carolina Piedmont. (Under the direction of DR. DAVID VINSON)

Crystalline bedrock weathering profiles in the southern Piedmont terrane have thicker soils and gentler slopes than mountainous terranes with their thin soils and steep slopes. The objective of this study was to understand watershed-scale baseflow and groundwater chemistry in relationship to weathering depth, and to assess landscape position (ridgetop, midslope, and base of slope) as a potential critical zone factor within the Piedmont.

This study took place at the recently established (2019-present) Redlair Observatory (RO) in Gaston County, North Carolina in the southern Piedmont. RO is part of the 1,200-acre Redlair Preserve, which protects *Magnolia macrophylla* and *Helianthus schweinitzii.* The climate at RO is humid and subtropical, with a mean annual temperature of 14.5°C. The geology consists of felsic and mafic metavolcanic rocks of the Charlotte Terrane overlain by Ultisols (Cecil soil series) and Entisols (Pacolet soil series).

Seventeen wells were installed among four zero-order to first-order watersheds, ~4-25 m deep. Monthly surface water baseflow sampling, seasonal groundwater sampling, high-resolution continuous loggers, and geospatial analyses were used to examine critical zone processes. Samples were analyzed for major ion concentrations and water isotopes (δD, $\delta^{18}O$). Groundwater ranged from -25.4 to -35.8‰ (δD) and from -4.6 to -7.9‰ ($\delta^{18}O$). Manual groundwater measurements and 10-minute increment loggers revealed that groundwater levels were shallowest in the late spring-early summer months and deepest in late fall-early winter months. However, not all wells responded to these warmer groundwater peaks and colder groundwater minimums on the same timeline. Water level and temperature patterns suggest that mean groundwater residence times are on the order of a season to a few months. Well depth seemed to be the most important factor

influencing groundwater chemistry in this study. Most notably, the calcium/sodium (Ca/Na) molar ratios of the shallow wells versus the deep wells reveal a varying degree of weathered material at depth. The deep wells had higher Ca/Na ratios of 0.34-1.72 (5-24 m depth below land surface) while the shallow wells had Ca/Na ratios ranging from 0.7-1.79 (4-21 m depth below land surface). This suggests that the deep wells were screened in less weathered material than the shallow wells, consistent with weathering of Na-plagioclase shallower in the weathering profile and Ca-plagioclase deeper in the weathering profile.

This study found that hydrologic processes occur quickly in these small (4.4-15.5 ha) headwater watersheds of the Piedmont. Understanding of critical zone processes is important for predicting how small watersheds will respond to climate change and urbanization influences. Locally, the results of this study may contribute to management of Redlair Preserve.

ACKNOWLEDGEMENTS

I would first like to thank Dr. David S. Vinson for all that he has done for me from the moment that I started this program. Without his patience, guidance, and support this project would not have been possible. Thank you, Dr. Vinson, for helping to push me to think critically and thoroughly about watershed hydrogeology.

Next, I would like to thank Dr. Martha Cary Eppes for her support as my committee member and professor. I appreciated all the challenges that she provided in her classes to refine my skills as a field geologist. And to my last committee member, Dr. Craig Allan, I am very appreciative of the advice he gave me on the foundations of surface water hydrology. Thank you to Jon Watkins for providing me with teaching and guidance on various analytical instruments to successfully complete my research. Thank you to all the UNC Charlotte Department of Department of Geography and Earth Sciences for their innumerable support. Thank you to Haywood Rankin, the NC Plant Conservation Program, Redlair Preserve, and Catawba Lands Conservancy. Establishment of Redlair Observatory was funded by Duke Energy Foundation Water Resources Fund and Catawba Lands Conservancy. Thank you to the McCreary Memorial Award scholarship for providing financial support for my research.

Further, I would like to thank my peers and frequent field assistants, Elizabeth Batianis and Samantha Berberich, for providing me with physical and emotional support during treks across Redlair.

Additionally, I would also like to thank my friends and family, specifically, my mother, Diane Horgan. I would not be the woman I am today without her constant encouragement and lending ear.

And lastly, I would like to thank Ian T. Dunning. During my program, Ian’s support was boundless, and I am grateful for his partnership.

TABLE OF CONTENTS

LIST OF TABLES

LIST OF FIGURES

1 INTRODUCTION

This study examined the hydrological processes that occur in small, forested watersheds in the central Piedmont of North Carolina. The Piedmont spans from Alabama to New Jersey and is characterized as a humid, hilly, terrane filled with small (<2 km^2), forested watersheds on thick weathering profiles derived from *in situ* crystalline rocks. Small, forested watersheds are recognized as important influencers on water quality of large river systems worldwide (Sklash and Farvolden, 1979; Aust and Blinn, 2004). Furthermore, the headwaters of these watersheds represent a large proportion of the stream length in major river systems (MacDonald and Coe, 2006; Alexander et al., 2007; O'Driscoll et al., 2010). Small streams have more contact with their banks than larger ones. Therefore, the groundwater-surface water interactions of small streams have the potential to greatly influence water quality of large river systems. Despite their importance, these small watersheds within the Piedmont region are under-studied by hydrologists, geochemists, and soil scientists. Relative to mountain and coastal plain systems, much of the hydrologic research regarding hillslopes and small watershed-scale critical zones relates to temperate mountainous regions with steep slopes and thin soils, which is the opposite of the Piedmont physiographic province of North America (Burns et al., 2003; Burt and McDonnell, 2015; Zimmer, 2017). Recently, the Calhoun Critical Zone Observatory, an intensively studied Piedmont forest on legacy agricultural land, has drawn attention to the role of natural weathering processes and legacy human activities (such as agriculture) on the chemistry of soils and waters in low-order forest streams and watersheds.

In the Piedmont, shallow groundwater interacts with a reactive silicate weathering profile consisting of *in situ* material (soil, saprolite, weathered bedrock, and unweathered bedrock). The Piedmont weathering profile can be studied in terms of the critical zone (CZ) concept, which extends from the top of the tree canopy to the lowest weathered bedrock (Chorover et al., 2011; Figure 1). Additionally, seasonal fluctuations of shallow groundwater levels relate to seasonal

patterns of stream flow and water quality and to the growing season (e.g., Zimmer and McGlynn, 2017). Therefore, there may be a relationship between seasonal groundwater fluctuations and water quality of small headwater streams, especially at baseflow when the groundwater component to streams is proportionally largest. The overall goal of this study was to examine, on the scale of zero-order and first-order watersheds, seasonal to annual hydrologic fluctuation, the possible influence of seasonal cycling imparted upon stream and groundwater chemistry, and to assess landscape position as a potential factor affecting groundwater chemistry. For this study, only the land surface down to the bedrock-to-saprolite transition was examined from the entire critical zone (Figure 1).

Research was conducted at Redlair Observatory (RO). RO is part of the larger 1,200-acre Redlair Preserve (Redlair Lane: 35°18'0.13"N, 81° 5'5.48"W). The observatory is situated on the southern Piedmont physiographic province on the South Fork of the Catawba River in Gaston County, NC (Figure 3). RO encompasses a portion of the larger preserve, which is owned and managed by the North Carolina Plant Conservation Program. Redlair Preserve has the mission of protecting the locally abundant *Magnolia macrophylla* (Bigleaf magnolia), a threatened tree species in North Carolina. All the watersheds in this study ultimately flow into the South Fork of the Catawba River, which is a principal tributary of the Catawba-Santee River System, a vital water resource for the Piedmont region of the North and South Carolina. The landscape position concept refers to four sub-watersheds located within the larger, regional South Fork of the Catawba River tributary and basin divide. The Piedmont lands that had been historically used for row-crop agriculture have more recently become forested and pastoral land uses. Portions of these lands have been revegetated and are managed landscapes that are surrounded by rapidly urbanizing regions. The watersheds in this study also have an extensive legacy of agricultural land-use that has influenced the geomorphology and hydrology of small watersheds and low-order streams (Trimble, 2008). More recently, Redlair and surrounding regions of the Concord-Gaston-Mecklenburg

County Metropolitan Statistical Area have seen a population increase >1.5 million as of 2019 (North Carolina Office of State Budget and Management).

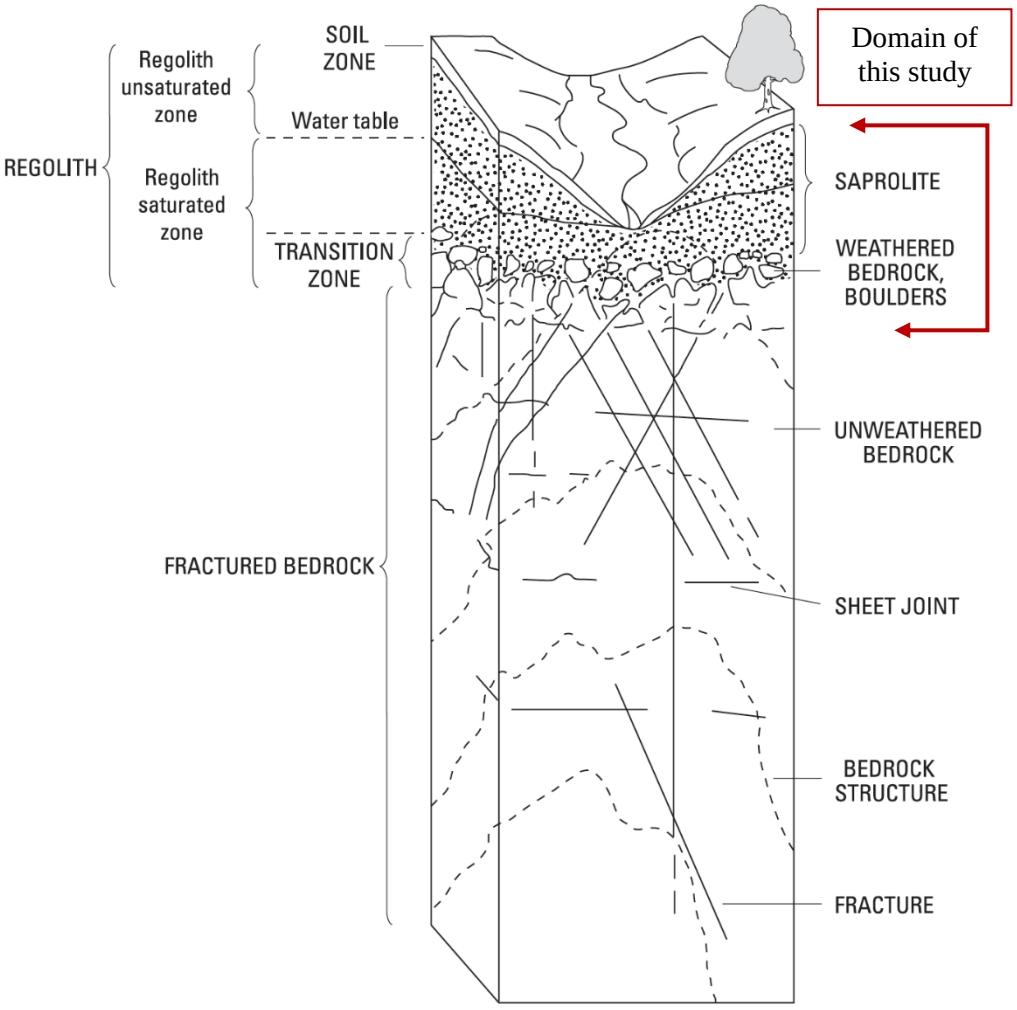

Figure 1. The critical zone is defined as the top of the tree canopy down to the bottom of weathered bedrock. The general groundwater system in this region of the Blue Ridge and Piedmont depends heavily upon intergranular flow within the crystalline bedrock. Within this diagram is the critical zone and the focus of this study highlighted in red (modified from Daniel and Dahlen, 2002).

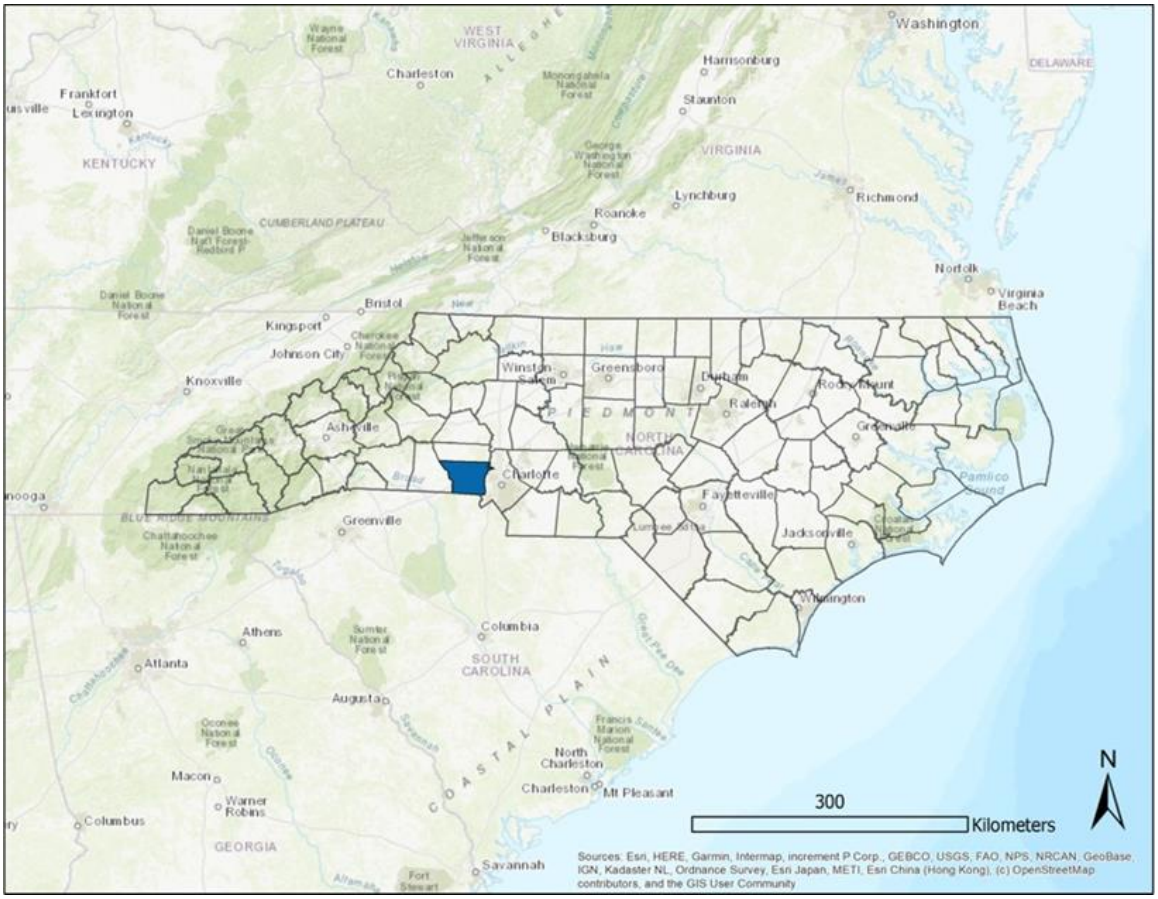

Figure 2. Location map showing the location of Gaston County (blue) within North Carolina.

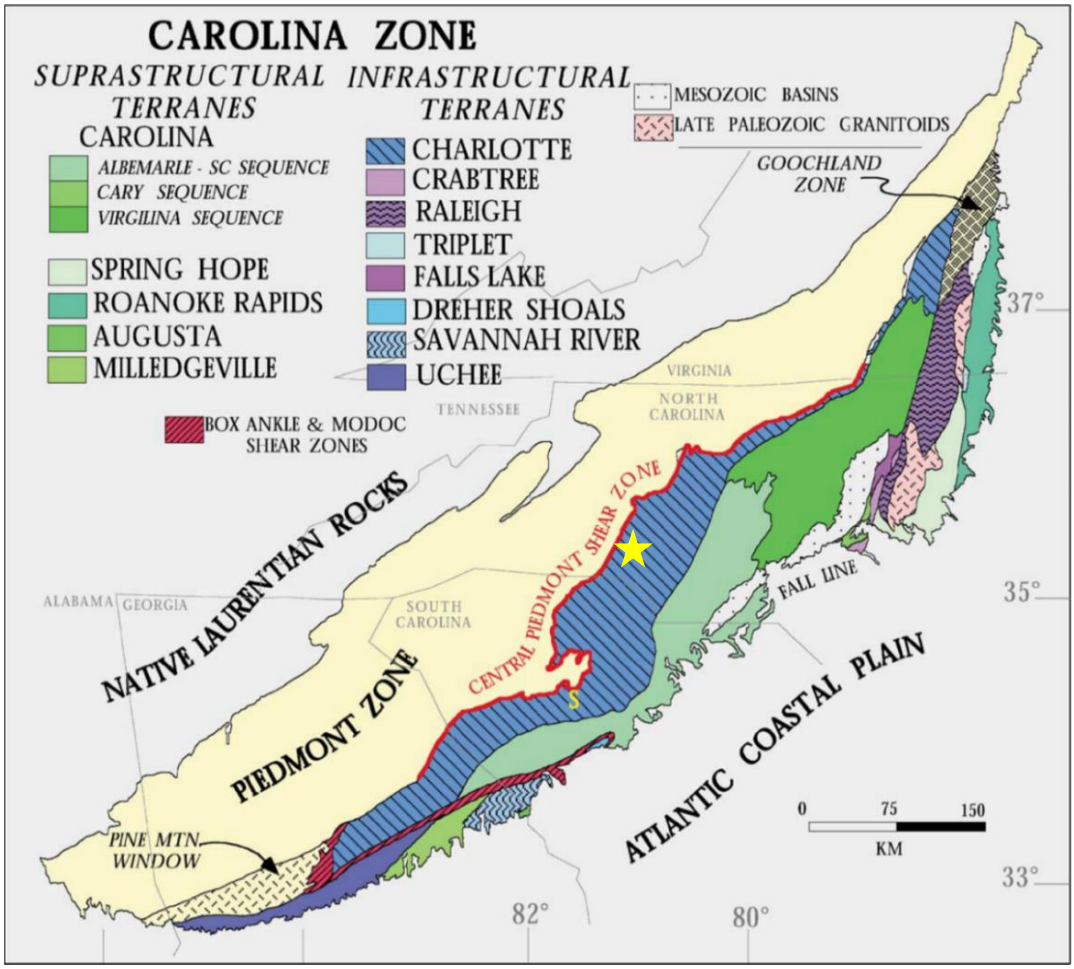

Figure 3. Geologic terranes found within the Carolina Zone. Location of the research site within the Charlotte Terrane is denoted by the yellow star (modified from Hibbard et al., 2002).

Redlair Observatory is well-suited for this study because it provides a topographic transect (roughly 1,200 m long) from a high-order river basin divide to the river floodplain. This landscape includes watersheds slightly incised into gentle ridgeline topography and deeply incised into steep slopes along the river valley. The map-scale lithology (rock type) is consistent across RO. This layout allows for a study design that incorporates zero- and first-order watersheds at different landscape positions along a large-scale geomorphic transect.

The catchment upgradient of a first-order stream (i.e., containing no upgradient channel), is referred to as a zero-order watershed. Zero-order watersheds are also poorly understood compared to first-order or higher-order watersheds in which runoff is concentrated into a stream

channel (Chorover et al., 2011; Heidbüchel et al., 2012). Essentially, all water flows in the zero-order watershed are in the subsurface when overland flow is not being generated by precipitation events. Within a zero-order watershed, we do not fully understand the chemical evolution of water or the timescale on which it occurs throughout these watersheds at the hillslope scale, water residence times, or chemical reactions within the weathering profile. These gaps in knowledge are due to hillslope heterogeneity and the lack of perennial stream channels in this province. Zero-order watersheds can be located at the hillslope, catchment, or watershed scale.

The physical position of a watershed within a landscape may influence critical zone processes. The CZ is important for many reasons: it is where carbon sequestration occurs, it may contain contaminants and pollutants, and it sustains terrestrial life (Wymore et al., 2017). Most significantly for the purposes of this research, the CZ is where the most rapid and influential chemical weathering occurs for small watersheds. Ions and nutrients are subsequently exported from watersheds. Element fluxes from small watersheds drive global element cycling in river systems (Chorover et al., 2011).

Zero-order and first-order watersheds are natural reactors that mix waters originating from precipitation and their topographic extents via evapotranspiration, overland flow, and through the subsurface portion of the critical zone (subsurface storm flow and groundwater flow in Figure 4). These small headwater watersheds may also exhibit contrasting reactivity depending on CZ factors such as: lithology, soils, slope, aspect, relief, depth to bedrock, stream incision, vegetation, hydrologic residence time, and climate (Chorover et al., 2011; Wymore et al 2016).

This study seeks to build upon Chorover and others' (2011) list of CZ factors by examining whether landscape position is a significant critical zone factor affecting element fluxes in watersheds. Landscape position and topography (slope) may affect where a watershed is situated within a hillslope: 1) top of the hillslope (ridgetop), (2) mid-slope, and slope base (riparian zone). This can potentially also affect watershed-scale CZ processes. Additionally, topography may influence the subsurface topography of the water table, and thus stream chemistry and elemental

fluxes as well. Previous studies have shown that watershed topography and geomorphology heavily can also influence baseflow (Price, 2011; Mesghi et al., 2014) and surface topography can greatly impact runoff flow distribution and rate (Farvolden, 1963; Vivoni et al., 2007; Price, 2011).

Three watersheds in this study occur at landscape positions broadly analogous to geomorphic settings seen across the Piedmont: (1) a headwaters stream (Duffy Creek) located at a high-level divide between two major order river basins (i.e., the Catawba and South Fork of the Catawba); (2) a mid-landscape position consisting of incised streams draining a mid-landscape slope complex (headwaters of South Rhyne Creek); and (3) a watershed at a lower landscape position that is incised into the foot of the mid-landscape slope complex and that discharges onto the legacy floodplain surface (North Rhyne Creek). These three first-order watersheds provide an example of 'headwater' streams that are not necessarily "in the headwaters" of a river system overall, but instead are low-order tributaries of a large river, in this case the South Fork of the Catawba River (Table 1).

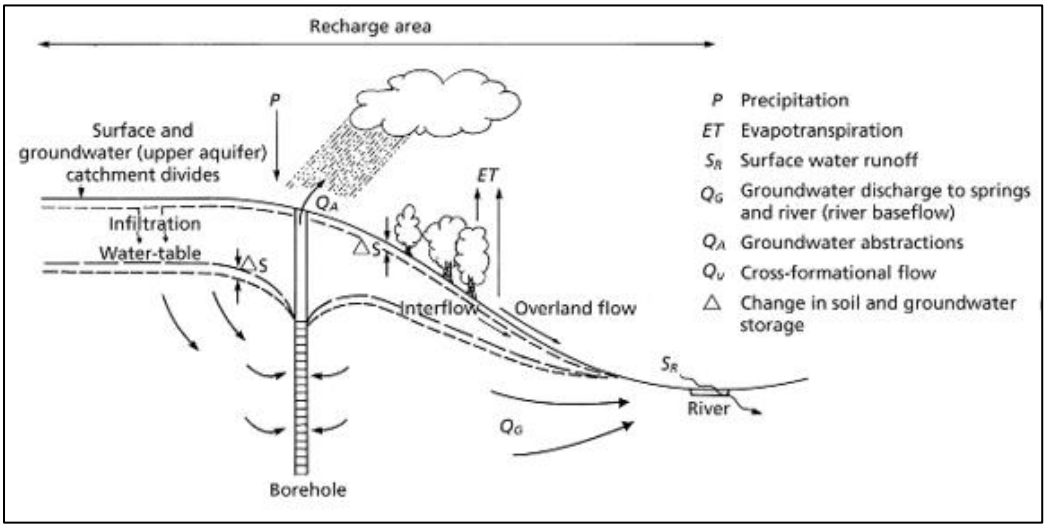

Figure 4. The subsurface portion of the critical zone includes groundwater flow, subsurface storm flow (interflow), and overland flow (modified from Hiscock and Bense, 2014).

2 HYPOTHESES

The watersheds examined in this study are in different landscape positions relative to the larger basin divide of the South Fork of the Catawba. Relative to the larger South Fork of the Catawba River basin divide, the watersheds in this study are in different landscape position. One is at the top of the ridgeline (closest to the divide), one is mid-slope, indicating the transition in topography from concave to convex, and one is at the base of the hillslope (closest to the outlet of the South Fork of the Catawba River). Two hypotheses related to this project involve factors that influence the soils of Redlair's first-order watershed streams and groundwater:

- Seasonal variations in the boundary of the water table affect the locations of weathering reactions within the subsurface, which will be evident as variance in stream chemistry, groundwater levels, and groundwater chemistry.
- Since topography influences the depth and intensity of soil weathering, the relationships between water table depth and watershed-scale chemistry will also vary with landscape position. This variation in landscape position will be visible in the cation chemistry, silica concentrations, or alkalinity concentrations of groundwater or baseflow stream samples.

These two hypotheses will improve understanding of hydrogeochemical processes in small Piedmont watersheds. The first hypothesis states that the water table fluctuation at each watershed could cause groundwater chemistry and stream chemistry to vary according to seasonal change of depth in the weathering profile. Since the watersheds are all located in the same study area, factors such as climate and map-scale lithology are uniform, allowing this research to focus on seasonal influences.

Table 1. Physical characteristics of each watershed incorporated in this study are presented here (USGS StreamStats program). These watersheds are predominantly undeveloped (rural) with little urban influence. South Rhyne was divided into an upper and lower portion for stream sampling purposes.

	Duffy	**Deep**	**South Rhyne**	**Lower South Rhyne**	**North Rhyne**
Latitude of Stream Sampling Site	35.298°	-	35.297°	35.296°	35.298°
Longitude of Stream Sampling Site	-81.083°	-	-81.090°	-81.095°	-81.095°
Area (ha)	6.4	12	4.4	15.5	4.5
Mean Basin Slope (%)	9.8	15.9	8.8	14.4	14
% Forested	83.3	91.0	43.3	78.8	100
% Impervious	0.2	0	0	0	0
% Urban	2.3	0	0.3	0.27	0
Distance from watershed boundary to S. Fork of Catawba River (km)	1.5	0.75	0.88	0.73	0.18

The second hypothesis involves landscape position, or how the physical position of a watershed may influence its hydrologic processes. At RO, one watershed is on a ridgeline, one is at the base of the hillslope, and one is situated in a mid-slope position. Since topography influences the depth and intensity of soil weathering, the relationships between water table depth and watershed chemistry may also vary based on the watershed's location on the hillslope. This landscape variation may be visible in the groundwater levels, ion chemistry, and alkalinity concentrations of groundwater and stream water. This research still provides insight into small, forested watersheds across the southern Piedmont.

A combination of groundwater and surface water chemistry paired with geomorphological measurements of these watersheds were used to examine the water residence timescale and seasonal variations of these watersheds. These hypotheses were investigated using the following approach: geomorphic analysis; continuous water table and water temperature measurements; monthly baseflow stream sampling and calculation of baseflow fluxes; and seasonal groundwater sampling at nested wells located at specific landscape positions within the watersheds. Samples were analyzed for isotopic composition, cation and anion concentrations, silica concentrations, and

alkalinity concentrations to understand the seasonal variability of weathering-derived ions and water quality compounds such as nitrate and phosphate.

3 Redlair Observatory: A Representative Critical Zone Research Site on the Southern Piedmont

Redlair Observatory was newly established at the beginning of this research project in 2019. The purpose of this section is to describe Redlair's suitability to address the research questions in this study, and to describe the permanent site conditions that were documented during the period of the study.

The climate at Redlair is humid and subtropical, typical for this region of North Carolina. The mean annual precipitation for North Carolina is 1,200 millimeters (for 1901-2019) with a mean annual temperature of about 14.5º Celsius (for 1901-2019; NCSU, 2019). The elevation at Redlair is approximately 230 m above sea level from the Duffy hilltop to the South Fork of the Catawba River to the west. This research project covered a transect of roughly 1,400 m with 200 m of topographic relief (Figure 5). The climate is uniform across the watersheds since they are close to one another. This allows for better understanding of how the changing seasons affect the watersheds.

3.1 Geology

This research occurs entirely on the Charlotte Terrane (Figure 3). The rocks of the Charlotte Terrane are likely Neoproterozoic to early Paleozoic in age (Hibbard et al., 2002). The Charlotte Terrane is characterized by plutonic and metavolcanic rocks (Goldsmith et al., 1985; Pippin et al., 2008). The protoliths likely originated from a volcanic island arc system, which explains why there are volcanic and intrusive rocks present in the same area (Dennis and Shervais, 1996; Hibbard et al., 2002). At the map scale, Goldsmith et al. (1985) determined that the Charlotte Terrane consists

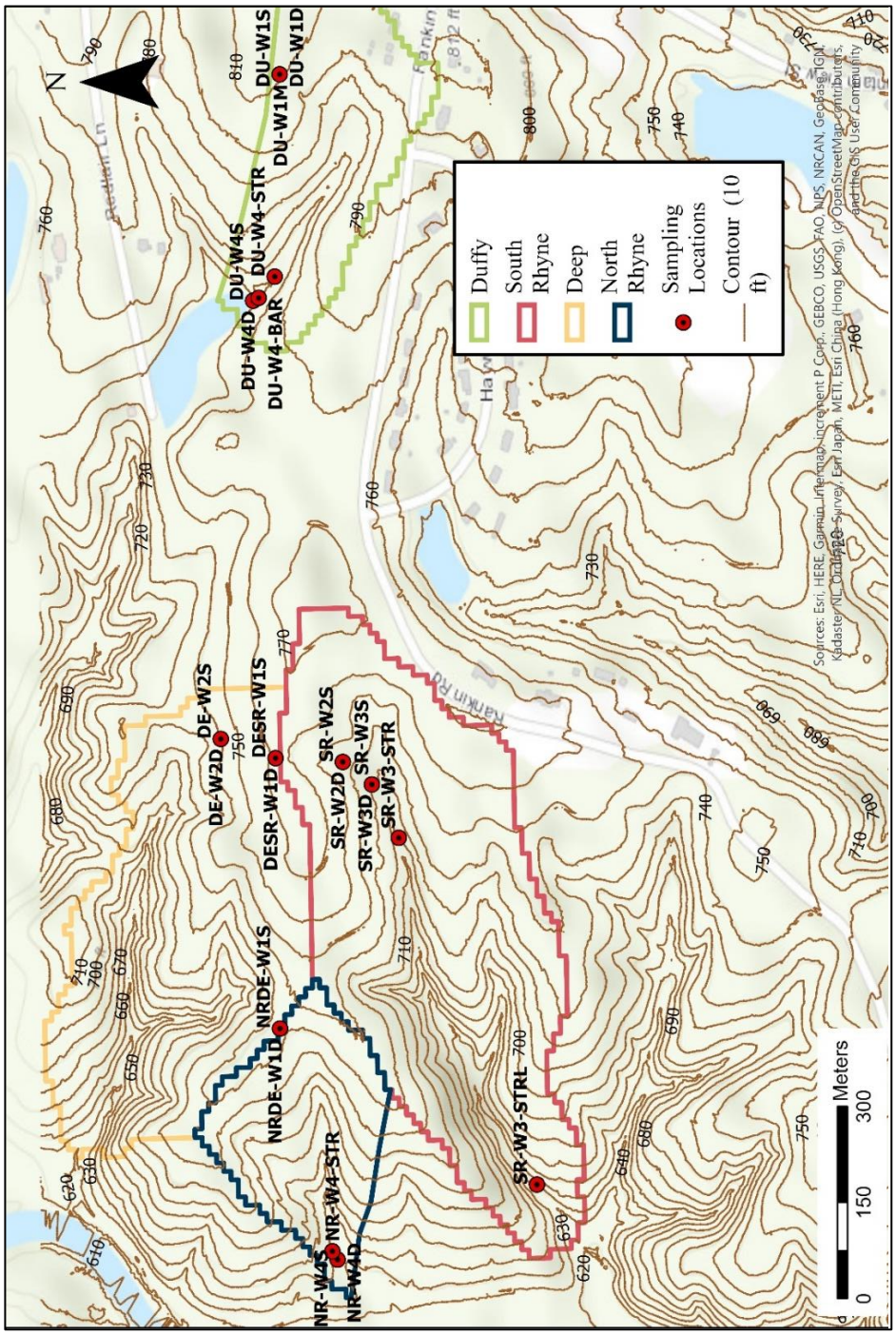

Figure 5. Topographic map of the study area derived from LiDAR DEM data (NCID.NC.gov). The contour lines are in 10-foot intervals.

of metaintrusive and metavolcanic rocks described as undivided felsic to mafic rocks. The Central Piedmont Shear Zone (or Boogertown Shear Zone) is a northeast-southwest trending structural feature that cuts through Redlair Preserve, northwest of the instrumented watersheds that comprise the core of RO. This shear zone separates the Kings Mountain Terrane (part of the Piedmont Zone) on the west from the Charlotte Terrane on the east.

The rocks at RO weather into three main soil types: sandy clay loam of the Cecil series, Pacolet fine sandy loam, and Pacolet sandy loam (unpublished Redlair soils map obtained from Redlair Observatory; Figure 6). These soil types are all formed *in situ* from mainly felsic igneous and metamorphic rocks parent material (Hearn et al., 1909). The two Pacolet series soils are in forested areas with steeper slopes or ridges, while the Cecil series soil is located on more subdued flatlands along divides (such as floodplains). One of the Pacolet soil series is comprised of sandy clay loam while the other is primarily sandy loam. More generically, these soils are defined as Entisols (Pacolet) and Ultisols (Cecil). Ultisols are defined as well-developed soils (with high acidity and in the B horizon). Entisols are defined as soils that have little to no soil development (US Department of Agriculture and National Resources Conservation Service, 2014). At Redlair, the Duffy watershed is situated in the Cecil series grading into the Pacolet series in the forested area. The North Rhyne and South Rhyne watersheds are in the Pacolet series. Additionally, the divide between North Rhyne and Deep Creek watersheds is comprised of mostly Cecil series soil.

Aspect can affect critical zone processes due to the strong influence that solar insolation has on both vegetation and soil properties. Studies have shown that south-facing slopes typically have thinner regolith (saprolite), and therefore slope creep is more likely to occur on south-facing slopes (West et al., 2014). A complete analysis of the influence of aspect on watershed dynamics is beyond the scope of this study but may be an important critical zone factor for future studies. Nevertheless, the watersheds studied herein are consistently characterized by both north-facing and south-facing slopes.

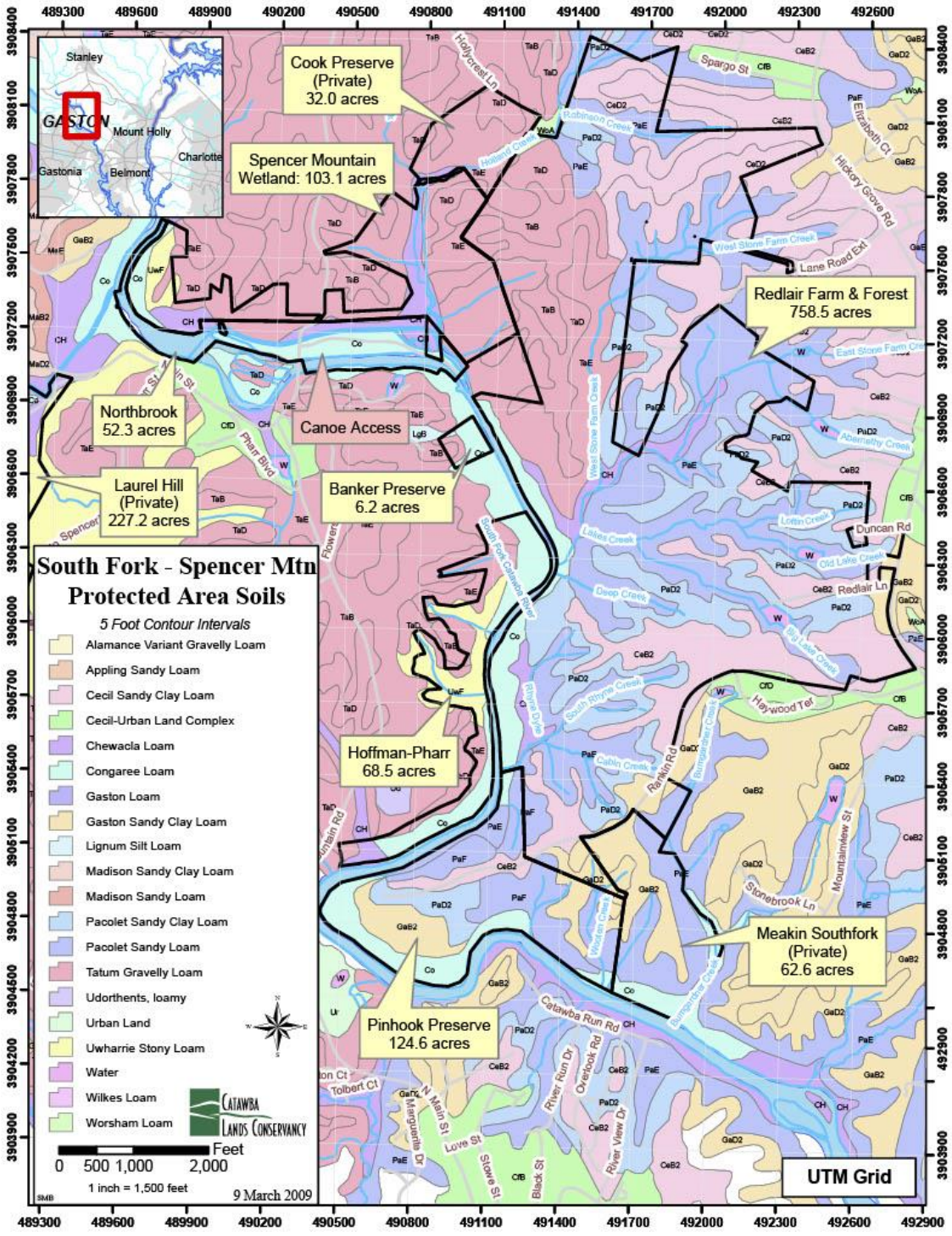

Figure 6. A map of the soils found at Redlair Observatory (outlined in black) and surrounding areas. The main soils found at Redlair include Pacolet fine sandy loam, Pacolet sandy loam, and sandy clay loam of the Cecil series (Catawba Lands Conservancy, 2009).

3.2 Hydrogeology

Topography profoundly affects the flow paths of groundwater flow systems. Groundwater and topography are interconnected by factors such as the elevation of recharge areas, the degree to which rivers incise the landscape, and the location and extent of low-lying areas that drain groundwater from hillside areas. The Piedmont is a local flow system, meaning that recharge originates at ridgetops or topographic high regions and discharge is located proximal to streams or rivers, or topographically low areas (Fetter, 2001). Redlair also exhibits a local flow system, as illustrated by Daniel and Dahlen (2002) (Figure 7). The local flow system at Redlair could influence groundwater levels, residence times, and chemistry. Studies have shown these systems result in fluctuating chemical signatures of seasonal water table variations at the hillslope scale (Hiscock and Bense, 2014). Groundwater in a local flow system is unlikely to cross watershed boundaries.

Figure 7 illustrates the groundwater flow system of the North Carolina Blue Ridge and Piedmont provinces. Within the region, infiltrated water moves downward through the unsaturated zone. Vertical movement within the saturated and unsaturated zone is dependent on the condition of the regolith or bedrock, often relying on intergranular flow or fractures (Daniel and Dahlen, 2002). Because the bedrock geology of Redlair consists of igneous and metamorphic rocks, most of the vertical movement of groundwater within the saprolite depends on intergranular flow along weathered grain boundaries and weathered fracture planes. Ultimately, the bedrock provides fast flow paths (fractures) for groundwater movement, but little storage. The saprolite provides storage (porosity) but is low in hydraulic conductivity (ease of water moving through the sediment).

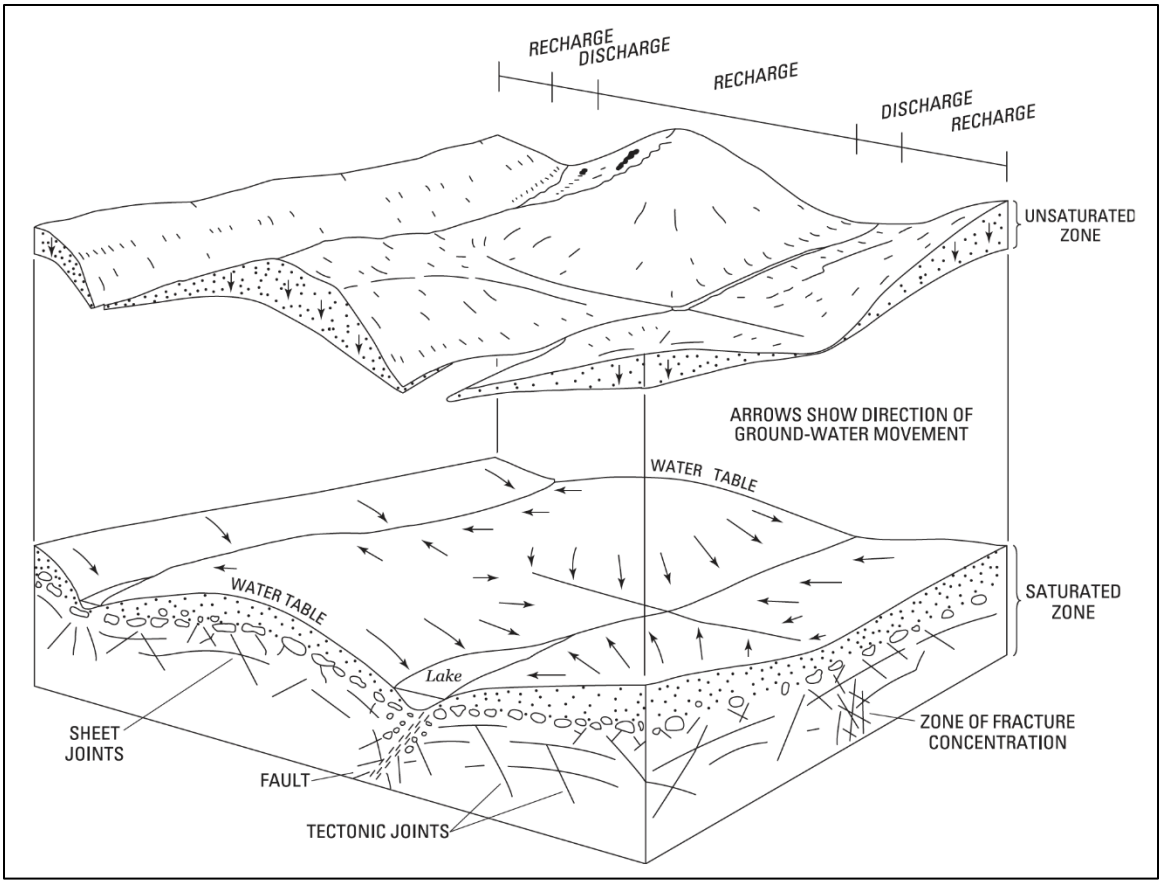

Figure 7. A conceptual diagram of the groundwater flow system of the Blue Ridge and Piedmont regions of North Carolina (Daniel and Dahlen, 2002). Once water infiltrates into the ground, it begins to move vertically and laterally away from the unsaturated zone (here, shown raised above the water table boundary) and towards the saturated zone. The Redlair Observatory represents a local flow system.

3.3 Historical Land Use

Historically, Redlair is representative of the overall southern and central Piedmont regions. These lands were used heavily for agriculture during the 1800s to ~1950s, which depleted the once nutrient-rich soils. This nutrient depletion led to abandonment of the lands, and subsequent reforestation of the uplands. The southern Piedmont has been slowly recovering ever since, with most of the land today being forested, agricultural, or urbanized. After European settlement, rapid clearing of forested uplands for agriculture led to an increase in gullying and erosion and the filling-in of established stream channels (Trimble, 2008). The filled channels then became deeply incised. This has led to further gully erosion across these landscapes.

4 METHODOLOGY

4.1 Study Site

Seventeen wells were drilled at two or three depth completions per location (Figure 8; Table 2). Well depth was dependent on the depth to competent bedrock from the ground surface. The wells and watersheds are also located on slopes of varying aspect.

4.2 Geomorphological measurements of watersheds

Geomorphological measurements were quantified to better constrain the physical attributes of these small watersheds. To analyze this relationship, channel heads – which represent the transition from zero to first-order watersheds – were identified in the field for the Duffy, North Rhyne, and South Rhyne streams. The method involved identifying channel heads by locating the uppermost extent of erosion and flow found in continuous stream banks (Jefferson and McGee, 2013). Channel head topography typically includes the convergence of multiple small streams or gullies (Julian et al., 2011). Field data collection included traversing the length of the three main streams investigated in this study to find their channel heads. Any additional tributaries to the streams were also noted and located. The field-based GPS coordinates were then compared to where they were identified in LiDAR maps. The transition between first and zero-order watershed is often indicated as amphitheater bowl-shaped topography (Julian et al., 2011; Jefferson and McGee, 2013). Lastly, the Strahler stream order of each watershed's channel network was based on 10 m contour lines. The stream orders were hand-drawn directly onto the contour map.

Hillslope slope and profile curvature were analyzed using ArcMap GIS based on LiDAR (2 points per meter) data acquired from NCID.NC.Gov (accessed 2020). The LiDAR data were used to construct a Digital Elevation Model (DEM) of the study area. Watershed analyses, including hypsometric curves and longitudinal channel profiles from channel head to outlet were also constructed using ArcMap GIS. The hypsometry tool was acquired from the San Francisco

State University Institute for Geographic Information Science (Davis, 2020). Additional ArcMap tools that were used included ‘profile’, ‘slope’, and ‘curvature’ acquired from the 3D Spatial Analyst toolbox and used on the DEM(s). Some analyses, including use of the slope, hypsometric, and curvature tools, required clipping the DEM rasters to the extent of the individual watershed shapefiles. Subsequent filling-in of holes in the DEMs also occurred. For the profile curvature tool, ArcGIS assigns number values to each pixel of the DEM. A negative value indicates a convex shape while a positive value indicates a concave shape. Measurements of the location of each of the sampling sites in terms of their elevation above the South Fork of the Catawba and their lateral distance from the major tributary were acquired from Google Earth and ArcMap GIS.

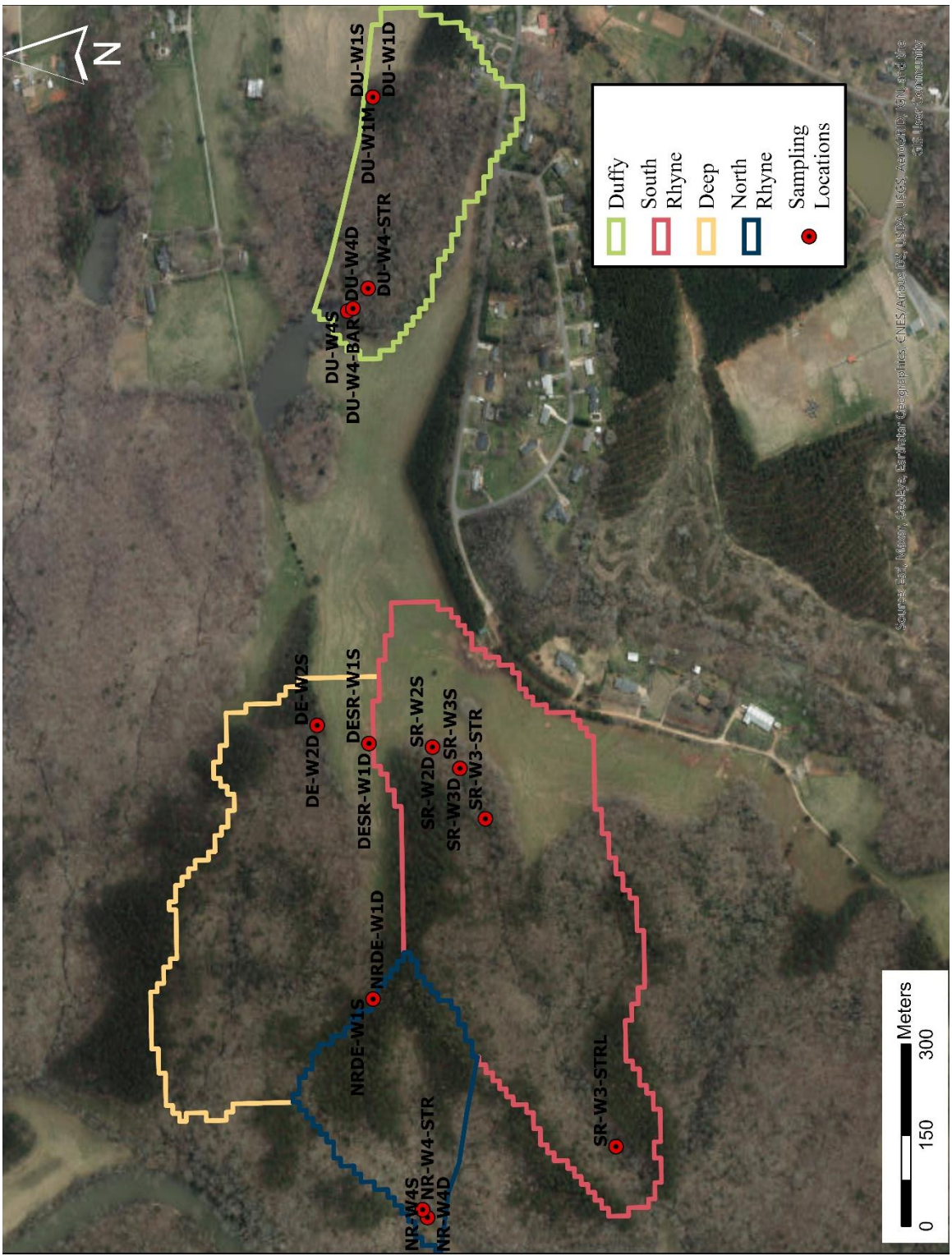

Figure 8. Satellite imagery of the Redlair Observatory with the four study watersheds of concern outlined. The sampling locations, which in this case includes the wells and the surface water locations, are also shown. (Source: Esri, Maxar, GeoEye, Earthstar Geographics, CNES/Airbus DS, USDA, USGS, AeroGRID, IGN, and the GIS User Community).

Table 2. The 17 wells and four stream sampling locations (STR) are listed in the table below. Since NRDE-W1 was dry throughout the study, some of its characteristics were not recorded. The last four rows are the streams.

Well Name	Latitude (decimal degrees)	Longitude (decimal degrees)	Height above land surface to top of well casing (meters)	Total well depth below land surface (meters)
DU-W1S	35.29900	-81.08176	0.77	16.16
DU-W1M	35.29900	-81.08176	0.84	21.04
DU-W1D	35.29900	-81.08176	0.86	24.39
DU-W4S	35.29900	-81.08440	0.00	4.27
DU-W4D	35.29900	-81.08440	0.00	6.10
DESR-W1D	35.29900	-81.08974	0.00	21.34
SR-W2S	35.29800	-81.08979	1.03	9.76
SR-W2D	35.29800	-81.08979	0.99	15.24
SR-W3S	35.29754	-81.09005	0.84	7.62
SR-W3D	35.29754	-81.09005	0.79	21.04
NR-W4S	35.29794	-81.09559	0.85	4.57
NR-W4D	35.29794	-81.09559	0.84	6.40
DE-W2S	35.29930	-81.08952	0.00	18.29
DE-W2D	35.29930	-81.08952	0.00	24.39
NRDE-W1S	35.29861	-81.09290		14.02
NRDE-W1D	35.29861	-81.09290		17.07
DU-W4-STR	35.29885	-81.08412		
SR-W3-STR	35.29706	-81.09076		
NR-W4-STR	35.29706	-81.09550		
SR-W3-STRL	35.29559	-81.09472		

4.3 Water levels

Water levels were recorded manually from fourteen wells and automated data loggers were used at five wells. Groundwater levels were measured manually monthly. Measurements were recorded as depth below land surface (bls) from a designated measurement point. A water level beeper was used to measure from the top of the identified measurement point (i.e., top of the well casing) to the depth at which the sensor hit the water level surface monthly. Additionally, Onset HOBO U20L Series Water Level Loggers were used to continuously record groundwater

temperature (Celsius) and water pressure (kPa) at five wells every 10 minutes (Table 3). There was also a barometric pressure logger located in the Duffy watershed (DU-W4-BAR on Figure 8). A seventh logger was in the North Rhyne stream (NR-W4-STR). The data from these loggers were downloaded approximately monthly. Manual barometric compensation was calculated based on the water pressure data from the HOBO loggers. The calculation goes as follows:

1. Determine the net pressure (kPa) based on the difference between the HOBO logger in the well and the barometric pressure logger.
2. Net pressure in kPa x 0.14503 x 0.703 = Height of water on top of the sensor in meters.
3. String length (m) – well stickup height (m) – height of water on top of sensor (m) = depth of water below the land surface (m).

Several measurements were used to calculate the depth to groundwater below the land surface: the height of the measurement point (MP) above the land surface, the length of the string from which the HOBO logger was hung, and the barometrically compensated data showing the height of the water on top of the sensor (refer to Table 3). The equation for calculating groundwater levels using the HOBO loggers is based upon the schematic in Figure 9. The groundwater levels calculated from the HOBO loggers were also measured in comparison with the monthly manual measurements of the depth from the MP to the water table using a water level beeper.

Table 3. Wells in this study, including those with HOBO data loggers are listed. Note that one logger was used as a barometric pressure logger to calibrate all groundwater levels from the other six loggers (DU-W4-BAR). Note that in the well names S = shallowest completion depth, M = intermediate, and D = deepest completion depth (BLS = below land surface).

Well Name	Latitude	Longitude	Top of Well Screen BLS (m)	Total Well Depth BLS (m)	Height of Measurement Point above land surface (m)	HOBO Logger String Length (m)
DU-W1S	35.298878	-81.081755	14.6	16.2	0.78	
DU-W1M	35.298878	-81.081755	19.5	21.0	0.79	

Well Name	Latitude	Longitude	Top of Well Screen BLS (m)	Total Well Depth BLS (m)	Height of Measurement Point above land surface (m)	HOBO Logger String Length (m)
DU-W1D	35.298878	-81.081755	22.9	24.4	0.79	
DU-W4S	35.298926	-81.084404	2.7	4.3	0	4.04
DU-W4D	35.298926	-81.084404	5.2	6.1	0	4.53
SR-W-2S	35.297879	-81.089785	8.2	9.8	0.95	
SR-W-2D	35.297879	-81.089785	13.7	15.2	0.95	8.41
SR-W3S	35.297540	-81.090048	6.1	7.6	0.73	
SR-W3D	35.297540	-81.090048	19.5	21.0	0.73	
DE-W2S	35.299303	-81.089517	16.8	18.3	0	
DE-W2D	35.299303	-81.089517	22.9	24.4	0	
DESR-W1S	35.298664	-81.089741	10.4	11.9	0	
DESR-W1D	35.298664	-81.089741	19.5	21.3	-0.12	17.95
NRDE-W1S	35.298612	-81.092895	12.5	14.0	0.82	
NRDE-W1D	35.298612	-81.092895	15.5	17.1	0.85	
NR-W4S	35.297940	-81.095592	3.0	4.6	0.84	4.64
NR-W4D	35.297940	-81.095592	5.8	6.4	0.82	
NR-W4-STR	35.298001	-81.095495				0.65
DU-W4-BAR	35.30830	-81.07230				0.67

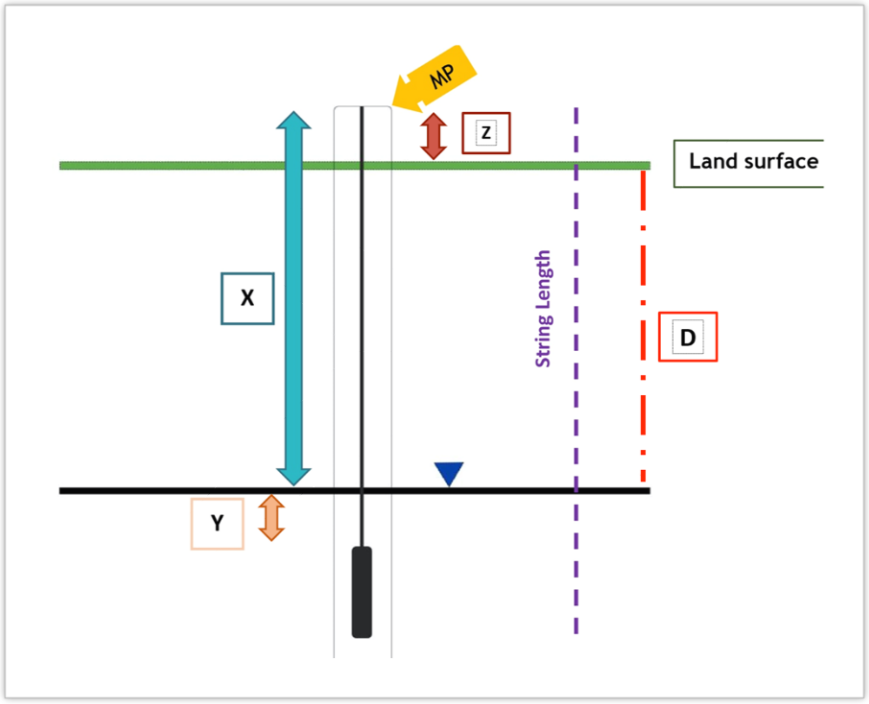

Figure 9**.** Schematic diagram depicting the U20L Series 1 HOBO logger sitting in a well below the ground surface. Several variables are needed to calculate the groundwater level below land surface. In this diagram, X represents the depth of water from the measurement point (MP) to the water table. Y represents the potential difference between the depth of the sensor below the ground and the distance from it and where the water table lies (i.e., height of water above the logger). Z represents the height of the MP above land surface. All these measurements are required to calculate the distance from the land surface down to the water table. D represents depth to groundwater below the land surface in meters. Figure is not to scale.

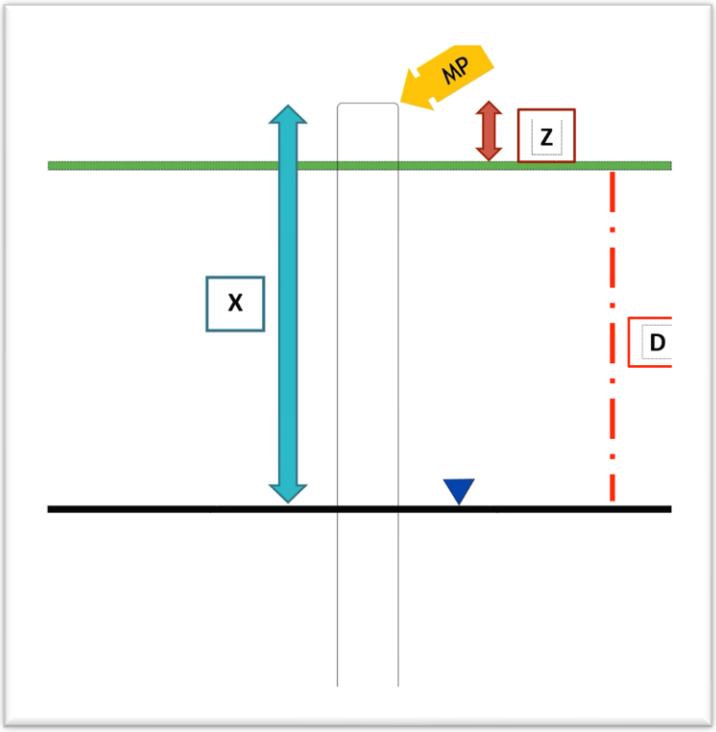

Figure 10. Manual groundwater measurements using a water level beeper. X represents the depth of the water from the MP and Z represents the height of the MP above land surface. Groundwater levels, recorded as depth bls (variable D), can be solved from manual groundwater measurements by X – Z = D. Figure is not to scale.

4.4 Groundwater sampling

Groundwater samples were collected seasonally from Spring 2019 to Summer 2020. Upon arrival at each well, depth to groundwater level was measured using a water level beeper, then the well was purged of stagnant water using a bailer or pump. Temperature, pH, specific conductance, and electronic conductivity were measured from pumpable wells until these parameters were stable, indicating fresher groundwater. At the start of the research project (Spring 2019 – Fall 2019), shallow wells were sampled using a GeoPump peristaltic pump at a rate of 100-1000 mL/min using in-line filtration, and deeper wells were sampled with a bailer and syringes. All groundwater samples were filtered in the field using 0.2 µm polyethersulfone filters. However, the Geopump was unable to collect water at depths greater than ~9 m beneath the land surface (bls), but several wells at Redlair were drilled deeper than 18.3 m bls. As a result, samples from that point on were

primarily collected using a Geotech Geosquirt 12 VDC Purge Pump, which can pump groundwater from depths of 27.4 m (90 ft) from October 7, 2019 and onward. The Geosquirt Purge Pump is capable of low-flow sampling, which is ideal for sampling groundwater from small-diameter and low-yielding monitoring wells with a minimum of disturbance. Use of the Geopump peristaltic pump continued at the two shallowest well locations: NR-W4 and DU-W4 (4.3–6.4 m deep).

Three wells were dry for the duration of this research project: NRDE-W4 shallow and deep and DESR-W1S (Figure 5).

4.5 Surface water sampling and stream discharge

Four stream sampling locations were identified within the three watersheds (DU-W4-STR, NR-W4-STR, SR-W3-STR, and SR-W3-STRL). Only one of the four stream locations ran perennially (SR-W3-STRL), while the other three were intermittent-to-ephemeral during the study period (SR-W3-STR, DU-W4-STR, NR-W4-STR).

Baseflow stream discharge was calculated using the volumetric discharge method. This included identifying a section along the stream with water flowing over a substrate. An aluminum rain downspout piece was fit to contain the stream flow into a 1000 mL volumetric beaker. Then, time was measured based on how long it took for a certain amount of the water to be captured in the beaker (typically a few seconds). This was repeated 3-5 times per site and after each sampling event. The volume of water collected, and time recorded varied each sampling event per stream location. Depending on the stream location and stream flow for a particular sampling event, discharge was calculated as volume of water over a given time, reported in L/min. During some sampling events, there was no streamflow, so some surface water parameters were not measurable. All values were recorded and reported in the Results section.

Surface water samples were collected monthly from Spring 2019 to Summer 2020 from flowing stream water. Samples were gathered by gently drawing the stream water into a syringe then transferring it to a polyethylene bottle. Use of a syringe helped to minimize the amount of

sediment in the water, which reduced filter loading and filtration time. Roughly four 60 mL syringe fills of stream water were needed to fill one 250 mL polyethylene bottle. Each stream's temperature, pH, specific conductance, and dissolved oxygen were immediately measured post-sampling using YSI single-parameter probes. The probes were placed directly into the flowing stream water facing upstream. Discharge measurements for each stream were also calculated at the time of sample collection as previously described. After collection, samples were taken to the laboratory for filtration using a vacuum pump and 0.2 µm polyethersulfone filters. These samples were stored at 4º C for subsequent laboratory analysis. SR-W3-STRL was a second sampling point along the South Rhyne stream, added in September of 2019. SR-W3-STRL was the most measurable stream of the four sampling locations selected. Occasionally, field parameters were not available due to logistical reasons (i.e., not having the meters available for fieldwork).

4.6 Laboratory Analysis

Water isotopes can be used as tracers to determine groundwater residence times as well as to follow the path of water through watersheds (Clark and Fritz, 1997; Buttle, 1998). Samples were collected and filtered in the field as previously mentioned and sealed in a crimp top vial for preservation. These samples were then stored in a refrigerator at 4º C. An LGR DLT-100 laser water isotope analyzer, calibrated using two commercially obtained standards, was used to analyze the samples for $\delta^{2}H$ and $\delta^{18}O$ (International Atomic Energy Agency, 2009).

Ion chromatography was used to analyze major anion (fluoride, nitrate [as NO_3^-], sulfate, phosphate, and chloride) and cation (calcium, sodium, potassium, and magnesium) concentrations in the monthly surface water samples and seasonal groundwater samples. Nitric acid was added at a final acidity of 0.5% to each sample bottle designated for cation analysis to preserve the samples at pH < 2. These samples were kept refrigerated prior to analysis.

Silica concentration was analyzed using a Lachat flow injection analyzer. Silica samples were refrigerated until analysis. Alkalinity samples were also stored in the same manner and were

analyzed following the Gran titration method (Gieskes and Rogers, 1973). Alkalinity concentration was reported in milliequivalents per liter (meq/L). A concentration of 0.1 normal hydrochloric acid was used to titrate each water sample.

Alkalinity concentration was calculated using the following:

$$Alkalinity = 1000 * \frac{(mL\ acid\ dispensed * 0.1)}{sample\ weight\ (g)}$$

Dissolved inorganic carbon (DIC) and stable carbon isotopes of DIC (δ^{13}C-DIC) were analyzed using a Picarro G2201-*i* carbon analyzer with Liaison and AutoMate peripherals for introducing DIC to the instrument. This analysis was calibrated using freshly made standards from bicarbonate and carbonate salts of known δ^{13}C.

5 RESULTS

5.1 Geomorphological measurements of watersheds

DEMs are provided for the entire study area, as well as individual watersheds in Figure 11-14. These images reveal the channel networks within the four sub-watersheds.

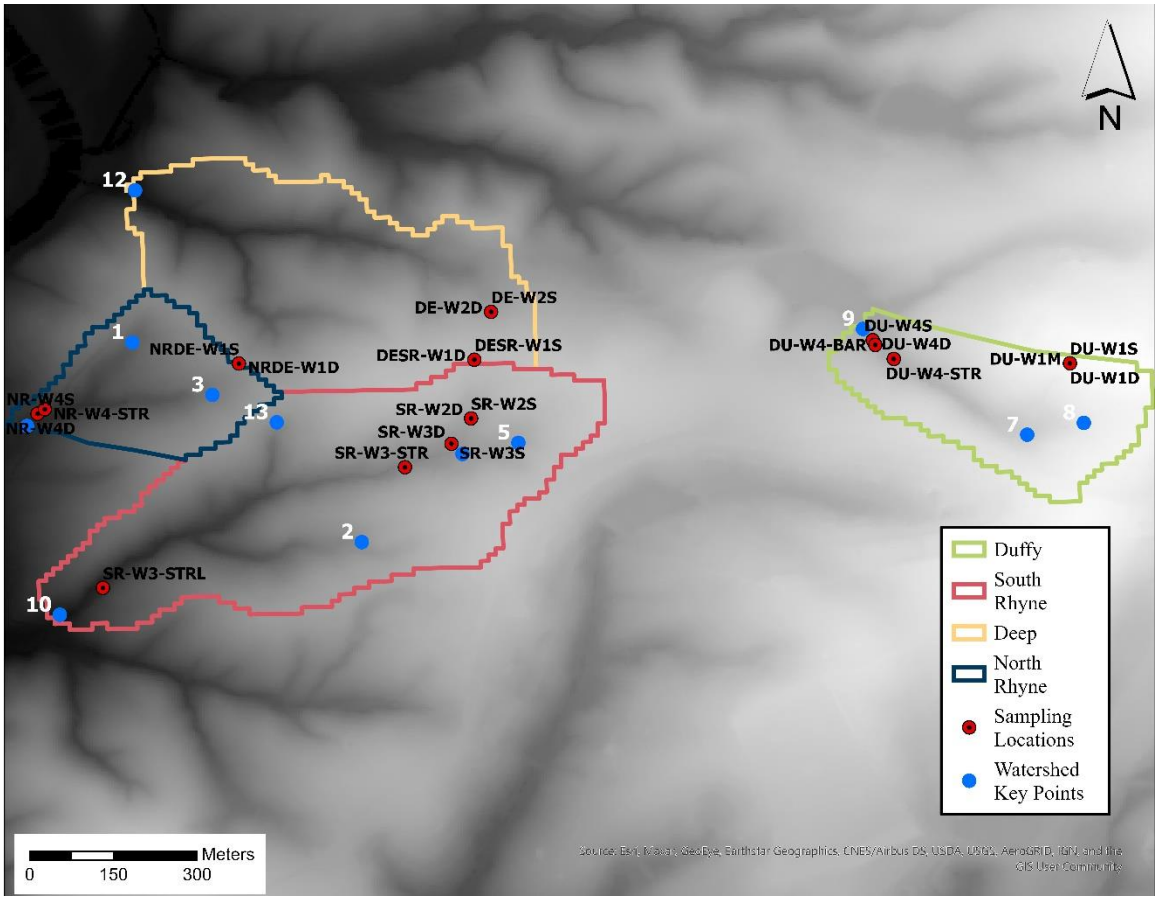

Figure 11. A DEM of the Redlair study area with associated watershed sampling locations and key points of interest (LiDAR data acquired from NCID.NC.Gov, accessed 2020).

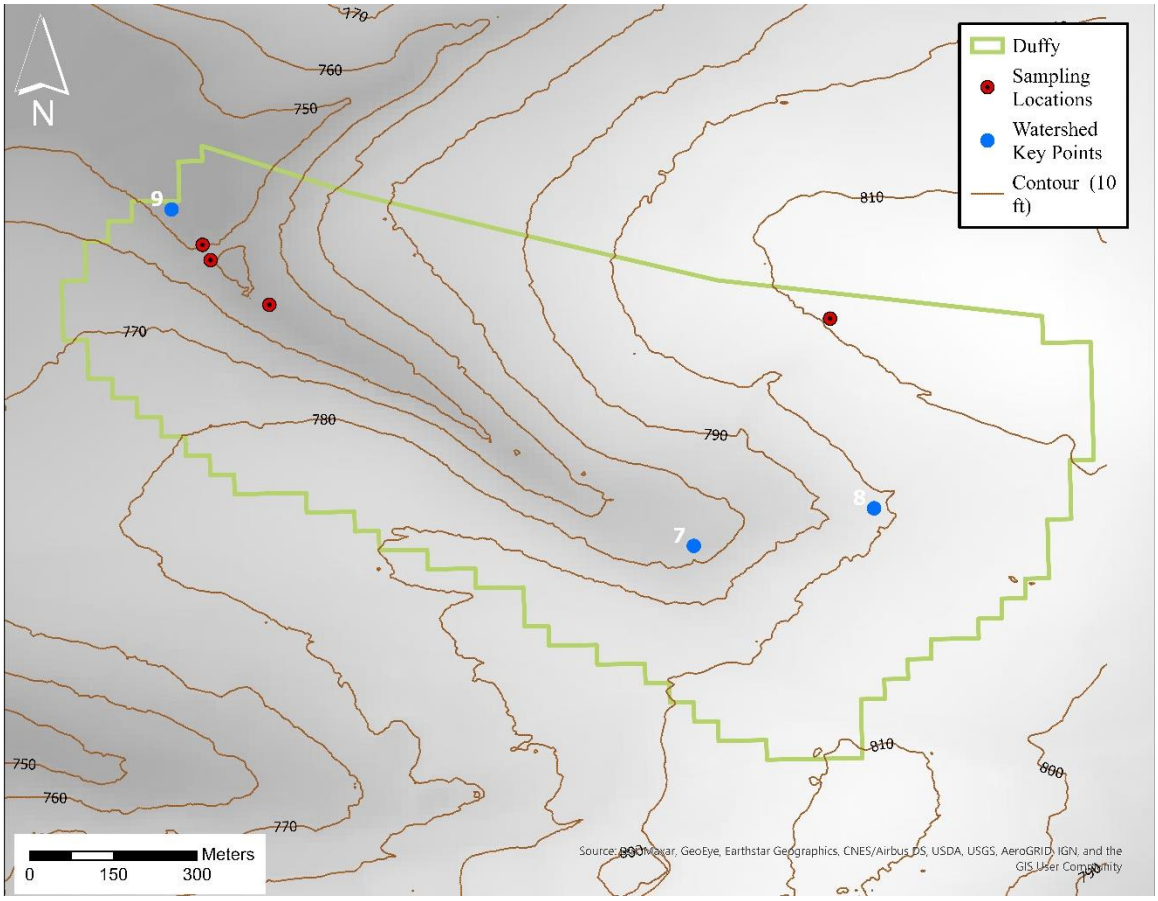

Figure 12. A DEM of the Duffy watershed sampling locations and key points of interest. Contour lines in 10-foot intervals are also shown to provide more detail. Points 7 and 8 were identified using field reconnaissance. Point 7 represents the transition in the watershed from zero- to first-order. Point 8 represents the channel head, which is where water first originates in the channel. Point 9 represents the outlet of the Duffy watershed (LiDAR data acquired from NCID.NC.Gov, accessed 2020).

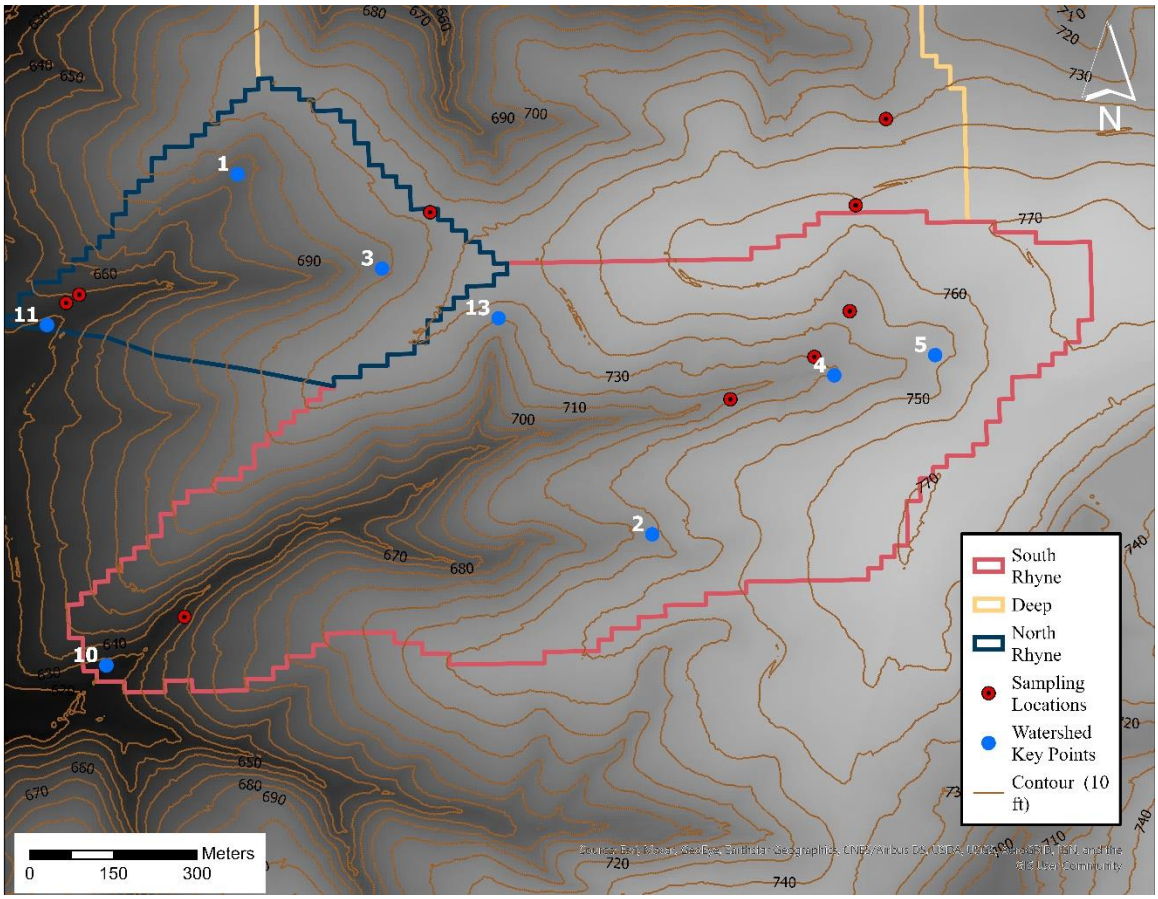

Figure 13. A DEM of the South Rhyne watershed sampling locations and key points of interest. Contour lines in 10-foot intervals are also shown to provide more detail. Here, point 4 represents the riprap at the fence delineating the cow pasture, where the main SR-W3-STR channel is located. Point 5 represents the channel head, which is where water first originates in the channel. Points 2 and 13 are channel heads of tributaries leading to the main portion of the South Rhyne. Points 2, 4, and 5 were identified using field reconnaissance. Point 10 represents the outlet of the Duffy watershed (LiDAR data acquired from NCID.NC.Gov, accessed 2020).

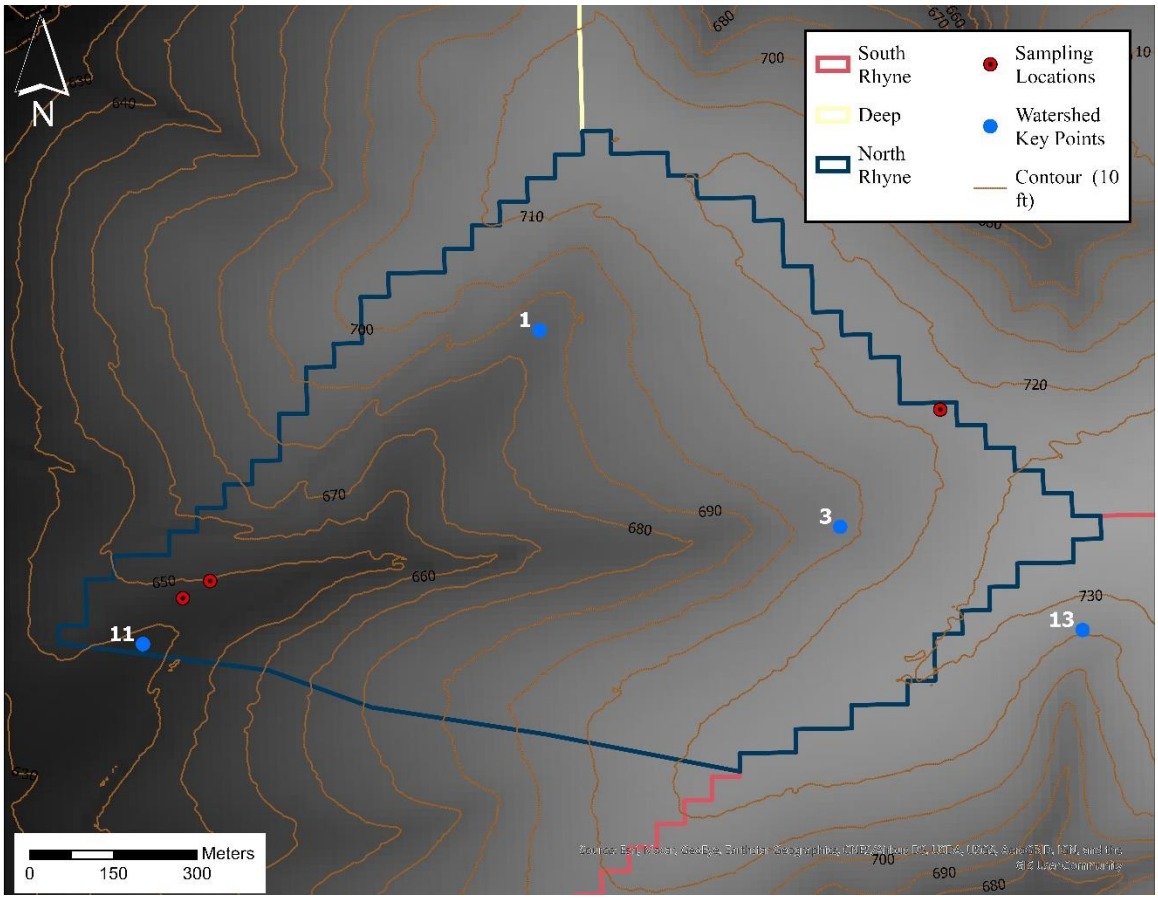

Figure 14. A DEM of the North Rhyne watershed sampling locations and key points of interest. Contour lines in 10-foot intervals are also shown to provide more detail. Point 3 represents the channel head, which is where water first originates in the channel. Points 1 and 3 were identified using field reconnaissance. Point 11 represents the outlet of the watershed (LiDAR data acquired from NCID.NC.Gov, accessed 2020).

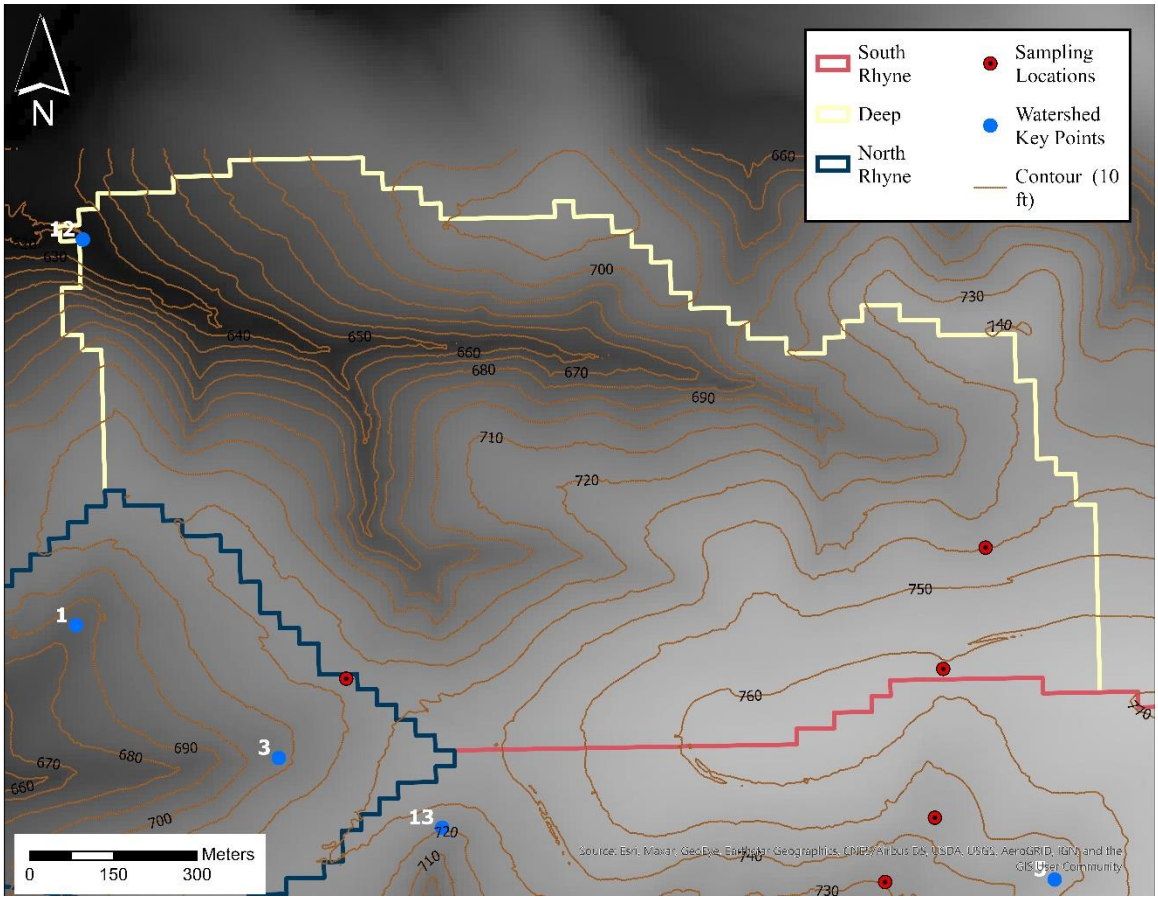

Figure 15. A DEM of the Deep watershed sampling locations and key points of interest. Contour lines in 10-foot intervals are also shown to provide more detail. Here, point 12 represents the outlet of the Deep watershed (LiDAR data acquired from NCID.NC.Gov, accessed 2020).

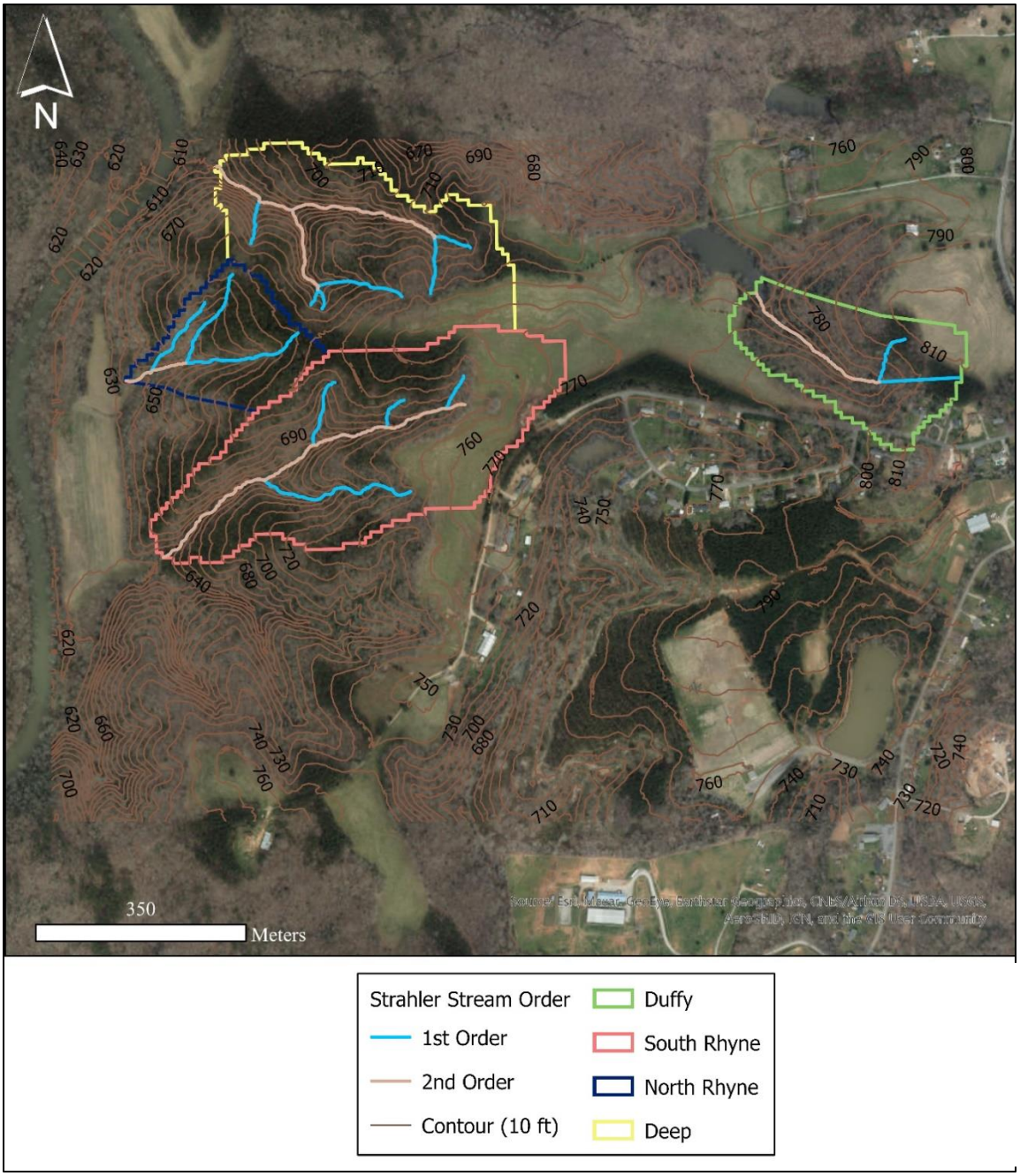

Figure 16. Map showing the streams of the four watersheds ranged from first- to second-order, with the initiation of the channel heads within the zeroth-order portion (Source: Esri, Maxar, GeoEye, Earthstar Geographics, CNES/Airbus DS, USDA, USGS, AeroGRID, IGN, and the GIS User Community).

On average, the Deep watershed had the steepest slope percent rise while the Duffy watershed had the gentlest (Table 4). It appears that the Deep and South Rhyne watersheds had the steepest slopes throughout the entirety of the stream channels in the watersheds when just based

off of Figure 17. However, according to Table 4, South Rhyne and North Rhyne had similar average slope percent rises.

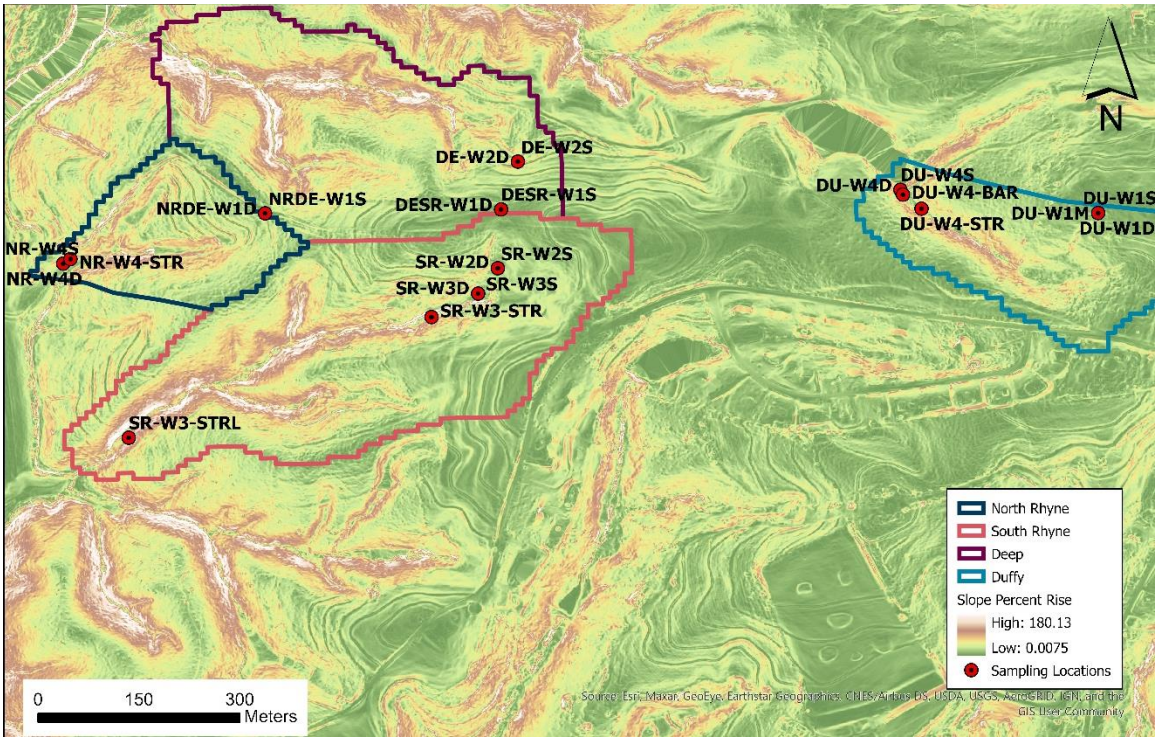

Figure 17. The Redlair Observatory study area colorized to show slope percent rise. The South Rhyne watershed has the steepest slopes, followed by Deep, whereas North Rhyne and Duffy have relatively gentler slopes.

Table 4. Curvature and average percent (%) slope rise of the four watersheds.

Watershed	Average Curvature	Average % Slope Rise
Duffy	-0.04	10.02
Deep	-0.05	21.06
South Rhyne	-0.03	17.64
North Rhyne	-0.03	17.42

The light pink color that seems to dominate much of the landscape in the watersheds represents roughly neutral curvature (i.e., neither concave nor convex; Figure 18-21). The color scheme of these figures also helps to emphasize the legacy agricultural contouring influences on the landscape from past land use, which otherwise could have been likely imperceptible within the

forest. The shades of green represent positive (i.e., concave topography) values, which seem to occur mostly around the stream valleys and paralleling the legacy contour imprints.

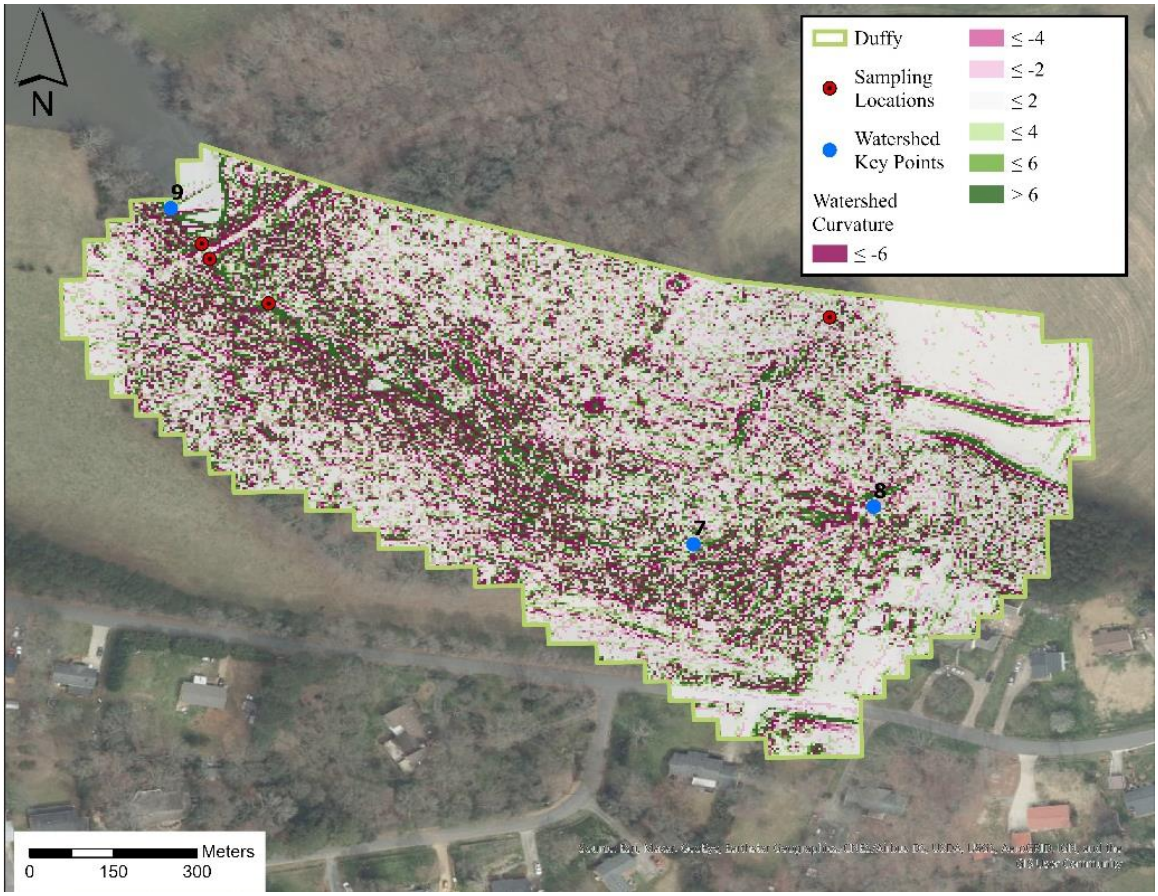

Figure 18. Colorized profile curvature map of the Duffy Watershed. The blue dots represent key locations within the watershed. Points 7 and 8 were identified using field reconnaissance. Point 7 represents the transition in the watershed from zero- to first-order. Point 8 represents the channel head, which is where water first originates in the channel. Point 9 represents the outlet of the Duffy watershed (LiDAR data acquired from NCID.NC.Gov, accessed 2020).

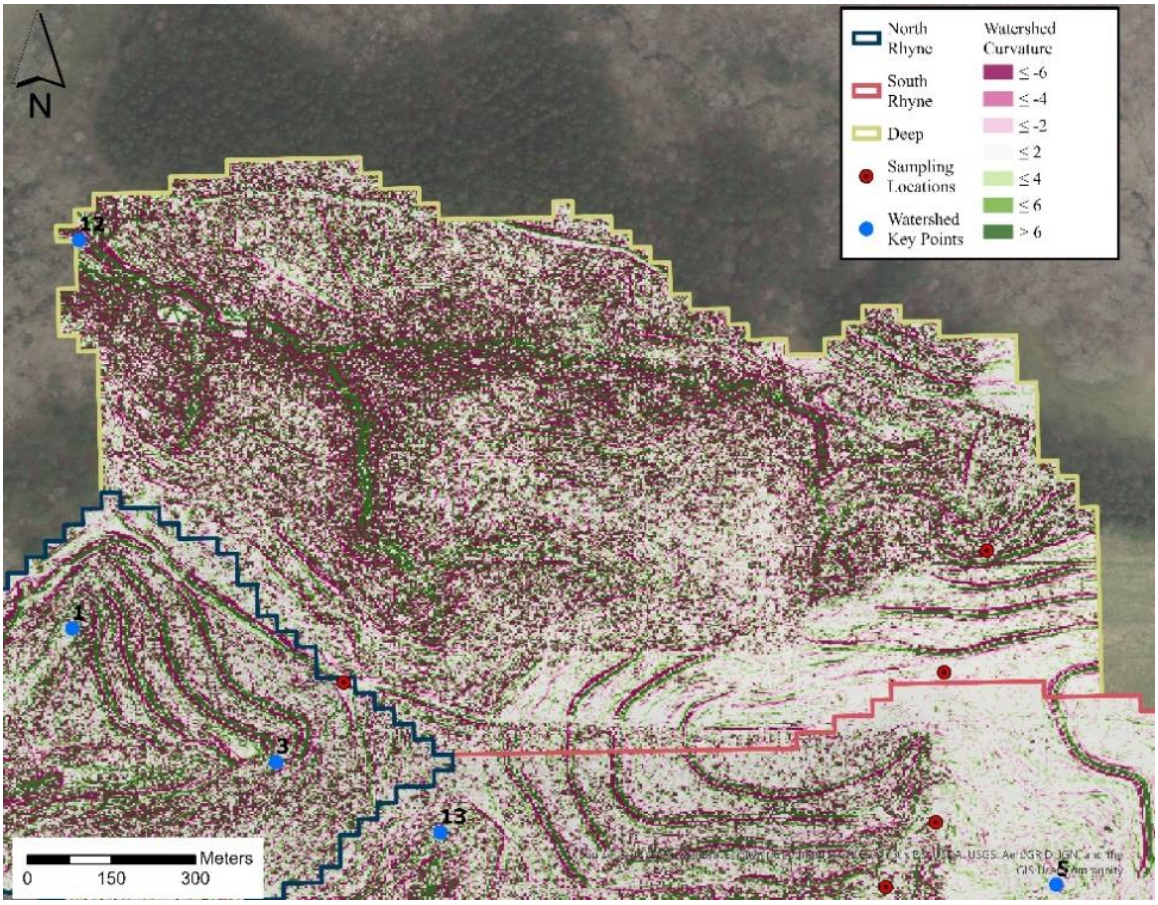

Figure 19. Colorized profile curvature map of the Deep Watershed. The blue dots represent key locations within the watershed. Here, point 12 represents the outlet of the Deep watershed (LiDAR data acquired from NCID.NC.Gov, accessed 2020).

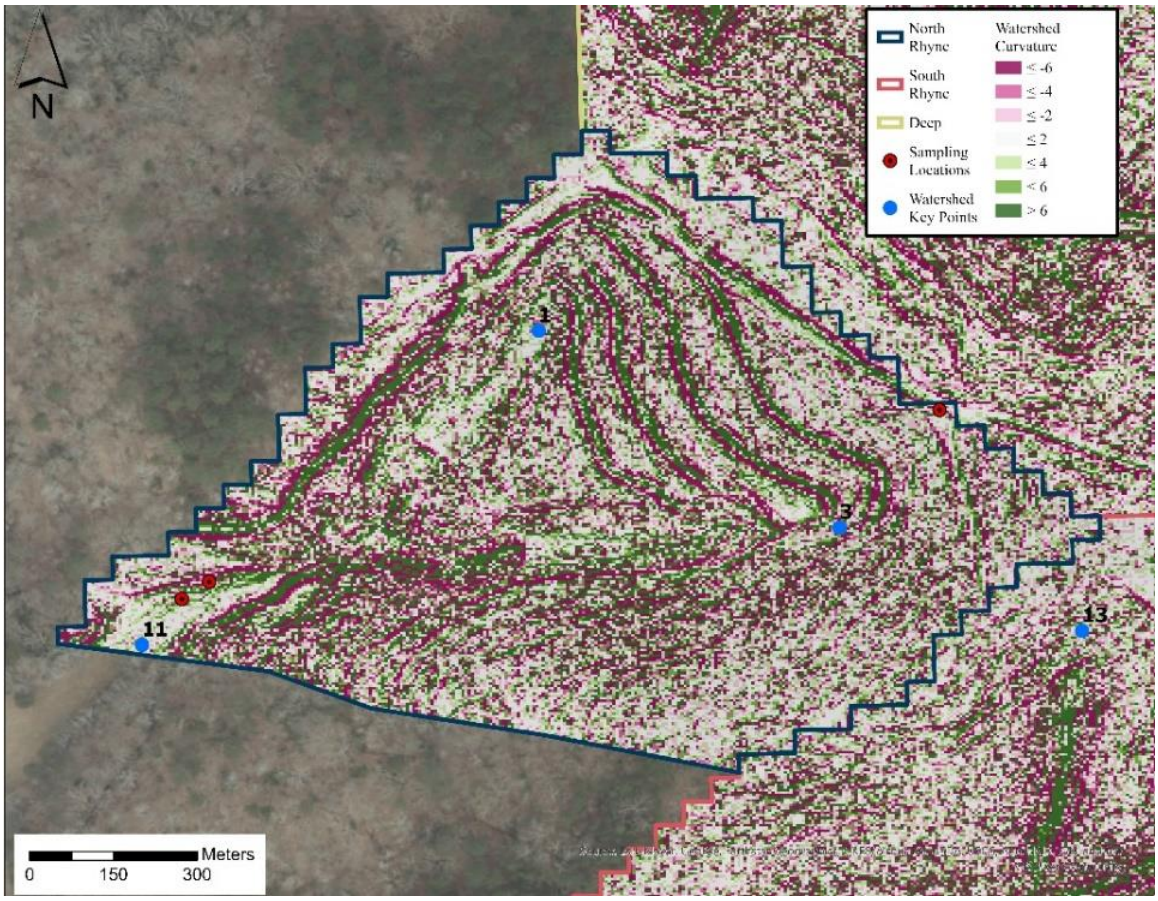

Figure 20. Colorized profile curvature map of the North Rhyne Watershed. The blue dots represent key locations within the watershed. Here, point 1 represents channel head of a tributary to the main stem of the North Rhyne channel. Point 3 represents the channel head, which is where water first originates in the channel. Points 1 and 3 were identified using field reconnaissance. Point 11 represents the outlet of the watershed (LiDAR data acquired from NCID.NC.Gov, accessed 2020).

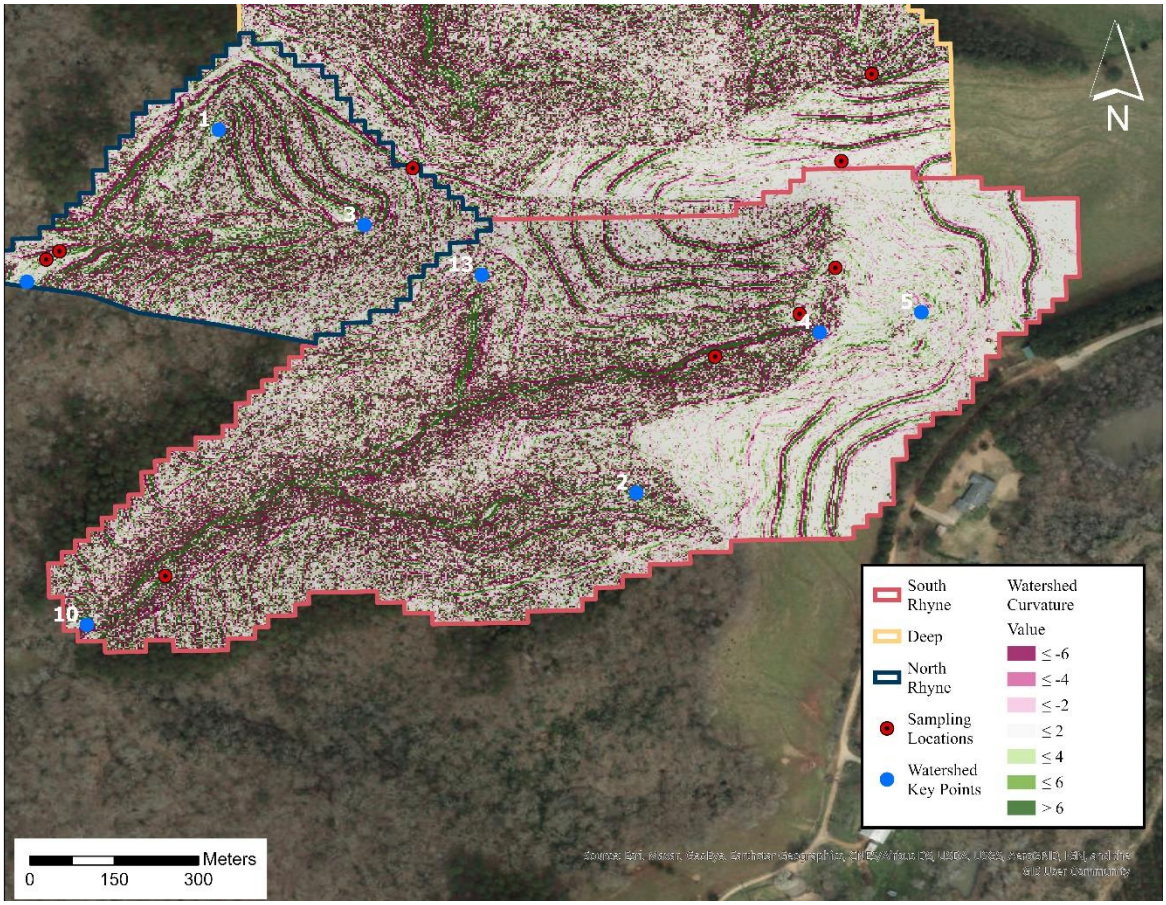

Figure 21. Colorized profile curvature map of the South Rhyne Watershed. The blue dots represent key locations within the watershed. Here, point 4 represents the riprap at the fence delineating the cow pasture, where the main SR-W3-STR channel is located. Point 5 represents the channel head, which is where water first originates in the channel. Points 2 and 13 are channel heads of tributaries leading to the main portion of the South Rhyne. Points 2, 4, and 5 were identified using field reconnaissance. Point 10 represents the outlet of the Duffy watershed (LiDAR data acquired from NCID.NC.Gov, accessed 2020).

The geomorphic shape of each watershed varies. A hypsometric curve graph is typically used to show the proportion of a surface above any elevation, as influenced by the proportional area. Essentially, it is a way of transposing a three-dimensional shape, in this case a watershed, onto a two-dimensional graph (Figure 22). Each watershed was analyzed to their outlet points at the South Fork of the Catawba River, including the Duffy watershed, which is the furthest from this major river. For Figure 22, the extent of the Duffy watershed is defined differently than the other figures showing Duffy. Plotting the locations of the wells in terms of proportional elevation

allows for a visual representation of where they are located along the entire watershed shape. The Duffy wells are plotted at the highest proportional elevation, while the North Rhyne well nest, closest to the South Fork of the Catawba River, is plotted at the lowest elevation. The NR-W4 well nest is located approximately 80% lower in elevation than the DU-W1 triple well nest. The South Rhyne and Deep watersheds, which are situated within and along the cow pasture, are generally situated at intermediate elevations.

The hypsometric curves display divergence in shape in the headwaters area but seem to show more similarities in the lower elevations. This type of geomorphologic analysis further supports the initial assertion that the watersheds are situated at different positions within the landscape; the Duffy watershed sits at overall higher elevations.

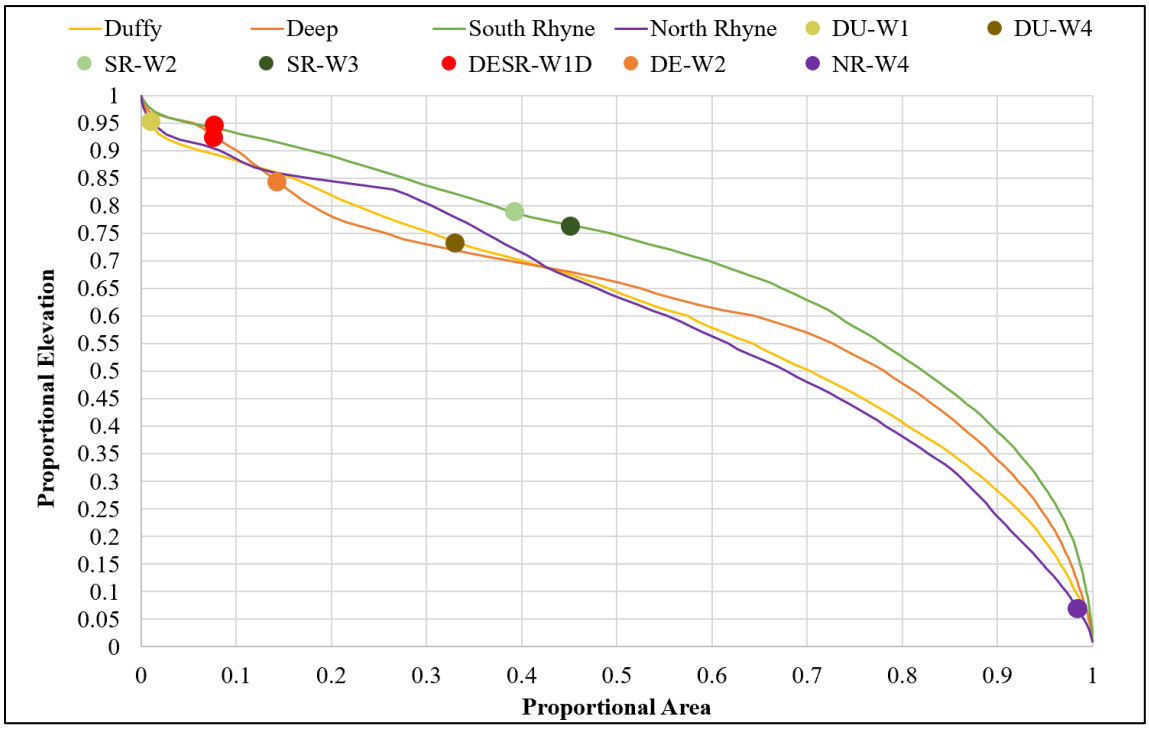

Figure 22. Hypsometric curves of the four watersheds. Proportional elevation is plotted against proportional area. Land elevation of the well nests associated with each watershed are also plotted on the respective curves.

Stream longitudinal profiles are also provided for the four streams (Figure 23). The Duffy stream ranges in elevation from just under 70 to ~75 m, which is the highest elevation of the three streams. The North Rhyne stream channel ranges in elevation from 60 to 64 m, and has the shortest horizontal distance (i.e., shortest channel). The South Rhyne stream has the longest stream channel, over 550 m long, and ranges in elevation from 58 to ~68 m. The Deep stream ranges is the second longest at over 400 m long, with elevations ranging from 58 to 65 m. Figure 5 reaffirms the topographic differences between average stream channel gradients of the watersheds.

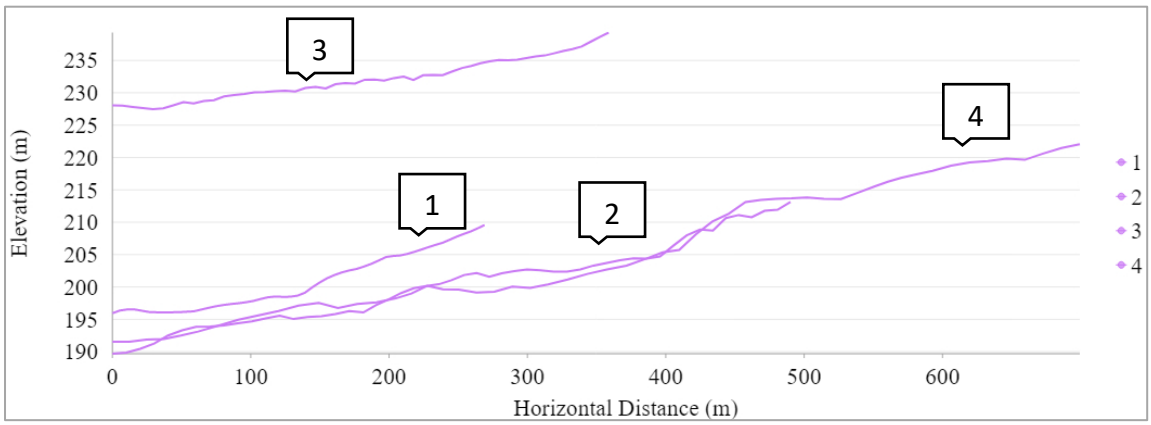

Figure 23. Longitudinal profiles of the four main stream channels located in the four different watersheds of the study. Line one (1) is the North Rhyne stream; line two (2) is Deep; line three (3) is Duffy; and line four (4) is the South Rhyne stream. A horizontal distance of zero (0) indicates the channel outlet, and the largest horizontal distance indicates the channel heads. Elevation is measured as relative to the land surface based on the LiDAR data (LiDAR data acquired from NCID.NC.Gov, accessed 2020).

5.2 Groundwater levels

Overall, water levels in the wells appear to be shallowest (that is, the closest to the land surface or the smallest depth below the land surface) in the late spring-early summer months and deepest (the farthest below the land surface or the largest depth below the land surface) in the late fall-early winter months (Table 5). There is not much variation in groundwater levels over time between the shallow and deep wells (Figure 24).

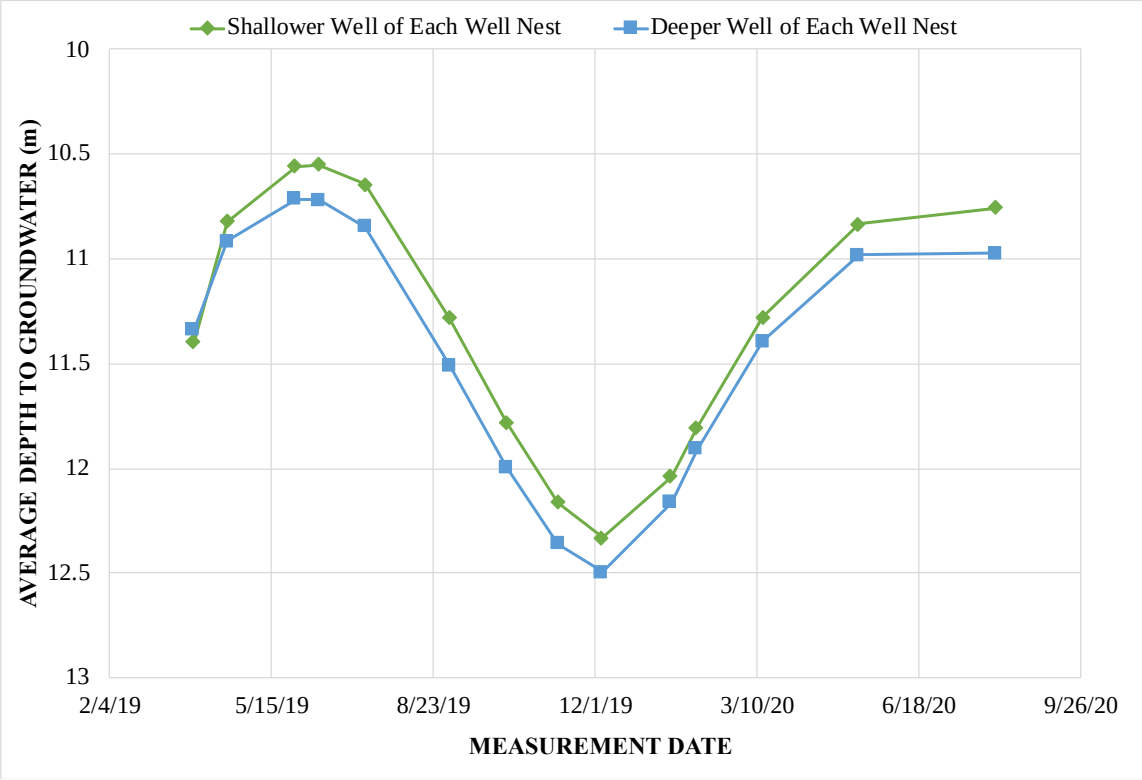

Figure 24. A visualization of groundwater level variations between March 2019 to August 2020 for deep and shallow wells all throughout the Redlair study area. Water levels were shallowest in the late spring-early summer months and deepest in the late fall-winter months.

Table 5. Manual groundwater level (GWL) measurement results from the water level beeper during the year 2020. The DU-W4 wells, which represent the riparian zone of the Duffy watershed, had their deepest GWLs occur in August 2020, but this could be because there was no late fall/early winter 2020 measurement.

Well Name	***Shallowest GWL Date***	***Deepest GWL Date***
DU-W1S	8/5/20	1/17/20
DU-W1M	8/5/20	1/17/20
DU-W1D	8/5/20	1/17/20
DU-W4S	3/14/20	8/5/20
DU-W4D	3/14/20	8/5/20
SR-W-2S	5/13/20	1/17/20
SR-W-2D	5/13/20	1/17/20
SR-W3S	5/13/20	1/17/20
SR-W3D	5/13/20	1/17/20
DESR-W1D	8/5/20	1/17/20

Well Name	*Shallowest GWL Date*	*Deepest GWL Date*
DE-W2S	8/6/20	1/17/20
DE-W2D	8/6/20	1/17/20
DESR-W1D	8/5/20	1/17/20
NR-W4S	5/12/20	1/17/20
NR-W4-D	5/12/20	1/17/20

In the Duffy watershed, there was little variability in groundwater levels for the wells at DU-W1 and DU-W4 well nests (Figure 25-26). Water levels dropped earlier in the riparian wells (DU-W4) than the ridgeline wells (DU-W1) during the study period. DU-W1 nest groundwater levels ranged from 10.5 to 12.5 m below land surface (bls). DU-W4 nest water levels ranged from 1.6 to 3.1 m depth bls. Additionally, the late fall to early winter groundwater level occurred sooner in the riparian than the ridgeline wells.

In the North Rhyne watershed, water levels fluctuated between 3 to 6 m depth bls (Figure 27). The NRDE-W1 ridgeline well nest, which represented the North Rhyne – Deep watershed divide, was dry throughout the study duration.

In the Deep watershed, the mid-slope well (DE-W2) had its spring peak occur earlier than the ridgeline well (DESR-W1). Water levels in DE-W2 well nest ranged from 11.8 to 12.4 m depth bls. The ridgeline well nested pair only had measurable groundwater levels in the deep well (DESR-W1D), while the shallow well (DESR-W1S) was dry throughout the duration of the study.

The South Rhyne watershed had three nested well pairs representing ridgeline, mid-slope, ad riparian topographic positions. The ridgeline well (DESR-W1D) had groundwater levels ranging from 14.6 to 15.3 m depth bls. Located roughly halfway down the hillslope (SR-W2), groundwater levels ranged from 8.0 to 9.0 m depth bls. This pattern is also observable in the South Rhyne watershed, which had its riparian wells (SR-W3) show shallower water levels earlier than the mid-

slope wells and spring peak occur earlier in the riparian and mid-slope well nests than the ridgeline well.

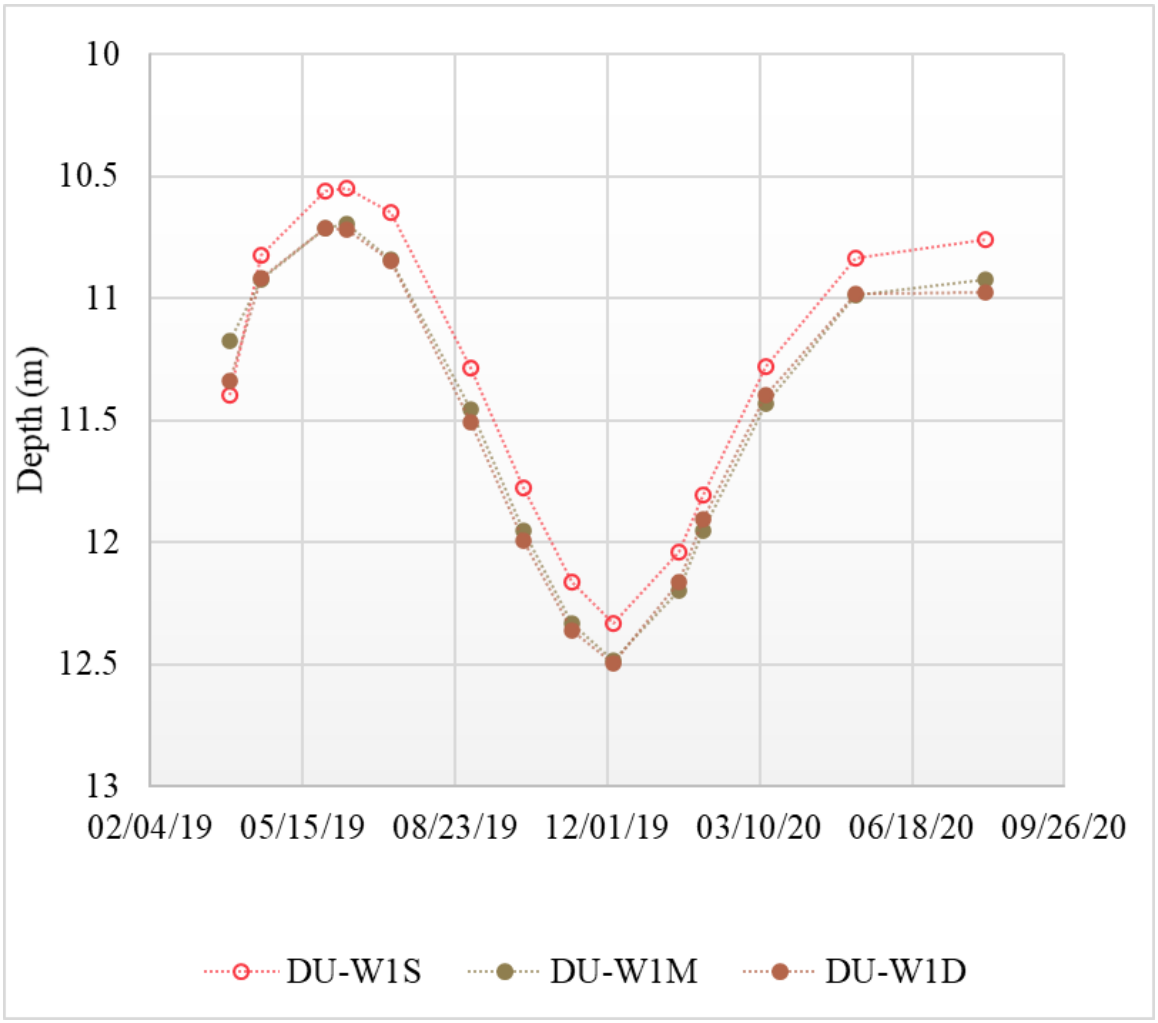

Figure 25. Manual groundwater levels reported as depth below land surface at the DU-W1 triple well nest within the Duffy watershed. This well nest represents ridgeline topography closer to the main watershed divide.

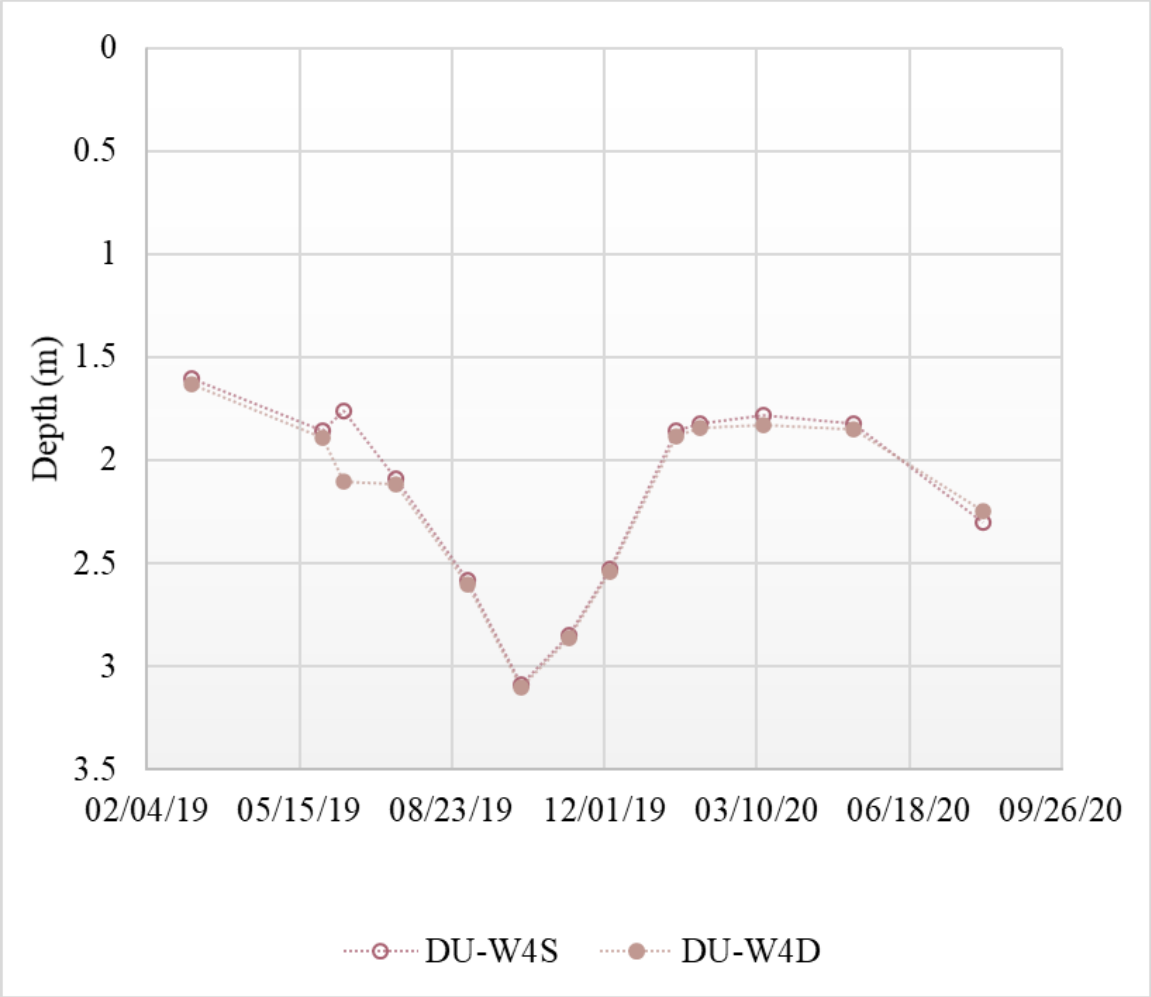

Figure 26. Manual groundwater levels reported as depth below land surface at the DU-W4 double well nest within the Duffy watershed. This well nest represents riparian zone closer to watershed outlet.

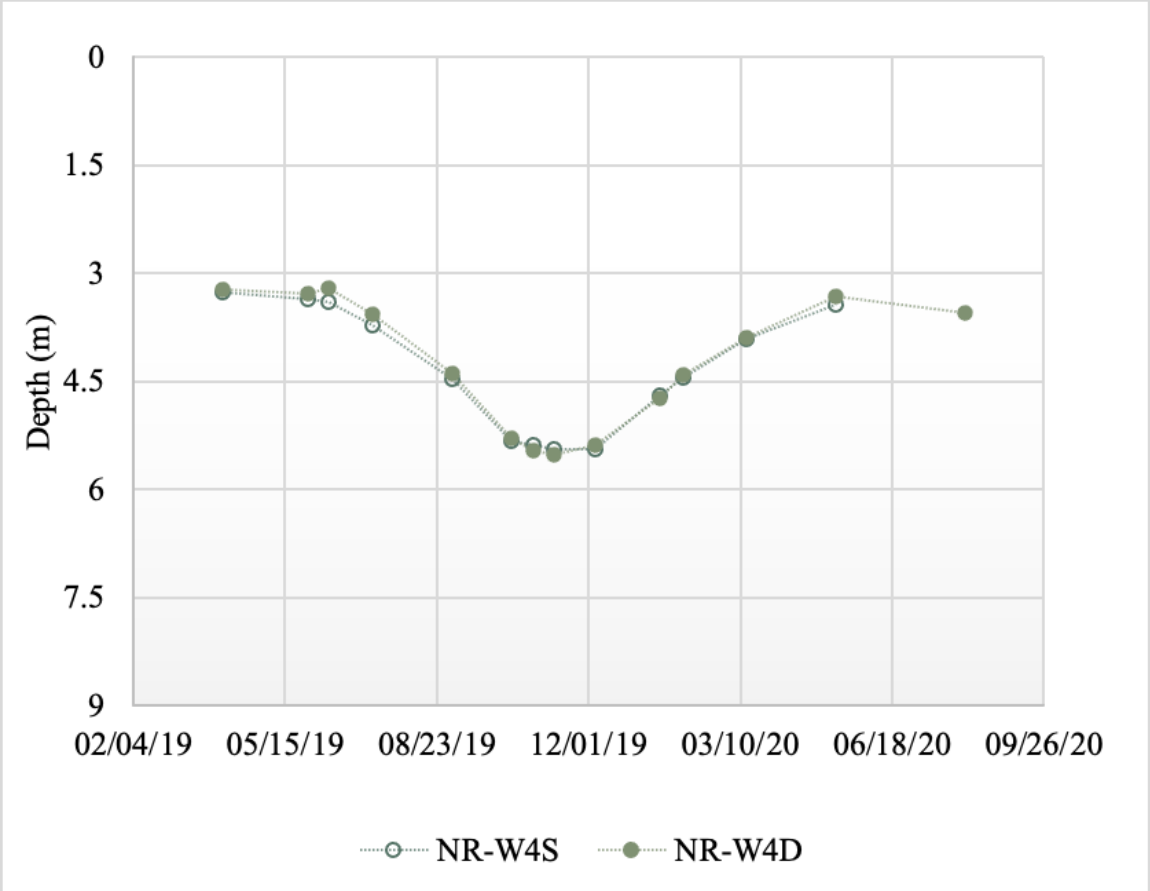

Figure 27. Manual groundwater levels reported as depth below land surface at the North Rhyne watershed.

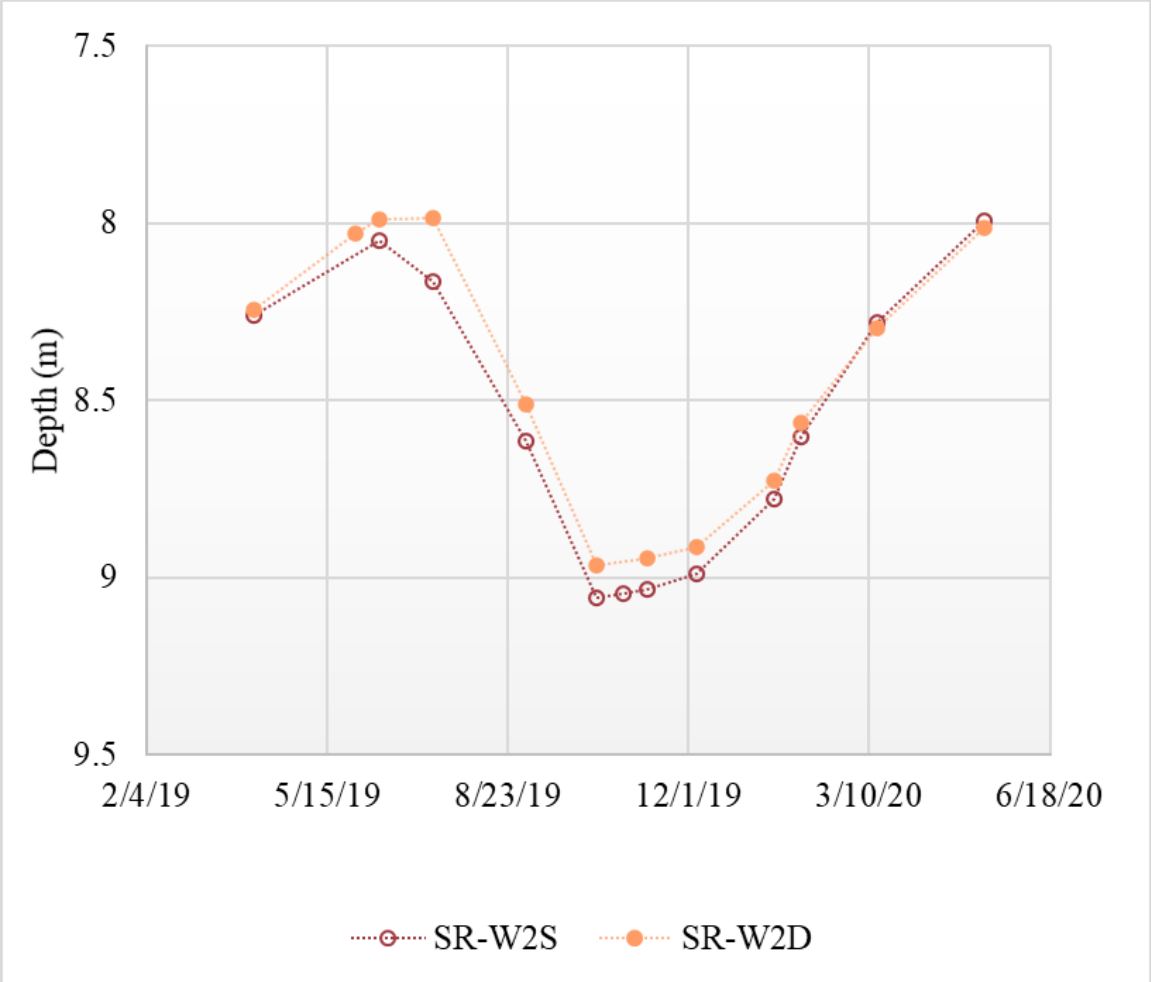

Figure 28. Manual groundwater levels reported as depth below land surface at SR-W2 well nest within the South Rhyne watershed. This well pair is located roughly mid-slope within the watershed.

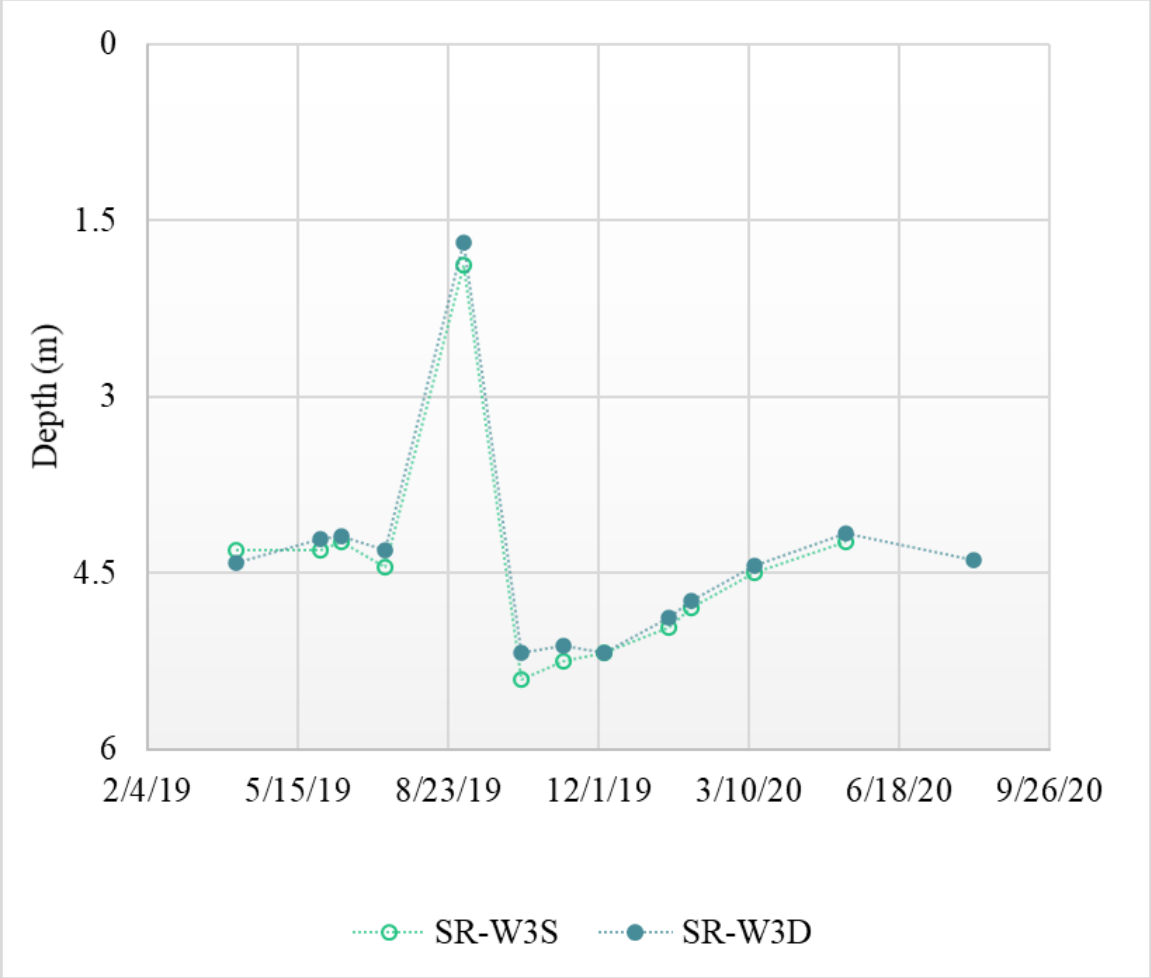

Figure 29. Manual groundwater levels reported as depth below land surface at SR-W3 well nest within the South Rhyne watershed. This well pair is in the riparian zone closer to the watershed outlet.

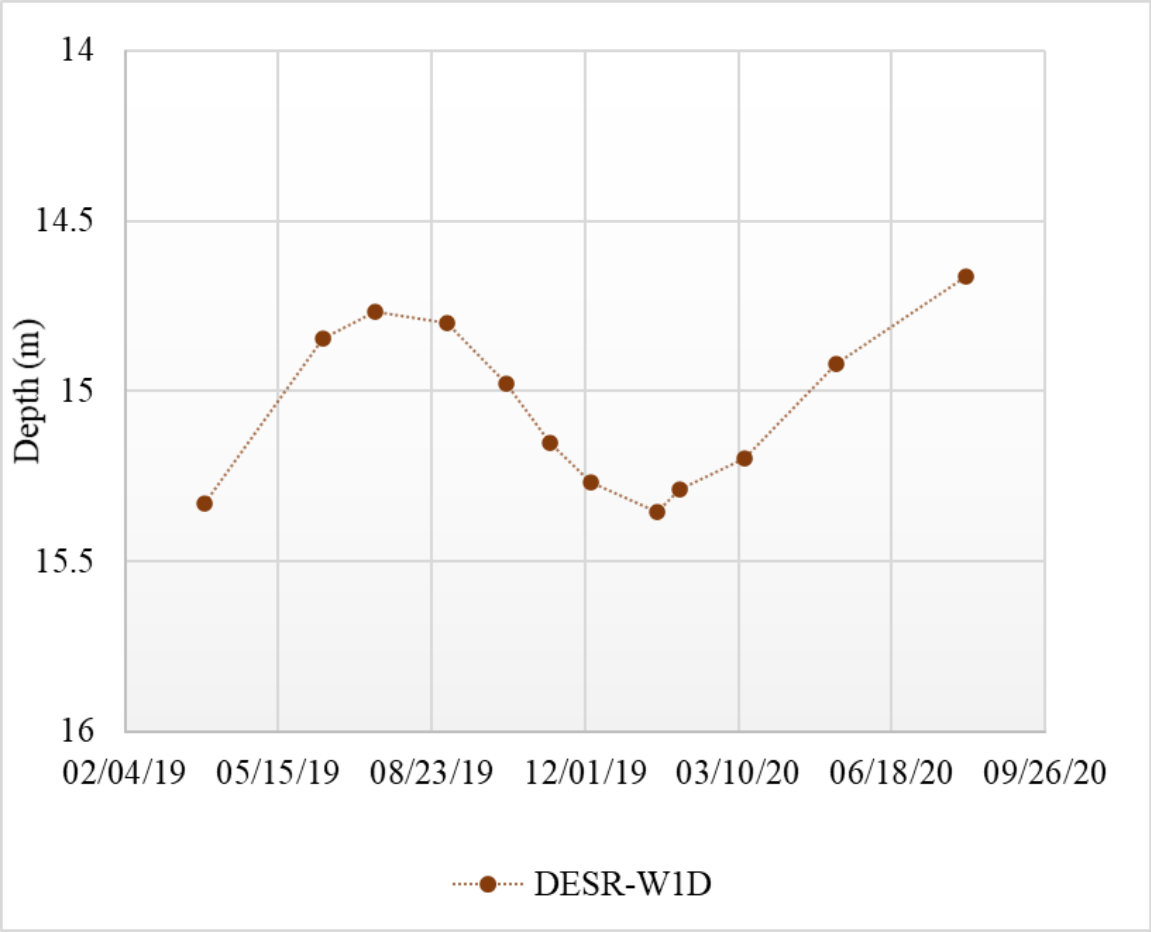

Figure 30. Manual groundwater measurements from the Deep-South Rhyne watershed divide. Although this location was a nested well pair, the shallow well (DESR-W1S) was dry for the duration of the study.

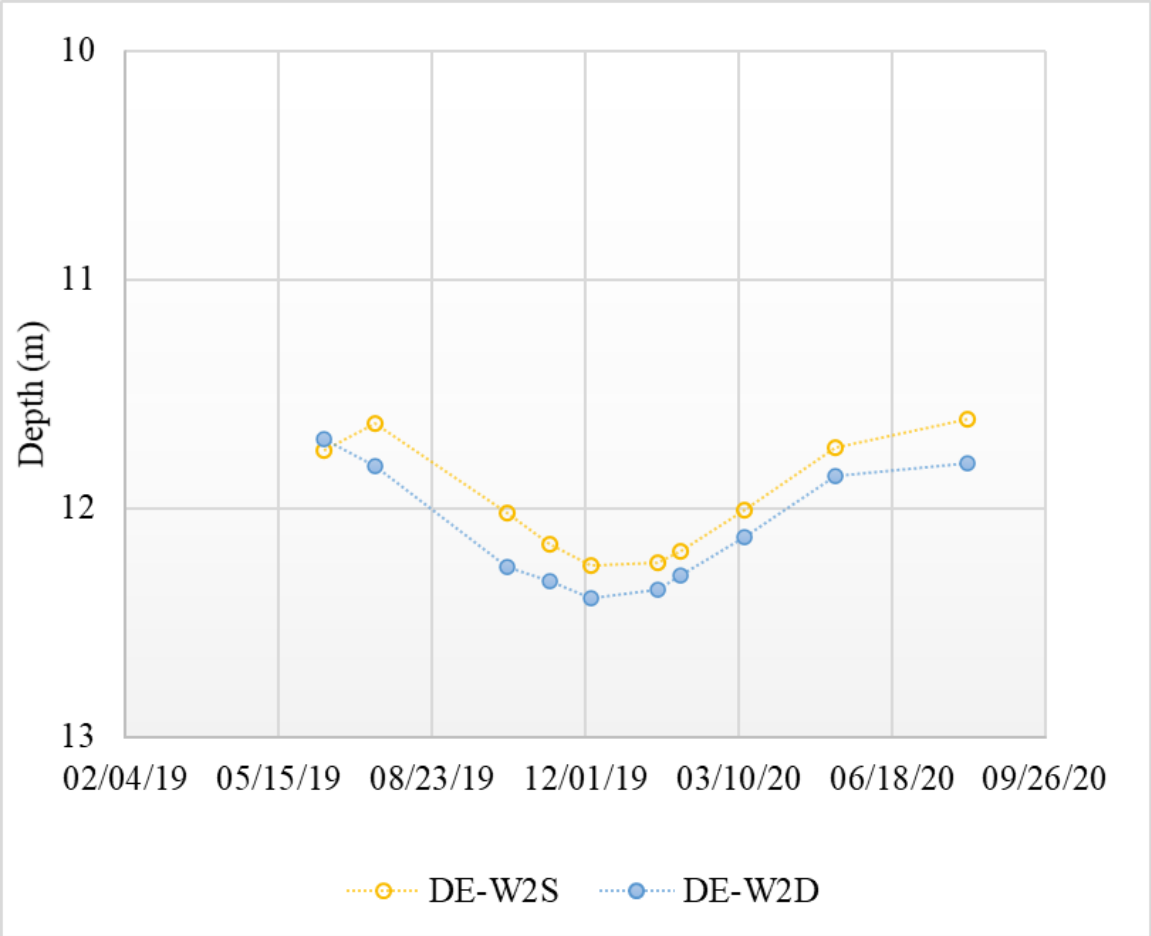

Figure 31. Manual groundwater levels reported as depth below land surface at DE-W2 within the Deep watershed.

The manual groundwater measurements were also compared to the groundwater measurements derived from the HOBO loggers. Manual barometric compensation was calculated using the barometric logger from the Duffy watershed. Even though there are dates in which some of the loggers were not active, the data indicate that the Duffy watershed had its winter minimum earliest, followed by the South Rhyne, North Rhyne, and DESR-W1D (Figure 32). The DESR-W1D logger shows the slowest response to reaching its winter minimum than the other four wells. A full data table with HOBO data has been posted to the Hydroshare online repository (Horgan et al., 2021).

A 1:1 plot shows the degree of variability between HOBO loggers and manual groundwater measurements per well (Figure 33-37). Overall, there was little discrepancy between the two in terms of depth to groundwater, confirming the automated measurements were accurate. The plot that showed the most variability (i.e., strayed from the 1:1 line) was DU-W4S, followed by DESR-W1D.

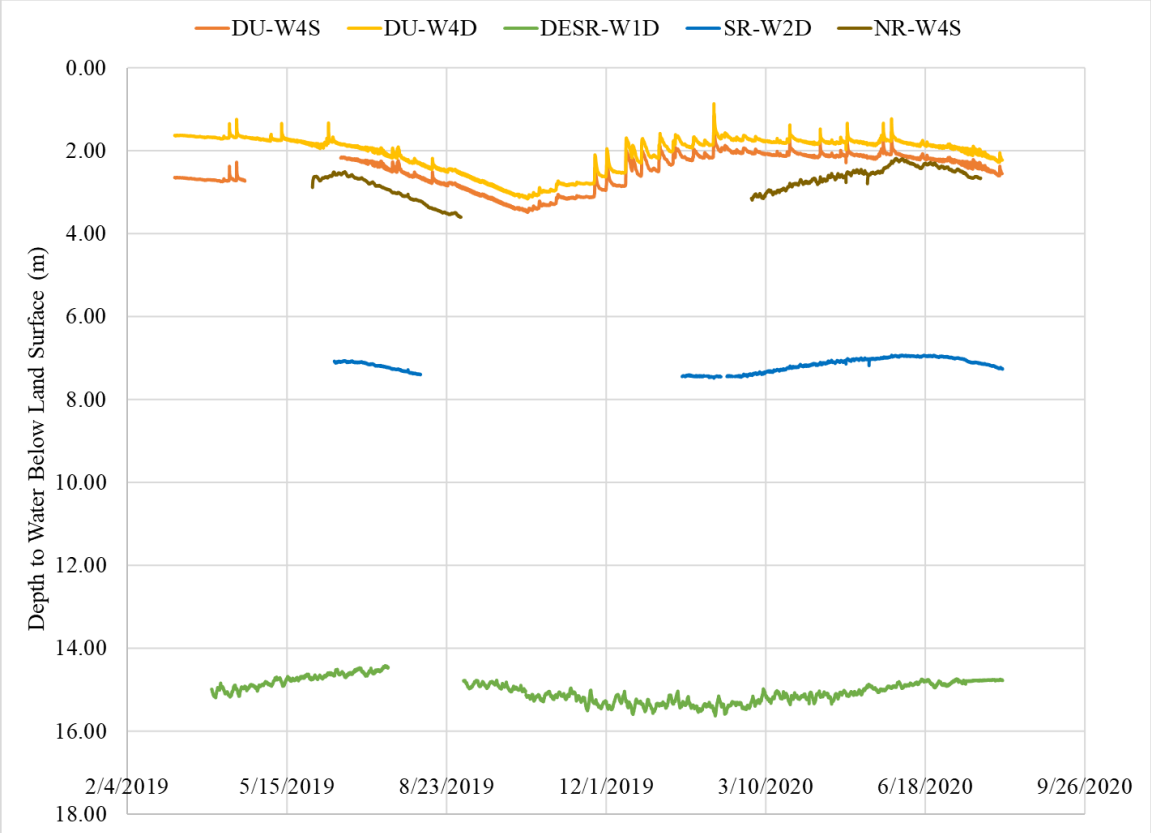

Figure 32. Five HOBO logger plots showing the wells' groundwater levels as depth below land surface. There were some periods where the loggers were not installed in the wells in this graph, or the loggers were dewatered, which are represented as gaps of time.

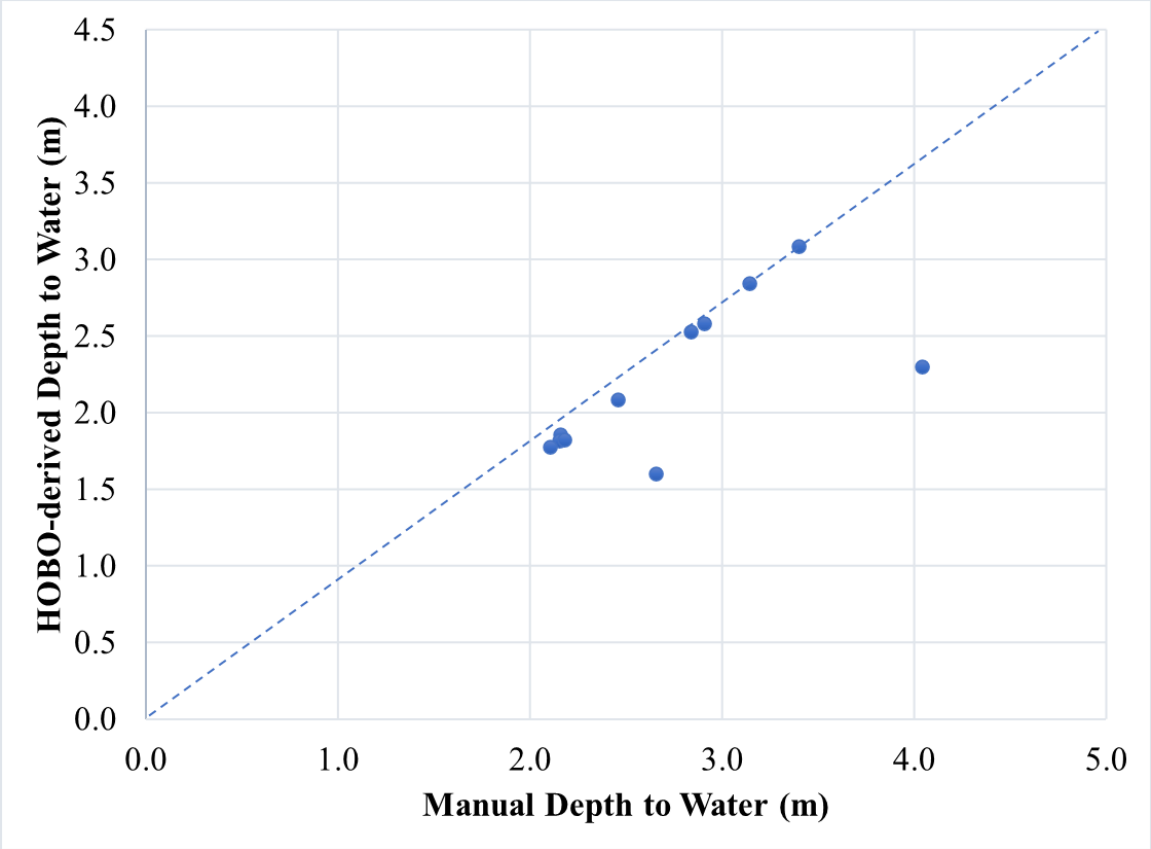

Figure 33. A 1:1 plot of DU-W4S showing the HOBO-derived groundwater levels (GWL) compared to the manually measured GWL. Similar measurements for both techniques plot along the 1:1 line.

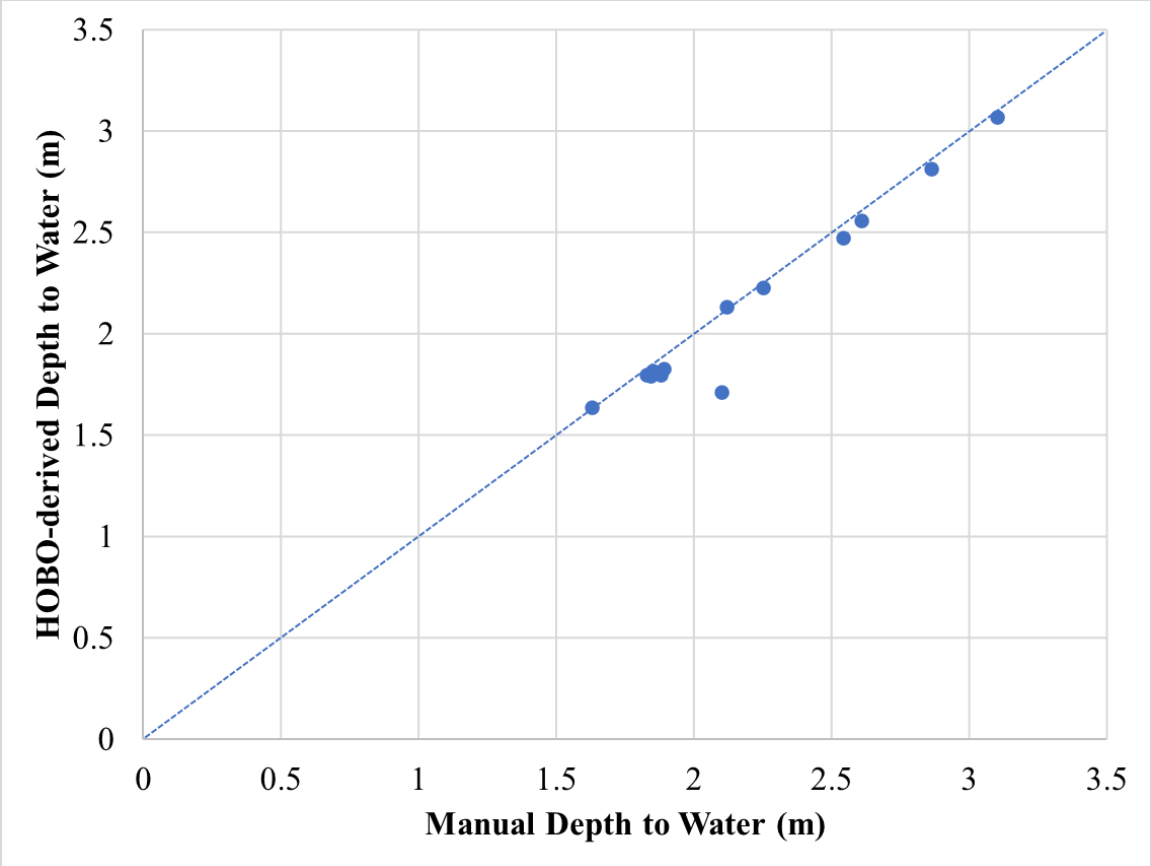

Figure 34. A 1:1 plot of DU-W4D showing the HOBO-derived groundwater levels (GWL) compared to the manually measured GWL. Similar measurements for both techniques plot along the 1:1 line.

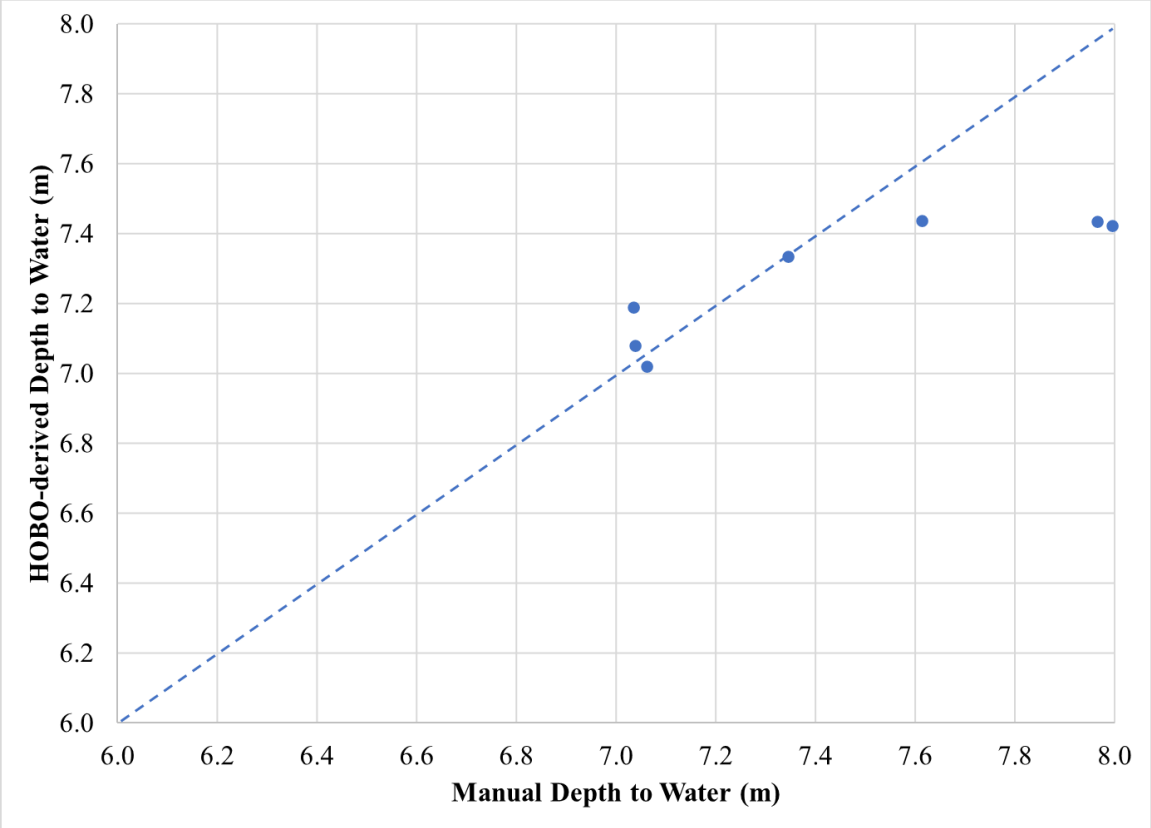

Figure 35. A 1:1 plot of SR-W2D showing the HOBO-derived groundwater levels (GWL) compared to the manually measured GWL. Similar measurements for both techniques plot along the 1:1 line.

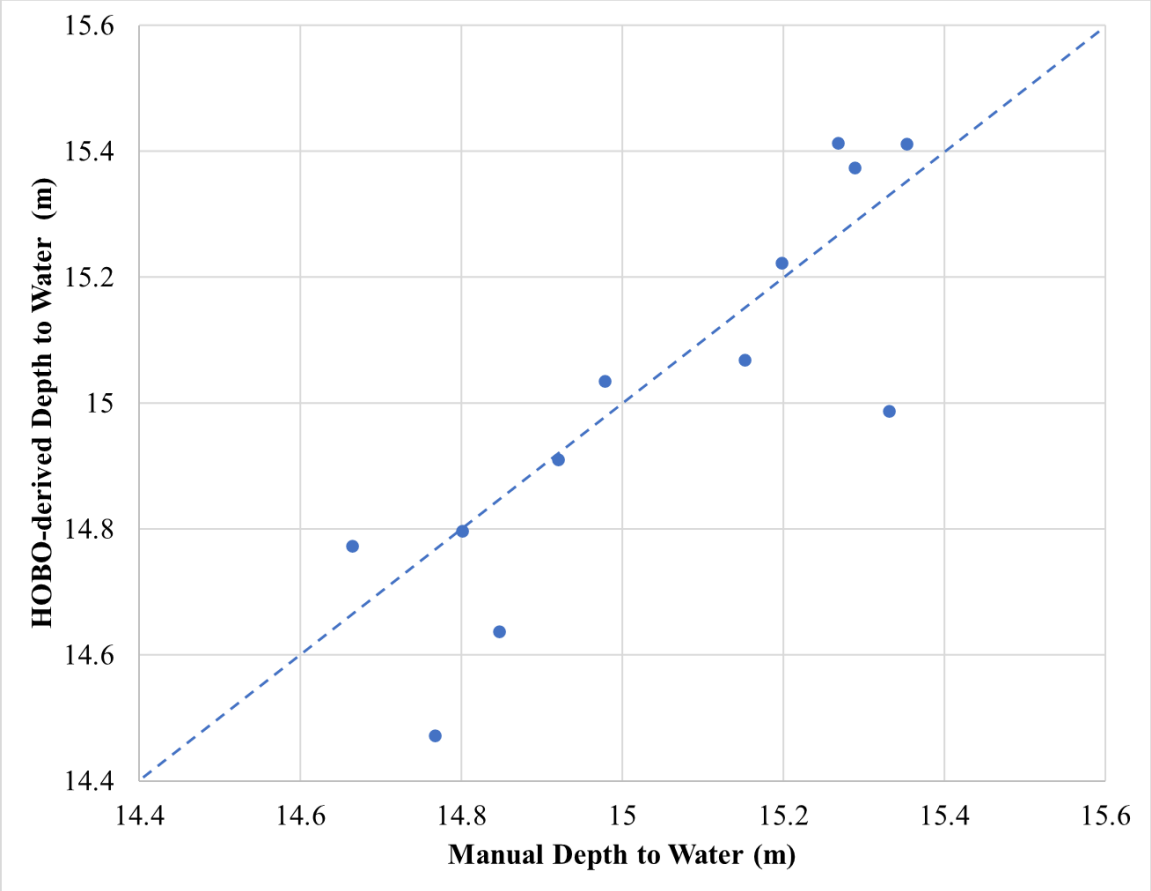

Figure 36**.** A 1:1 plot of DESR-W1D showing the HOBO-derived groundwater levels (GWL) compared to the manually measured GWL. Similar measurements for both techniques plot along the 1:1 line.

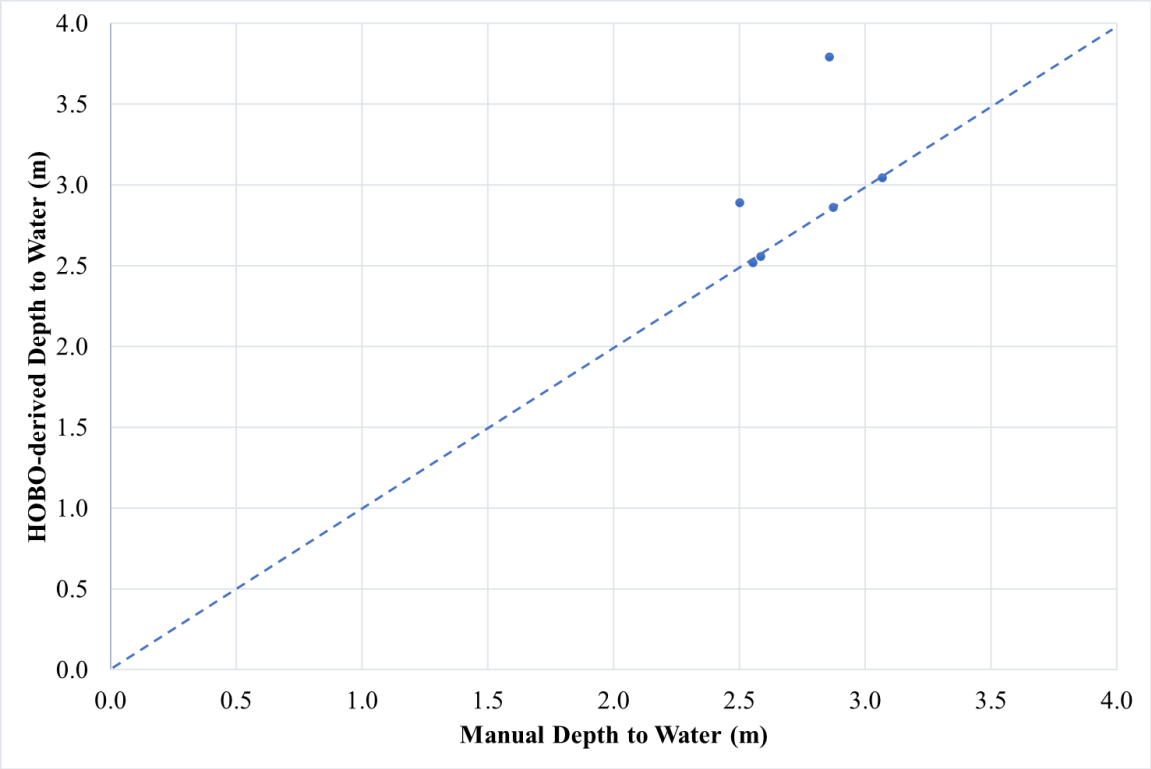

Figure 37. A 1:1 plot of NR-W4S showing the HOBO-derived groundwater levels (GWL) compared to the manually measured GWL. Similar measurements for both techniques plot along the 1:1 line.

The HOBO loggers also continuously recorded groundwater temperatures (Figure 38). The highest temperatures were found in the late summer months July and August. The coldest temperatures were found during the late winter season February and March. SR-W2D exhibited the least variability in groundwater temperatures throughout the study period (Figure 38). SR-W2D had its summer peak having occurred later in the year, around the time that the other four wells were reaching their winter minimums. Overall groundwater temperature did not exceed 16.0ºC at SR-W2D. DU-W4S had the highest groundwater temperatures of the loggers, with a peak temperature of 18.8º C. DESR-W1D also had a HOBO logger, but the temperature data proved to be unreliable for analysis. Manual groundwater temperatures ranged on average from 15.2-19.0ºC. Air temperature for the same period ranged from to -5.9 to 33.5ºC (Figure 39).

Table 6. Average manual groundwater temperatures per well from October 2019-August 2020. Barometric pressure for the same chosen period is provided, too. Of the mean groundwater temperatures, DESR-W1D had the highest and NR-W4S had the lowest.

WELL	AVERAGE TEMPERATURE (ºC)
DU-W1S	17.6
DU-W1M	18.1
DU-W1D	17.6
DU-W4S	17.1
DU-W4D	16.7
SR-W2S	16.7
SRW2D	17.3
SR-W3S	17.0
SR-W3D	16.3
DESR-W1D	19.0
DE-W2S	18.3
DE-W2D	17.9
NR-W4S	15.2
NR-W4D	15.5
DU-W4-BAR	13.9

The North Rhyne stream HOBO logger was also compared to the barometric air temperature from the logger in the Duffy watershed (Figure 40). The North Rhyne stream appears to have slightly cooler temperature in the summer months than the air temperature. In the winter season, the opposite is found, where the stream temperature is slightly warmer than the air temperature. This plot indicates that overall, the air and stream temperatures were mostly aligned with each other.

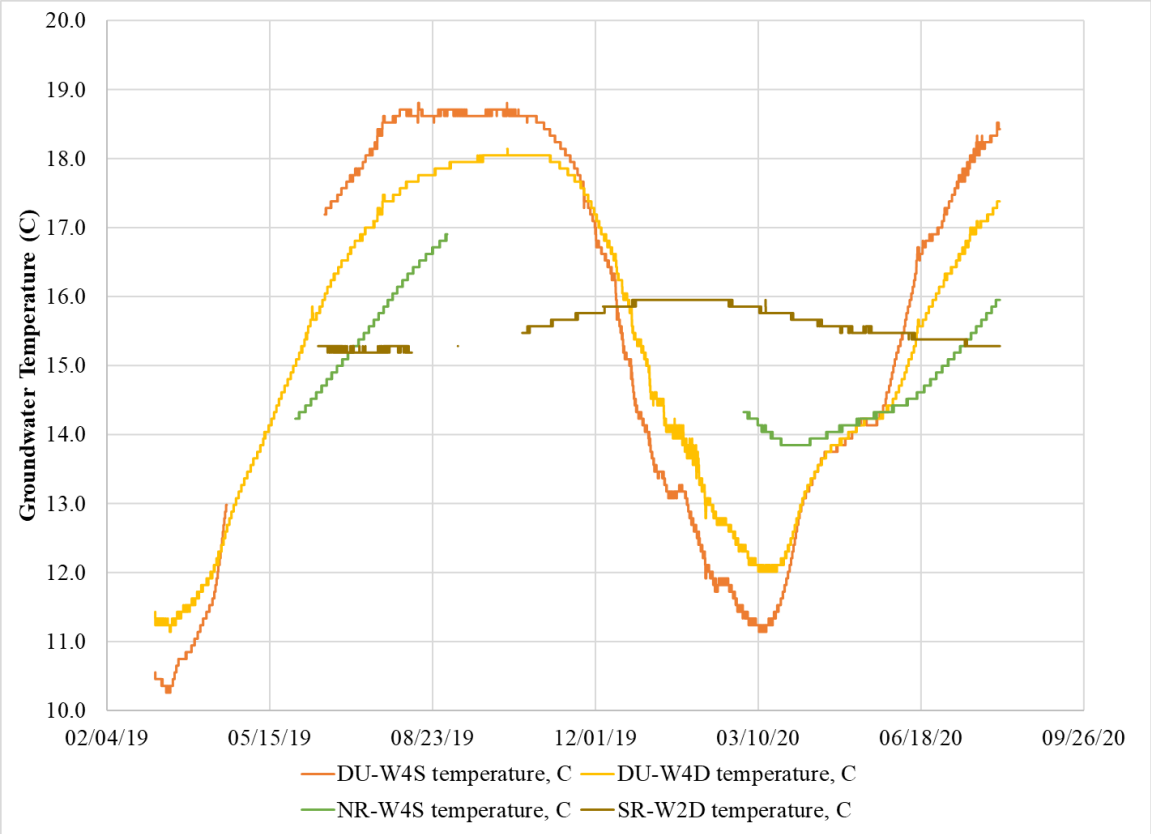

Figure 38. Groundwater HOBO logger temperature time series plot for four loggers. While DESR-W1D also contained a HOBO logger, the temperature data proved to be unreliable.

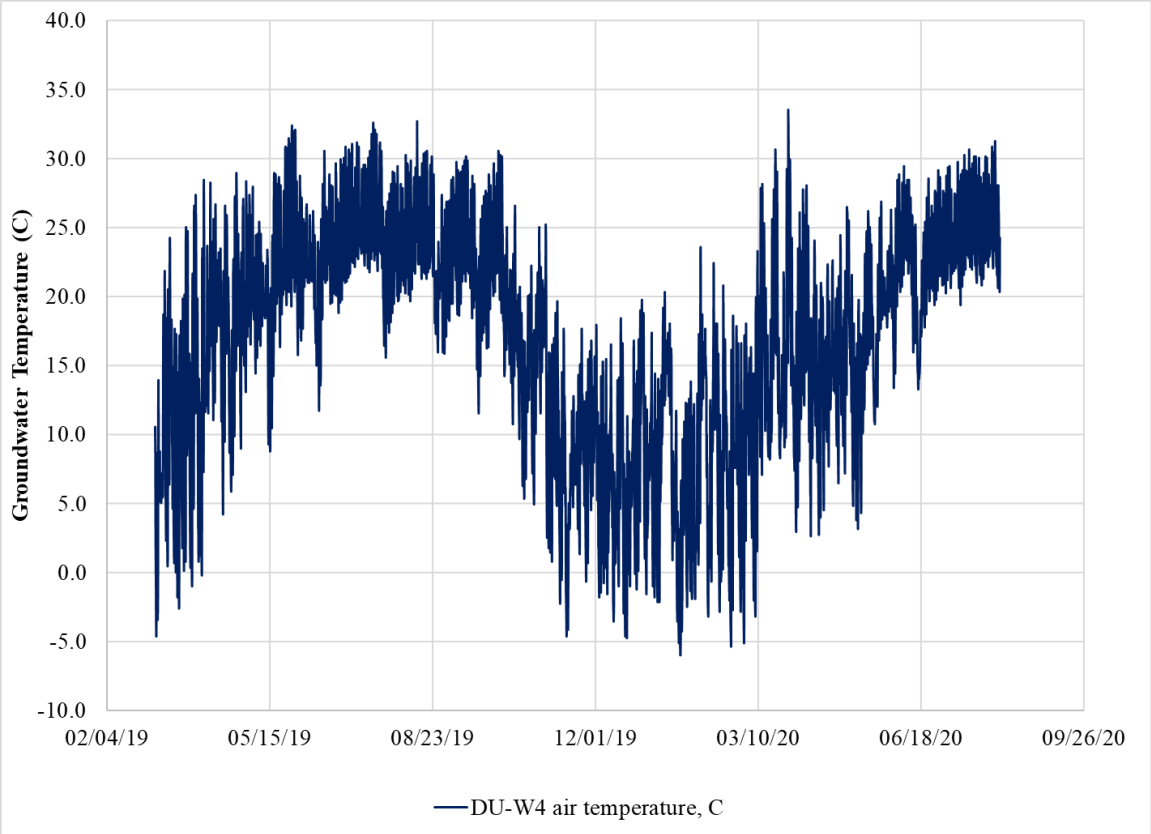

Figure 39. Air temperature time series for the barometric logger located in the riparian zone of the Duffy watershed.

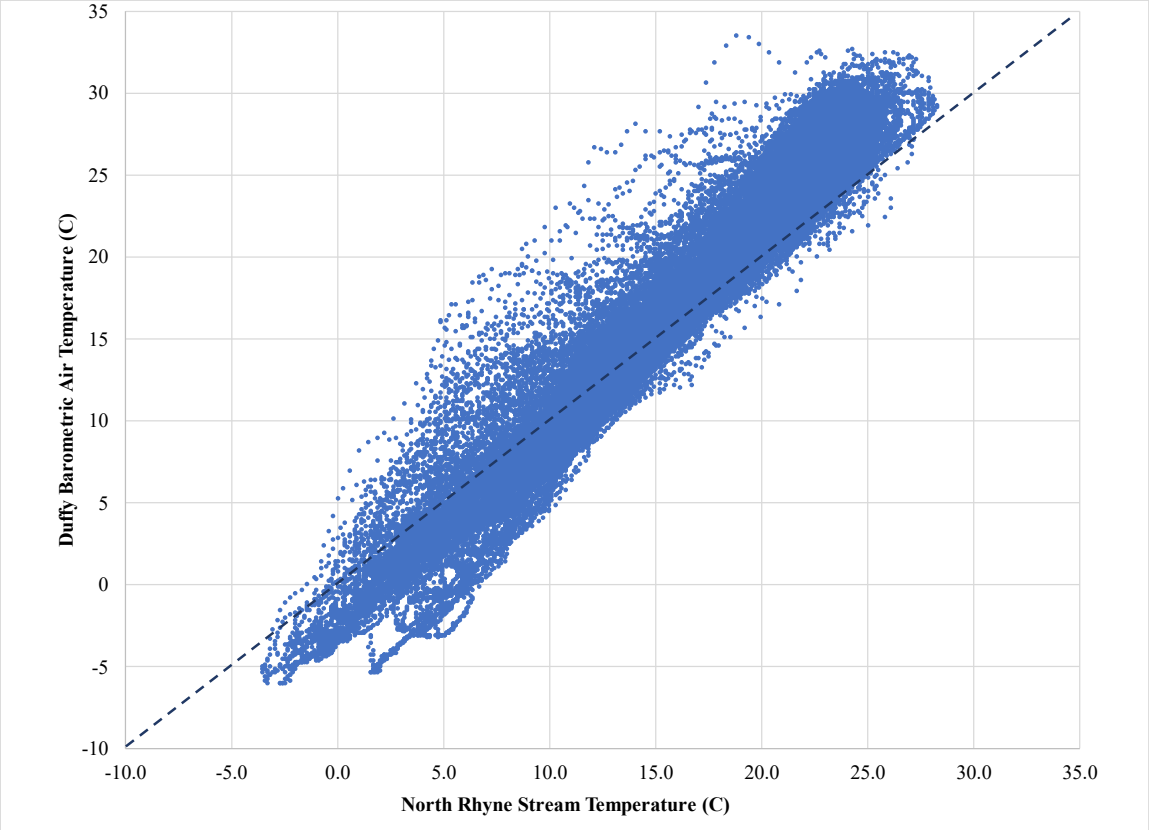

Figure 40. A 1:1 plot of the North Rhyne stream temperature and barometric air temperature based off HOBO loggers. In the summer months, the stream temperature is slightly cooler than the air temperature. However, in the winter the stream temperature is slightly warmer than the air temperature.

5.3 Stream discharge and surface water chemistry

Discharge measurements varied per stream location and the month at which it was sampled (Table 7). Three of the four stream sampling locations were dry for more than 75% of the total sampling events (DU-W4-STR, NR-W4-STR, and SR-W3-STR). The following data are from SR-W3-STRL, which was the fourth stream sampling site added in September 2019 in response to the other locations being overwhelmingly dry. Discharge values for SR-W3-STRL varied significantly from having no flow to a maximum flow rate of 21 L/min. The average rate was 2.1 L/min across the four stream locations. The accuracy of these discharge measurements is reliant upon the assumption that total flow was captured through the rain gutter and into the volumetric beaker.

Field parameters of surface water chemistry varied for temperature (Temp), pH, electrical conductivity (EC), and dissolved oxygen (DO). DU-W4-STR had the highest temperature and EC values, both occurring in August 2020. SR-W3-STRL seemed to have the most neutral pH values year-round, with a maximum pH of 7.7 in July 2019.

Table 7. Discharge measurements for the four stream sampling locations from May 2019 – August 2020 recorded as L/min. For the duration of this project, most of the streams were unable to be sampled and are therefore blacked-out. Asterisk-marked samples are those that had very low flow with poorly measured or unmeasurable flow.

Date		Sampled Y/N	Temp (C)	pH	DO (mg/L)	EC (us/cm)	Discharge Estimate (L/min)
5/30/19							
	DU-W4-STR	Y					
	NR-W4-STR	Y					
	SR-W3-STR	Y					
	SR-W3-STRL	N					
6/13/19							
	DU-W4-STR	Y	19.4	7.0	6.26	83.2	
	NR-W4-STR	Y	16.8	5.8	3.1	65.5	
	SR-W3-STR	N					
	SR-W3-STRL	N					
7/12/19							
	DU-W4-STR	N					No flow
	NR-W4-STR	Y	19.5	6.3	7.3	5.1	0.2
	SR-W3-STR	N					No flow
	SR-W3-STRL	Y	23	7.7	7.2	7.9	No flow
9/2/19							
	DU-W4-STR	N					No flow
	NR-W4-STR	N					No flow
	SR-W3-STR	N					No flow
	SR-W3-STRL	Y	20.5	7.1	7.6	72.3	5.5
10/11/19							
	DU-W4-STR	N					No flow
	NR-W4-STR	N					No flow
	SR-W3-STR	N					No flow
	SR-W3-STRL	Y	16.1	6.6	7.07	64.7	2.1

Date		Sampled Y/N	Temp (C)	pH	DO (mg/L)	EC (us/cm)	Discharge Estimate (L/min)
11/8/19							
	DU-W4-STR	N					No flow
	NR-W4-STR	N					No flow
	SR-W3-STR	N					No flow
	SR-W3-STRL	Y					1.8
12/5/19							
	DU-W4-STR	N					No flow
	NR-W4-STR	N					No flow
	SR-W3-STR	N					No flow
	SR-W3-STRL	Y	8.5	6.2	10.5	49.6	5.5
1/17/20							
	DU-W4-STR	N					No flow
	NR-W4-STR	N					No flow
	SR-W3-STR	Y	7.7	6.2	11.4	41.2	0.18
	SR-W3-STRL	Y	8.1	6.5	11	43.8	11.6
2/2/20							
	DU-W4-STR	Y	9	5.9	9.9	51	2.3*
	NR-W4-STR	N					No flow
	SR-W3-STR	Y	8.8	5.8	6.0	49.1	1.4
	SR-W3-STRL	Y	8.5	6.2	10.9	44.9	16.6
3/14/20							
	DU-W4-STR	Y	14.1	6.4	9.9	78.4	2.3
	NR-W4-STR	N					No flow
	SR-W3-STR	Y	14	6.4	11.3	69.9	2.1
	SR-W3-STRL	Y	13.8	6.4	10.8	52.5	21.5
5/12/20-5/13/20							
	DU-W4-STR	Y	13.1	6.7	9.6	86.2	4.5
	NR-W4-STR	Y	13.1	6.0	4.6	51.9	No flow
	SR-W3-STR	N					No flow
	SR-W3-STRL	Y	11.7	6.5	9.5	52.3	10
8/5/20-8/6/20							
	DU-W4-STR	Y	23.3	7.2	5.1	123.3	No flow
	NR-W4-STR	Y	21.4	6.3	6.7	78.3	No flow
	SR-W3-STR	N					No flow

Date		Sampled Y/N	Temp (C)	pH	DO (mg/L)	EC (us/cm)	Discharge Estimate (L/min)
	SR-W3-STRL	Y	22.4	6.8	7.31	74.6	13.7

5.4 Groundwater chemistry

There were no significant temporal trends in groundwater ion concentrations during the period of the study. The results presented herein define relationships between shallow and deep groundwater. Sodium and calcium were the highest major ions reported on average at each of the four watersheds.

pH levels ranged from 5.5-7.5, although SR-W3S had an anomalously high value of 12.1 in May 2019. Dissolved oxygen ranged from 1.2 mg/L (DE-W2S) to 9.4 mg/L (DESR-W1D). Sodium concentrations ranged from 3.2 mg/L (DU-W1S) to 74.8 mg/L (SR-W3S). Potassium concentrations ranged from 0.6 mg/L (SR-W2S) to 47.4 mg/L (DU-W1M). Magnesium concentrations in wells varied not being present (DU-W1M) to 6.3 mg/L (DU-W1D). Calcium concentrations ranged from 2.5 mg/L (SR-W2S) to 31.0 mg/L (DU-W1D). Chloride concentrations ranged from 2.1 mg/L (DU-W1S and DU-W4D) to 7.3 mg/L (SR-W3S). Chloride concentrations were low overall, generally less than 10% of total ion equivalents, which is expected for these undeveloped watersheds. Nitrate concentrations did vary temporally however, based on the location of the well. Nitrate was generally non-existent at most wells for the duration of the study but did appear in some wells at concentrations up to 4.8 mg/L in NR-W4S and DE-W2D. Phosphate concentrations were found to be like nitrate, and only appearing at higher ranges at specific wells. Sulfate concentrations ranged from 0.9 mg/L (DU-W1D) to 47.3 mg/L (DE-W2S). DU-W1S had an abnormally high sulfate concentration of 197 mg/L, which was not incorporated into the statistical analyses presented in Table 8. Alkalinity, determined by conducting titrations, ranged from 0.4 meq/L (DU-W4S) to 5.1 meq/L (DU-W1M). A complete data table of groundwater chemistry has been posted to the Hydroshare online repository (Horgan et al., 2021).

Table 8. Major chemical properties of the groundwater samples from Redlair per well. SD = standard deviation from the mean. *n* = number of observations. Nitrate concentrations are mg/L as NO_3^-.

Well	Parameter	Minimum	Maximum	Median	Mean	SD	*n*
DU-W1S							
	field pH	6.2	7.5	6.7	6.8	0.6	5
	Dissolved oxygen (mg/L)	3.8	8.1	7.5	6.7	1.7	5
	Sodium (mg/L)	3.2	20.0	4.9	7.7	7.0	5
	Potassium (mg/L)	1.2	2.2	1.7	1.6	0.4	5
	Magnesium (mg/L)	1.2	1.4	1.3	1.3	0.1	5
	Calcium (mg/L)	7.4	16.3	8.2	10.1	3.7	5
	Chloride (mg/L)	2.1	2.2	2.2	2.2	0.1	4
	Nitrate (mg/L)	1.0	1.5	1.2	1.2	0.2	4
	Phosphate (mg/L)	0.0	0.0	0.0	0.0	0.0	4
	Sulfate (mg/L)	1.2	2.1	1.6	1.6	0.5	4
	Alkalinity (meq/L)	0.5	1.5	0.7	0.9	0.4	5
DU-W1M							
	field pH	6.9	11.5	11.3	10.2	2.2	4
	Dissolved oxygen (mg/L)	1.9	5.6	3.9	3.8	1.5	4
	Sodium (mg/L)	28.3	67.0	39.4	46.9	18.7	5
	Potassium (mg/L)	5.2	47.4	23.2	23.4	16.9	5
	Magnesium (mg/L)	0.0	3.8	1.0	1.4	1.6	5
	Calcium (mg/L)	6.6	19.3	13.8	12.2	5.5	5
	Chloride (mg/L)	2.7	7.0	4.0	4.1	1.8	5
	Nitrate (mg/L)	0.2	0.9	0.6	0.6	0.3	5
	Phosphate (mg/L)	0.0	0.7	0.1	0.3	0.3	5
	Sulfate (mg/L)	14.9	39.3	18.6	21.6	10.2	5
	Alkalinity (meq/L)	2.2	5.1	2.7	3.2	1.3	4
DU-W1D							
	field pH	6.7	7.3	6.9	7.0	0.2	4
	Dissolved oxygen (mg/L)	1.8	3.1	2.2	2.3	0.5	4
	Sodium (mg/L)	10.7	13.8	12.0	12.0	1.2	5
	Potassium (mg/L)	2.4	5.7	3.6	4.1	1.3	5
	Magnesium (mg/L)	4.5	6.3	6.2	5.8	0.8	5
	Calcium (mg/L)	22.7	31.0	30.1	28.2	3.4	5
	Chloride (mg/L)	2.7	8.6	6.0	5.4	2.4	5

Well	Parameter	Minimum	Maximum	Median	Mean	SD	*n*
	Nitrate (mg/L)	0.0	0.7	0.3	0.3	0.3	5
	Phosphate (mg/L)	0.0	0.0	0.0	0.0	0.0	5
	Sulfate (mg/L)	0.9	8.0	5.0	4.1	2.9	5
	Alkalinity (meq/L)	2.2	2.6	2.5	2.4	0.2	5
DU-W4S							
	field pH	5.7	6.3	5.9	6.0	0.3	6
	Dissolved oxygen (mg/L)	2.6	5.0	3.6	3.7	0.9	6
	Sodium (mg/L)	4.1	9.2	5.8	6.0	1.7	7
	Potassium (mg/L)	0.9	2.2	1.8	1.6	0.5	7
	Magnesium (mg/L)	2.7	4.4	3.2	3.4	0.7	7
	Calcium (mg/L)	6.5	9.8	7.7	7.9	1.4	7
	Chloride (mg/L)	2.8	3.4	3.1	3.2	0.2	7
	Nitrate (mg/L)	0.0	1.2	0.2	0.3	0.4	7
	Phosphate (mg/L)	0.0	0.1	0.0	0.0	0.1	7
	Sulfate (mg/L)	3.2	19.5	16.1	14.5	5.4	7
	Alkalinity (meq/L)	0.4	0.9	0.6	0.6	0.2	6
DU-W4D							
	field pH	5.8	6.5	6.1	6.1	0.3	6
	Dissolved oxygen (mg/L)	1.8	5.0	3.6	3.5	1.3	6
	Sodium (mg/L)	4.7	8.3	6.1	6.4	1.2	7
	Potassium (mg/L)	1.0	2.0	1.6	1.5	0.4	7
	Magnesium (mg/L)	3.4	4.6	3.8	3.9	0.5	7
	Calcium (mg/L)	8.7	12.4	9.5	9.9	1.2	7
	Chloride (mg/L)	2.1	3.4	3.2	3.0	0.4	7
	Nitrate (mg/L)	0.0	1.0	0.7	0.5	0.5	7
	Phosphate (mg/L)	0.0	0.0	0.0	0.0	0.0	7
	Sulfate (mg/L)	3.0	19.3	13.9	14.0	5.4	7
	Alkalinity (meq/L)	0.5	0.9	0.6	0.7	0.1	6
DESR-W1D							
	field pH	5.9	6.9	6.4	6.4	0.4	4
	Dissolved oxygen (mg/L)	2.8	9.4	6.3	6.2	2.8	4
	Sodium (mg/L)	6.9	8.8	7.3	7.5	0.7	5
	Potassium (mg/L)	1.2	3.1	1.4	2.0	0.9	5
	Magnesium (mg/L)	3.1	5.3	3.2	3.8	1.0	5
	Calcium (mg/L)	5.9	13.8	6.1	8.6	3.7	5

Well	Parameter	Minimum	Maximum	Median	Mean	SD	*n*
	Chloride (mg/L)	3.4	4.4	4.3	4.1	0.4	5
	Nitrate (mg/L)	0.0	3.6	3.1	2.6	1.5	5
	Phosphate (mg/L)	0.0	0.2	0.1	0.1	0.1	5
	Sulfate (mg/L)	1.5	3.8	1.6	2.1	1.0	5
	Alkalinity (meq/L)	0.6	1.4	0.7	0.9	0.3	5
SR-W2S							
	field pH	5.7	6.6	6.0	6.1	0.4	4
	Dissolved oxygen (mg/L)	6.3	7.9	7.3	7.2	0.7	4
	Sodium (mg/L)	14.5	18.1	14.8	15.7	1.6	5
	Potassium (mg/L)	0.6	1.6	0.9	1.0	0.4	5
	Magnesium (mg/L)	0.8	2.0	1.0	1.1	0.5	5
	Calcium (mg/L)	2.5	7.0	3.6	4.2	1.8	5
	Chloride (mg/L)	3.3	4.4	3.4	3.6	0.4	5
	Nitrate (mg/L)	1.3	3.4	2.7	2.6	0.8	5
	Phosphate (mg/L)	0.0	0.1	0.0	0.0	0.0	5
	Sulfate (mg/L)	1.8	4.5	2.7	2.9	1.1	5
	Alkalinity (meq/L)	0.7	0.9	0.7	0.8	0.1	5
SR-W2D							
	field pH	6.4	6.8	6.6	6.6	0.2	4
	Dissolved oxygen (mg/L)	1.8	5.6	4.7	4.2	1.7	4
	Sodium (mg/L)	9.3	11.8	11.1	10.9	1.0	5
	Potassium (mg/L)	1.8	2.7	2.4	2.3	0.3	5
	Magnesium (mg/L)	3.8	4.7	4.3	4.2	0.4	5
	Calcium (mg/L)	11.1	13.6	12.7	12.6	1.0	5
	Chloride (mg/L)	2.9	3.1	3.1	3.0	0.1	5
	Nitrate (mg/L)	0.0	1.5	0.7	0.6	0.6	5
	Phosphate (mg/L)	0.0	0.0	0.0	0.0	0.0	5
	Sulfate (mg/L)	1.6	5.5	2.4	3.2	1.9	5
	Alkalinity (meq/L)	1.2	1.5	1.3	1.3	0.1	5
SR-W3S							
	field pH	7.0	12.1	7.6	8.3	2.1	5
	Dissolved oxygen (mg/L)	2.1	5.8	4.8	4.3	1.5	5
	Sodium (mg/L)	21.3	74.8	23.8	34.9	22.6	5
	Potassium (mg/L)	1.2	2.4	1.8	1.8	0.4	5
	Magnesium (mg/L)	0.2	2.2	1.7	1.4	0.8	5

Well	Parameter	Minimum	Maximum	Median	Mean	SD	*n*
	Calcium (mg/L)	13.8	24.7	21.1	20.3	4.5	5
	Chloride (mg/L)	3.1	7.3	3.3	4.2	1.8	5
	Nitrate (mg/L)	0.0	1.2	0.5	0.5	0.5	5
	Phosphate (mg/L)	0.1	0.3	0.1	0.2	0.1	5
	Sulfate (mg/L)	2.5	30.5	2.7	9.4	12.1	5
	Alkalinity (meq/L)	2.1	3.6	2.1	2.5	0.7	5
SR-W3D							
	field pH	6.1	8.8	7.3	7.4	1.0	5
	Dissolved oxygen (mg/L)	1.4	6.0	2.7	3.6	2.2	5
	Sodium (mg/L)	7.1	24.0	10.5	11.9	7.0	5
	Potassium (mg/L)	1.9	3.6	2.2	2.6	0.9	5
	Magnesium (mg/L)	1.8	5.6	2.8	3.5	1.6	5
	Calcium (mg/L)	9.8	18.2	14.3	14.2	3.7	5
	Chloride (mg/L)	3.0	3.5	3.3	3.2	0.2	5
	Nitrate (mg/L)	0.0	0.8	0.1	0.2	0.3	5
	Phosphate (mg/L)	0.0	0.0	0.0	0.0	0.0	5
	Sulfate (mg/L)	1.4	8.3	5.0	4.9	3.0	5
	Alkalinity (meq/L)	0.9	1.8	1.4	1.3	0.4	5
NR-W4S							
	field pH	5.5	6.7	5.9	6.0	0.5	5
	Dissolved oxygen (mg/L)	4.5	7.8	5.0	5.6	1.5	5
	Sodium (mg/L)	12.4	20.7	16.8	16.7	3.4	5
	Potassium (mg/L)	0.7	1.9	0.9	1.1	0.6	5
	Magnesium (mg/L)	1.2	2.5	1.5	1.7	0.6	5
	Calcium (mg/L)	4.9	9.0	5.2	6.0	2.0	5
	Chloride (mg/L)	2.9	4.7	4.4	4.1	0.8	5
	Nitrate (mg/L)	0.0	4.8	0.3	1.4	2.3	5
	Phosphate (mg/L)	0.0	0.0	0.0	0.0	0.0	5
	Sulfate (mg/L)	1.6	22.1	16.3	14.1	8.8	5
	Alkalinity (meq/L)	0.7	0.8	0.8	0.7	0.1	5
NR-W4D							
	field pH	5.9	6.9	6.4	6.4	0.4	5
	Dissolved oxygen (mg/L)	1.8	6.1	3.8	4.1	1.7	5
	Sodium (mg/L)	6.9	24.0	13.3	14.3	6.2	5

Well	Parameter	Minimum	Maximum	Median	Mean	SD	*n*
	Potassium (mg/L)	1.0	3.9	1.4	2.1	1.3	5
	Magnesium (mg/L)	1.6	4.6	2.8	3.1	1.3	5
	Calcium (mg/L)	6.7	30.2	16.2	17.4	9.1	5
	Chloride (mg/L)	3.9	4.3	4.2	4.1	0.2	5
	Nitrate (mg/L)	0.0	0.1	0.0	0.0	0.1	5
	Phosphate (mg/L)	0.0	0.0	0.0	0.0	0.0	5
	Sulfate (mg/L)	5.8	17.7	14.6	12.3	5.3	5
	Alkalinity (meq/L)	0.5	2.6	1.7	1.5	0.8	5
DE-W2S							
	field pH	6.6	7.0	6.9	6.9	0.2	4
	Dissolved oxygen (mg/L)	1.2	3.5	1.7	2.1	1.2	4
	Sodium (mg/L)	4.4	44.4	8.3	19.1	18.0	5
	Potassium (mg/L)	1.6	5.3	2.8	3.4	1.5	5
	Magnesium (mg/L)	1.8	4.0	3.4	3.2	0.8	5
	Calcium (mg/L)	4.0	13.7	6.8	8.0	3.8	5
	Chloride (mg/L)	2.4	3.8	3.1	3.0	0.6	5
	Nitrate (mg/L)	0.1	2.3	0.6	0.8	0.8	5
	Phosphate (mg/L)	0.0	3.0	1.3	1.2	1.3	5
	Sulfate (mg/L)	2.6	47.3	5.1	16.5	19.5	5
	Alkalinity (meq/L)	1.0	1.3	1.2	1.1	0.1	5
DE-W2D							
	field pH	6.1	6.2	6.1	6.2	0.0	4
	Dissolved oxygen (mg/L)	2.2	7.1	4.1	4.4	2.1	4
	Sodium (mg/L)	4.5	8.6	6.8	6.6	1.5	5
	Potassium (mg/L)	1.7	5.0	2.5	2.9	1.4	5
	Magnesium (mg/L)	2.5	3.3	2.7	2.8	0.3	5
	Calcium (mg/L)	5.8	9.0	6.8	7.3	1.5	5
	Chloride (mg/L)	2.6	4.0	3.3	3.3	0.5	5
	Nitrate (mg/L)	0.1	4.8	4.1	2.7	2.4	5
	Phosphate (mg/L)	0.0	2.4	0.2	0.7	1.0	5
	Sulfate (mg/L)	1.0	16.7	1.6	5.0	6.7	5
	Alkalinity (meq/L)	0.6	0.8	0.7	0.7	0.1	5

Alkalinity concentrations, which are linked to pH, ranged from 0.4 to 3.6 meq/L (Figure 41). Nitrate concentrations in the pasture wells – located in the South Rhyne and Deep watersheds

– were higher than the non-agricultural wells (Figure 42). Overall, nitrate concentrations ranged from below detection to 4.8 mg/L. Chloride and fluoride concentrations were relatively low at all wells in the study area from 2.1-6.5 mg/L and 0.07-0.58 mg/L, respectively (Figure 43-44). This does not include an anomalous chloride concentration found at DU-W1M (7.0 mg/L).

Phosphate concentrations were also generally low (<0.2 mg/L), except for those wells located in the cow pasture (SR-W3 [0-0.3 mg/L] and DE-W2 [0-3.2 mg/L]; Figure 45).

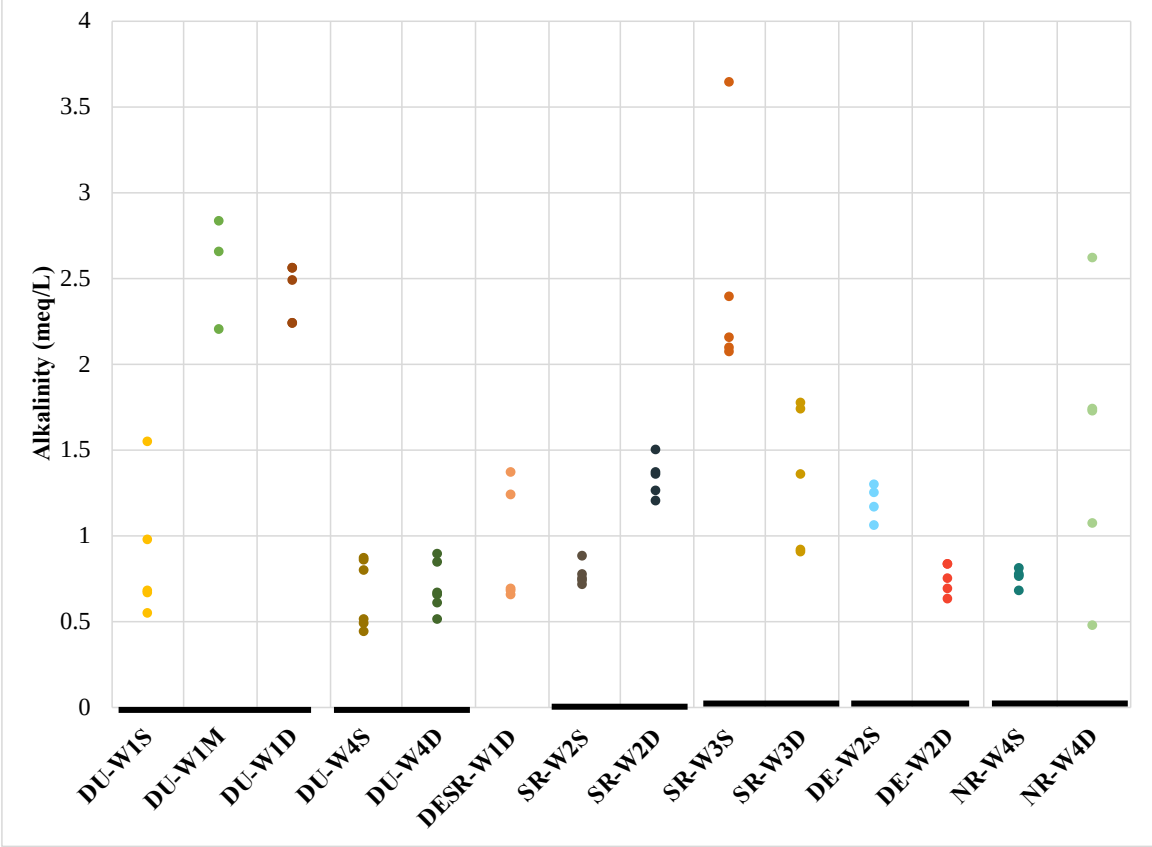

Figure 41**.** Alkalinity concentrations per well. DU-W4S had the lowest alkalinity concentration while SR-W3S had the highest.

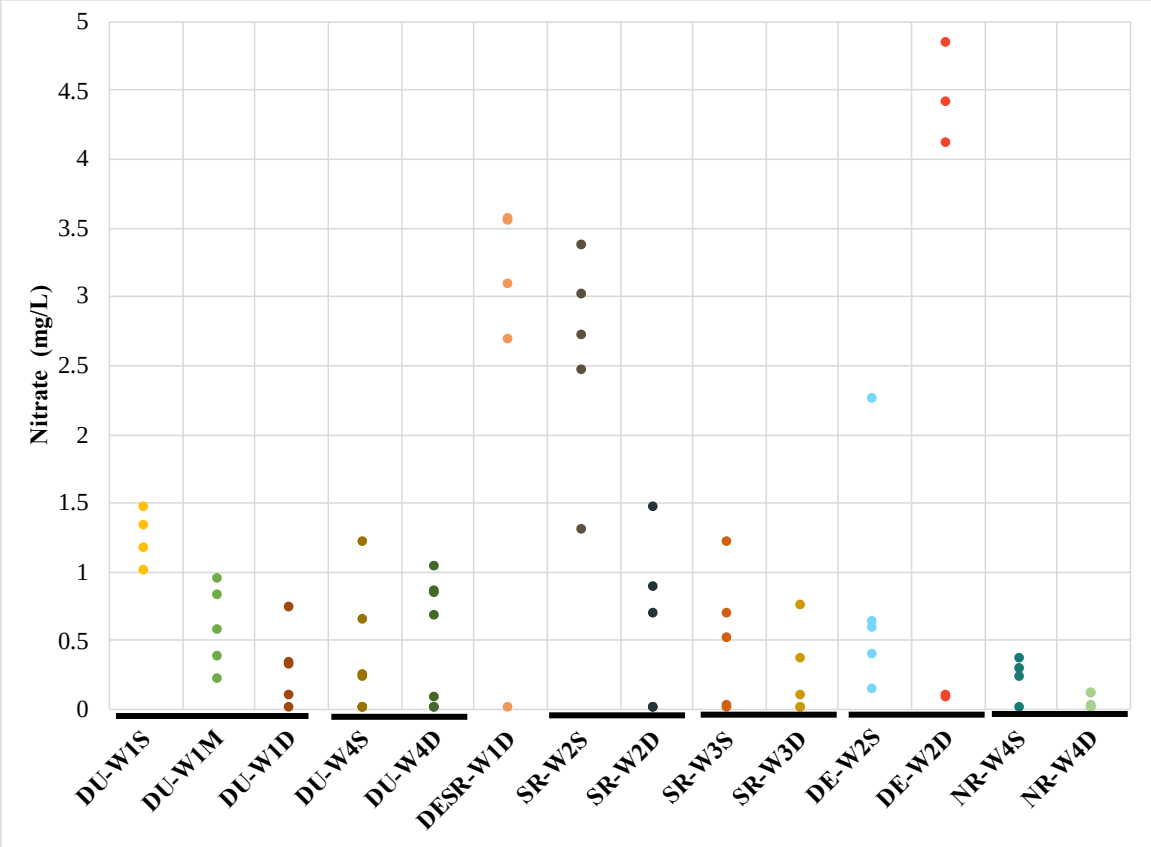

Figure 42. Nitrate (NO_3^-) concentrations per well. DE-W2D had the highest overall nitrate concentrations while NR-W4D had the lowest.

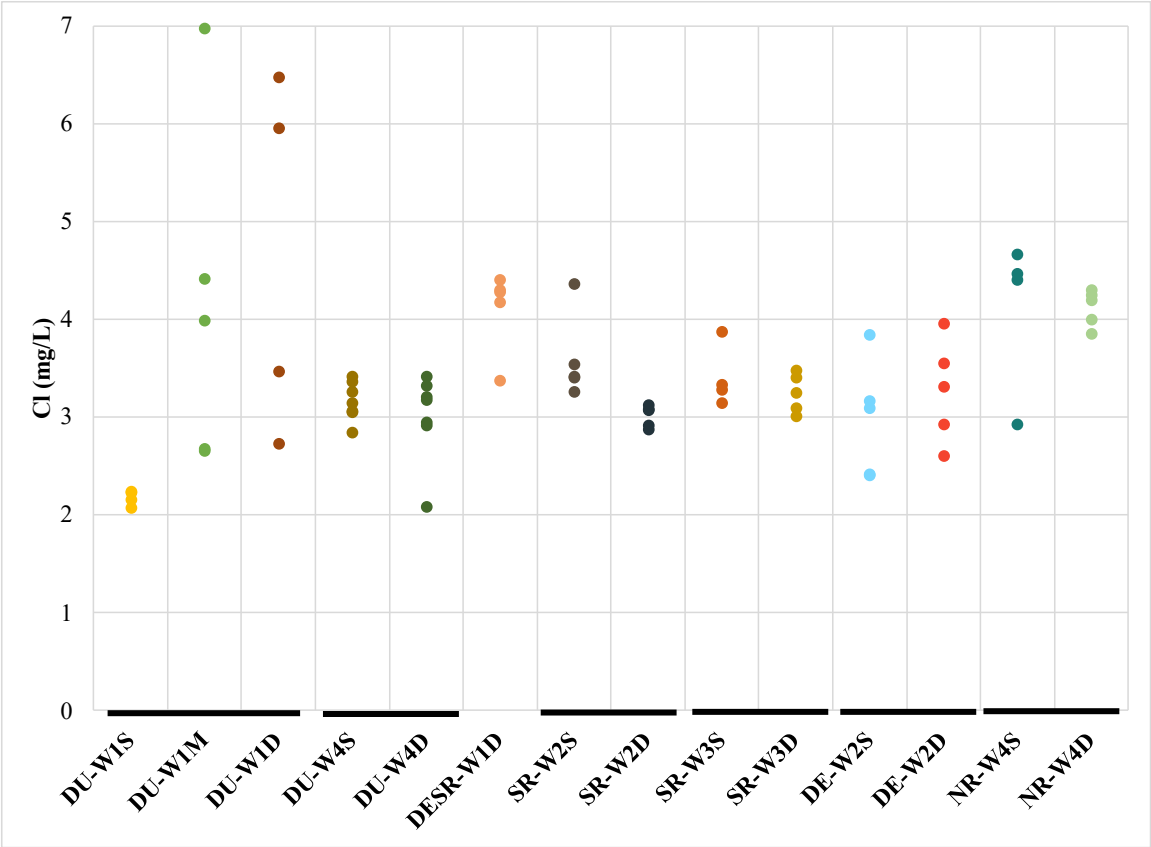

Figure 43. Chloride concentrations per well. DU-W1M had the highest chloride concentration during the study period.

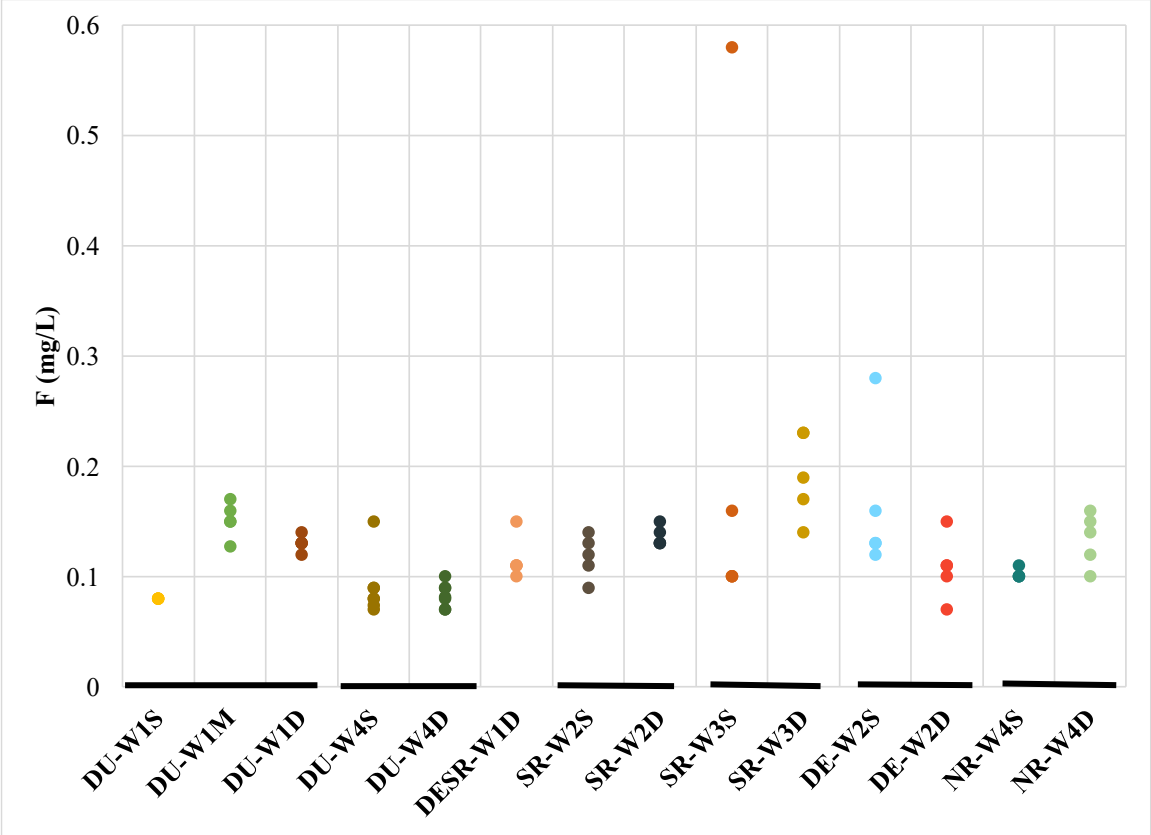

Figure 44. Fluoride concentrations per well. SR-W3S had the overall highest fluoride concentration at 0.6 mg/L in May 2019. DU-W1S had fluoride concentrations of 0.1 mg/L for all sampling events in which fluoride was analyzed.

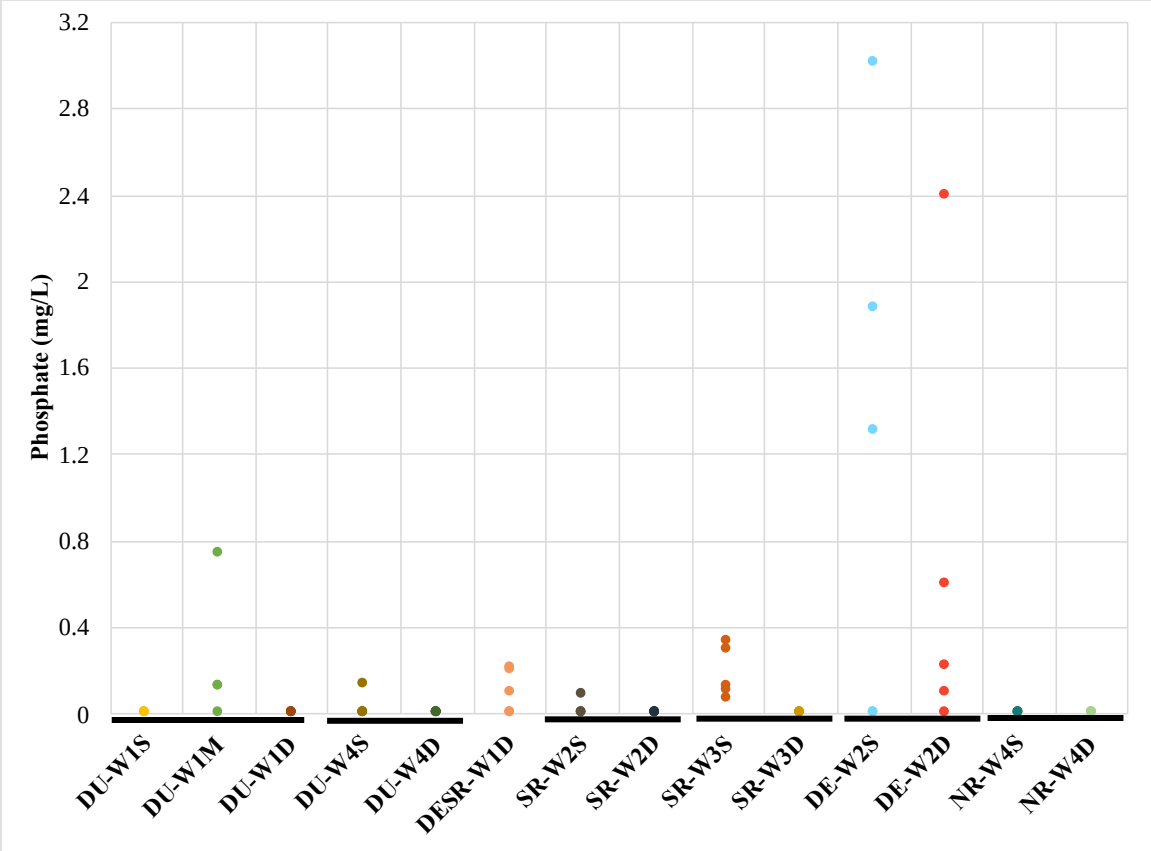

Figure 45. Phosphate concentrations per well. Phosphate concentrations were overall low at the wells, aside from some of the wells located in the pasture (DE-W2 and SR-W3).

Magnesium did not exhibit spatial variability between the watersheds, with concentrations ranging from 0.1 to 6.3 mg/L (Figure 46). Potassium concentrations ranged from 0.7 to 4.6 mg/L, aside from at DU-W1M, where values were greater than 5.0 mg/L (Figure 47). The deeper wells largely had higher concentrations of potassium than the shallow wells. Like potassium, the deep wells also had higher concentrations of calcium than the shallow wells. Calcium concentrations ranged from 2.5 to 31.0 mg/L (Figure 48). Sodium concentrations were generally higher in shallow wells, with SR-W3S having the highest concentration of 74.8 mg/L. Calcium and sodium are important indicators of the degree of weathered rock. Thus, it is important to also consider the calcium/sodium molar ratio (Figure 50). The calcium-sodium molar ratio (Ca/Na) can be used as a proxy to infer the degree of weathered subsurface material. A two-sample t-test was used to analyze for differences in Ca/Na molar ratios between the shallow wells and deep wells. The two-tailed test

was significant at the $p<0.0005$ level, indicating a significant difference in Ca/Na ratios for shallow versus deep groundwater.

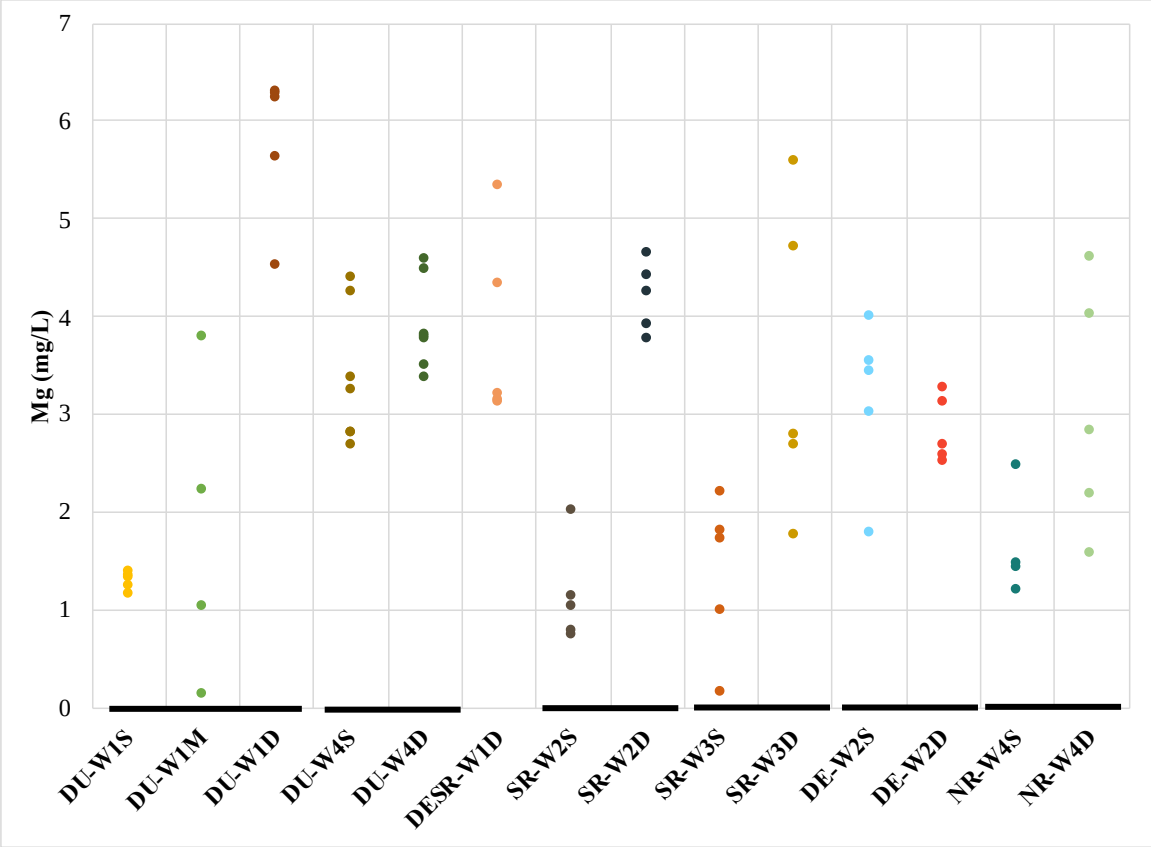

Figure 46. Magnesium concentrations per well. Magnesium varied widely both among the different watersheds and each nest well pair. However, it seems that the deeper well in each well cluster had higher magnesium concentrations than the shallow well from the same cluster.

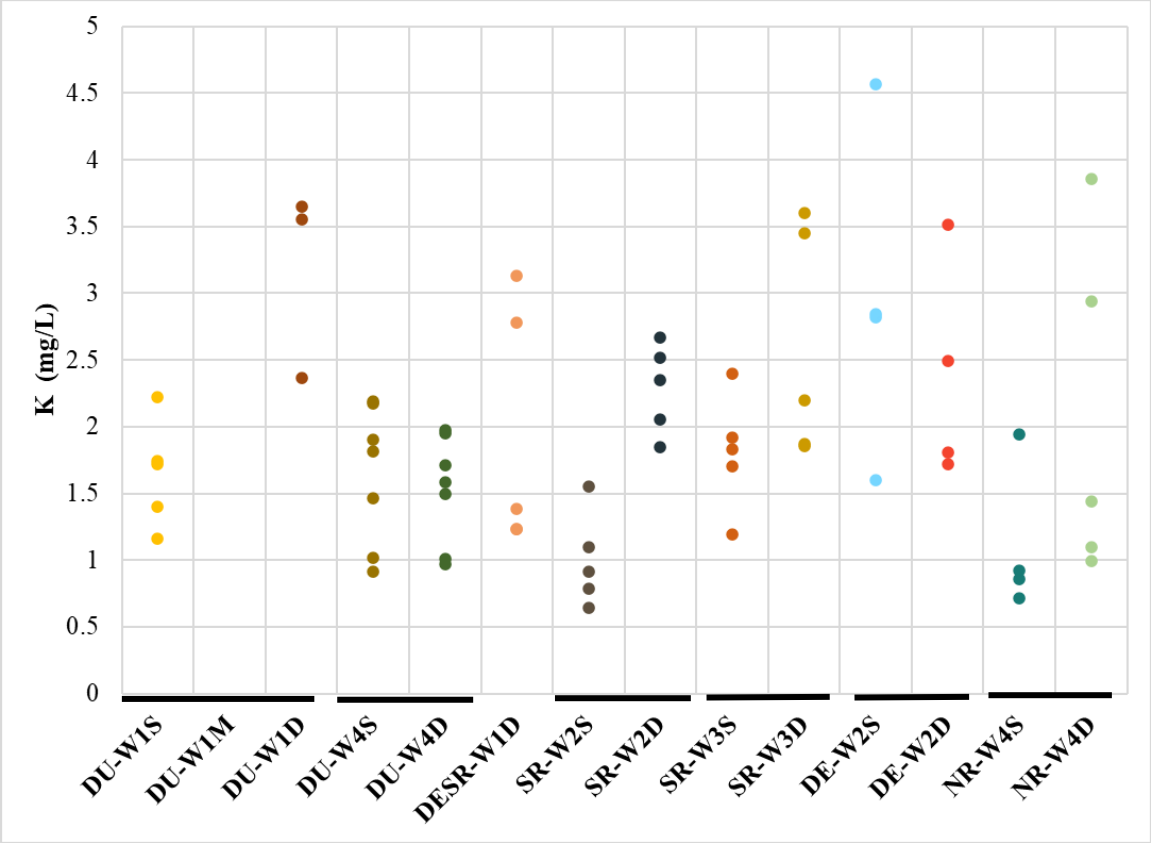

Figure 47. Potassium concentrations per well. DU-W1M, which represents an intermediate depth in the well nest triplet, had the highest concentration and range of potassium concentrations (>5 mg/L, not included). The other wells did not exhibit nearly as much variability.

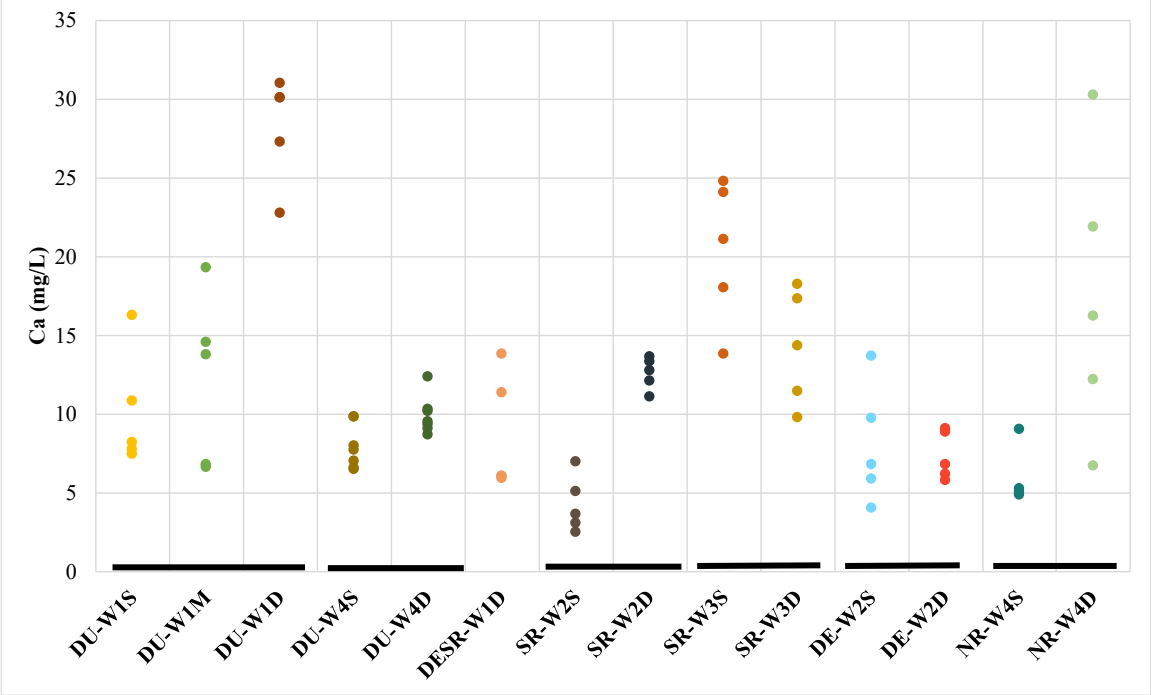

Figure 48. Calcium concentrations per well. The deeper wells tended to have higher concentrations of calcium than the shallower wells.

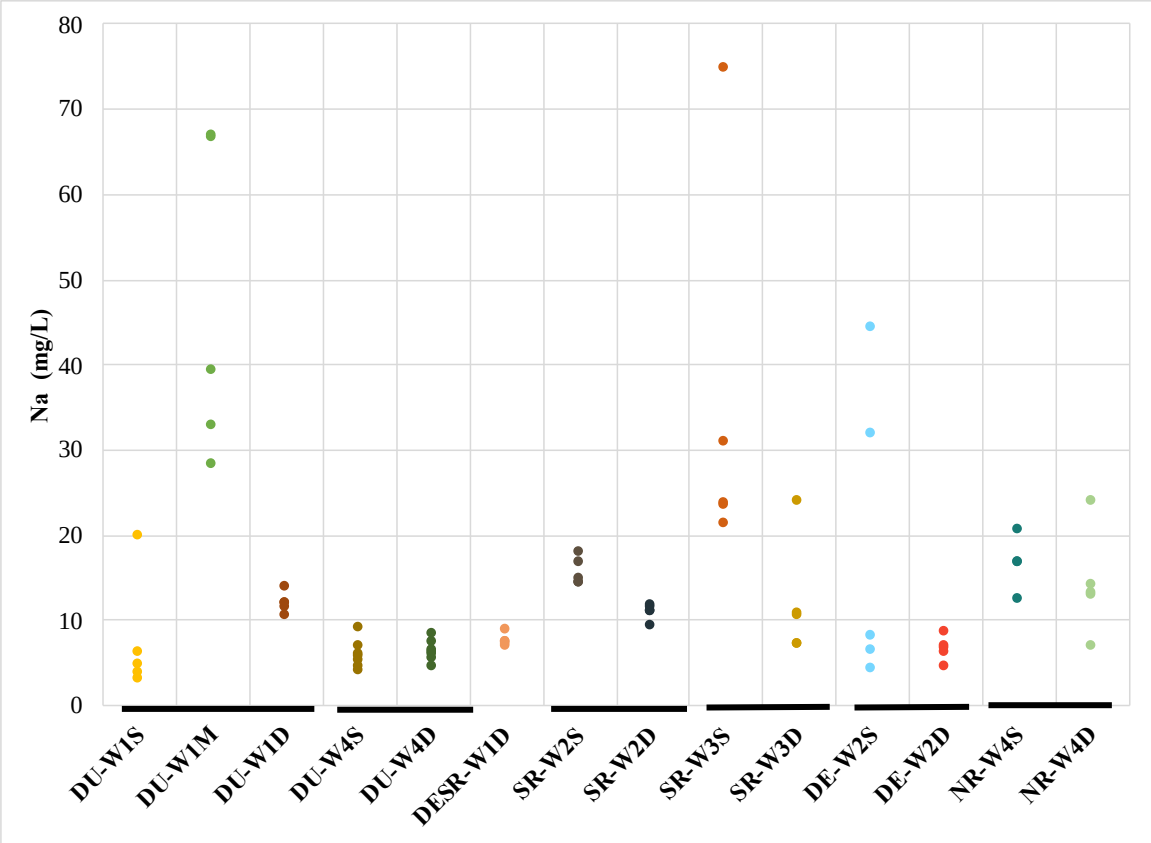

Figure 49. Sodium concentrations per well. In many cases, the shallower wells at each cluster had higher sodium concentrations than the deeper wells.

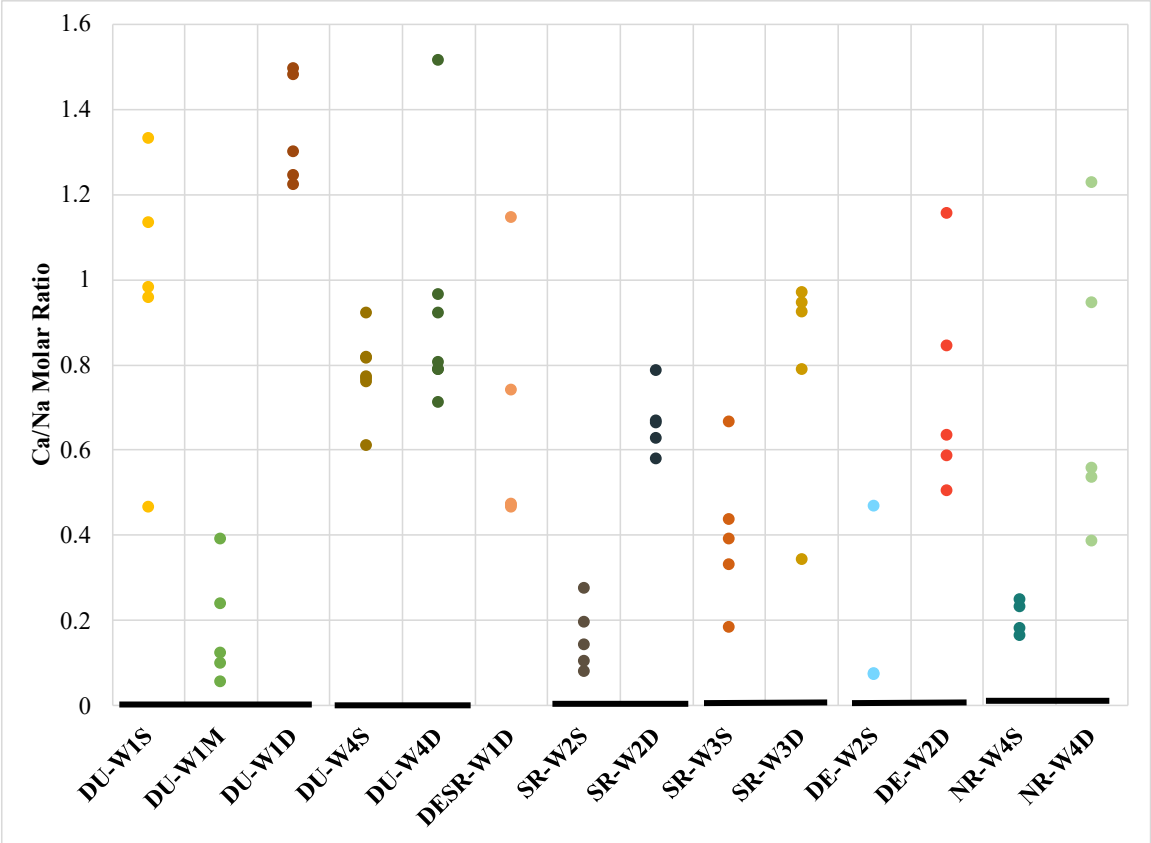

Figure 50. Dot plot showing the calcium/sodium (Ca/Na) molar ratio per well. At each well cluster, the deeper wells had a higher Ca/Na ratio while the shallow wells had lower Ca/Na ratios.

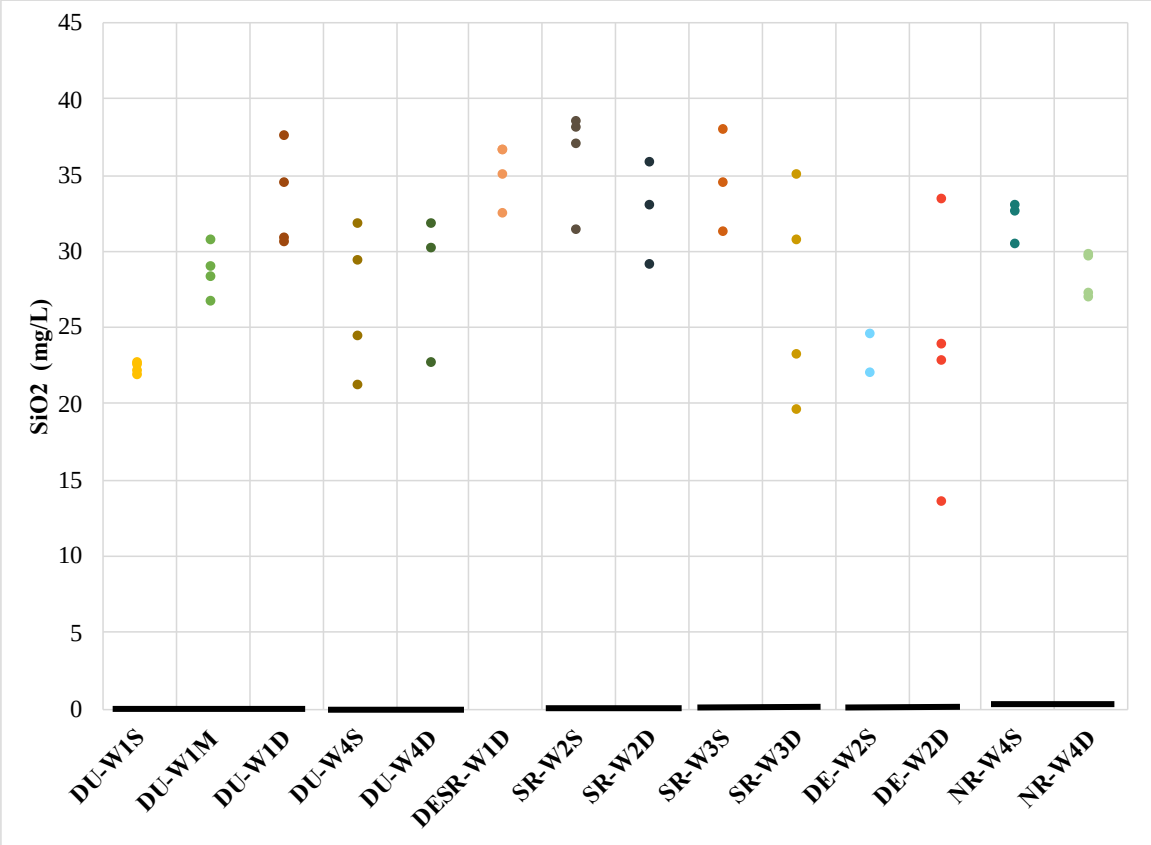

Figure 51. Silica concentrations per well.

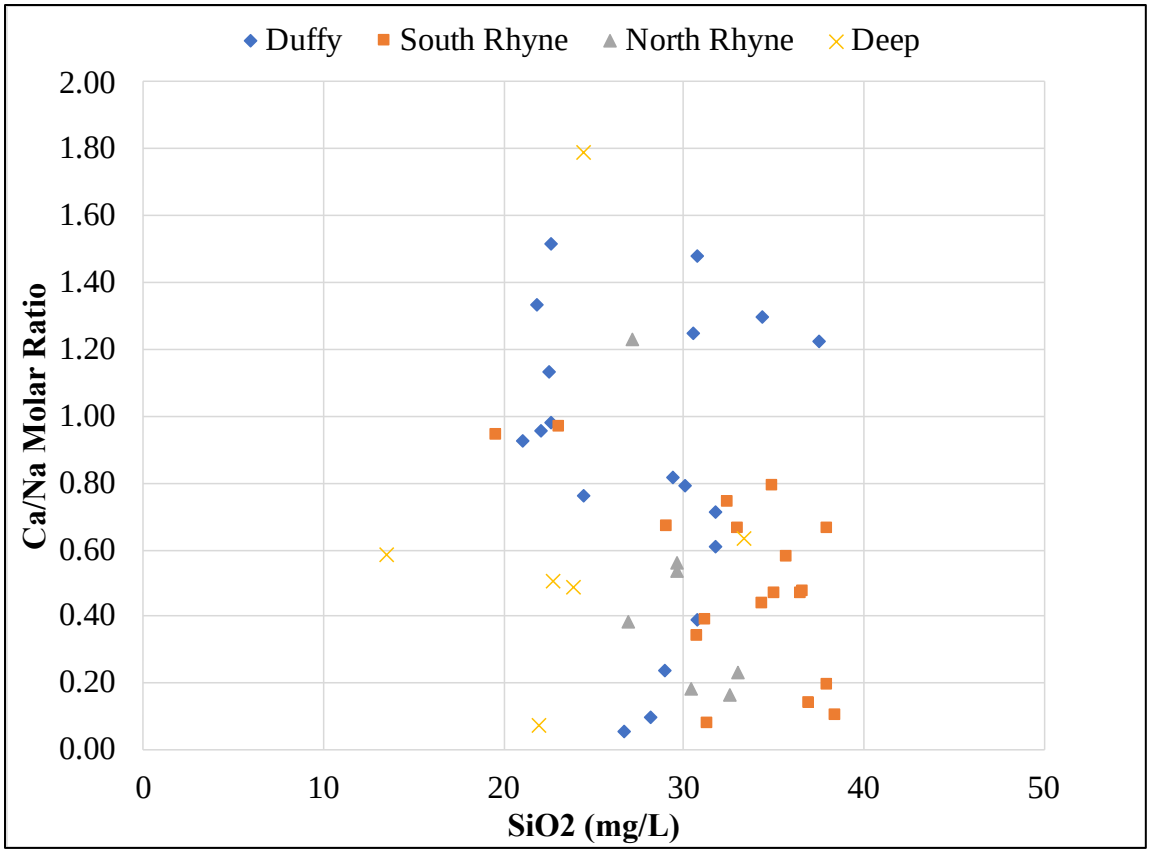

Figure 52. Relationship between silica concentration and Ca/Na molar ratio. The correlation coefficient between these two variables is -0.47, which implies a negative relationship between silica concentration and Ca/Na.

The Ca/Na ratios of the streams seemed to plot roughly intermediate between the shallow and deep groundwaters (Figure 53). The South Rhyne stream, which was sampled at two different locations along the stream channel, had the highest overall Ca/Na ratio (0.5-1.5). The North Rhyne stream had the lowest Ca/Na ratio (0.2-0.3).

Silica concentrations in the streams also fall roughly intermediate between the shallow and deep wells (Figure 54). Stream silica concentrations had a median value of 29.6 mg/L, shallow groundwater had a median value of 29.1 mg/L, and deep groundwater had a median value of 31.3 mg/L.

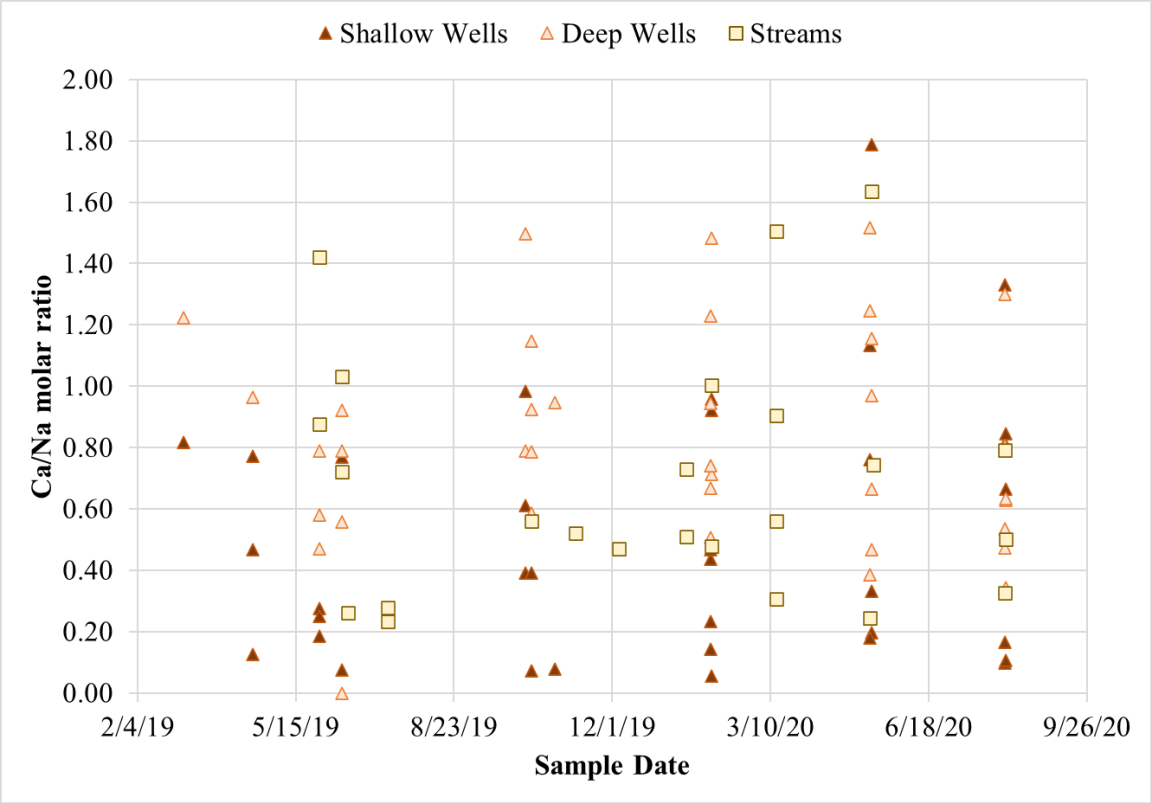

Figure 53. Ca/Na molar ratios color-coordinated and plotted per watershed with respective streams (squares). This figure illustrates that the Ca/Na ratios of the streams plot roughly intermediate between the shallow wells (dark triangles) and deep wells (light triangles).

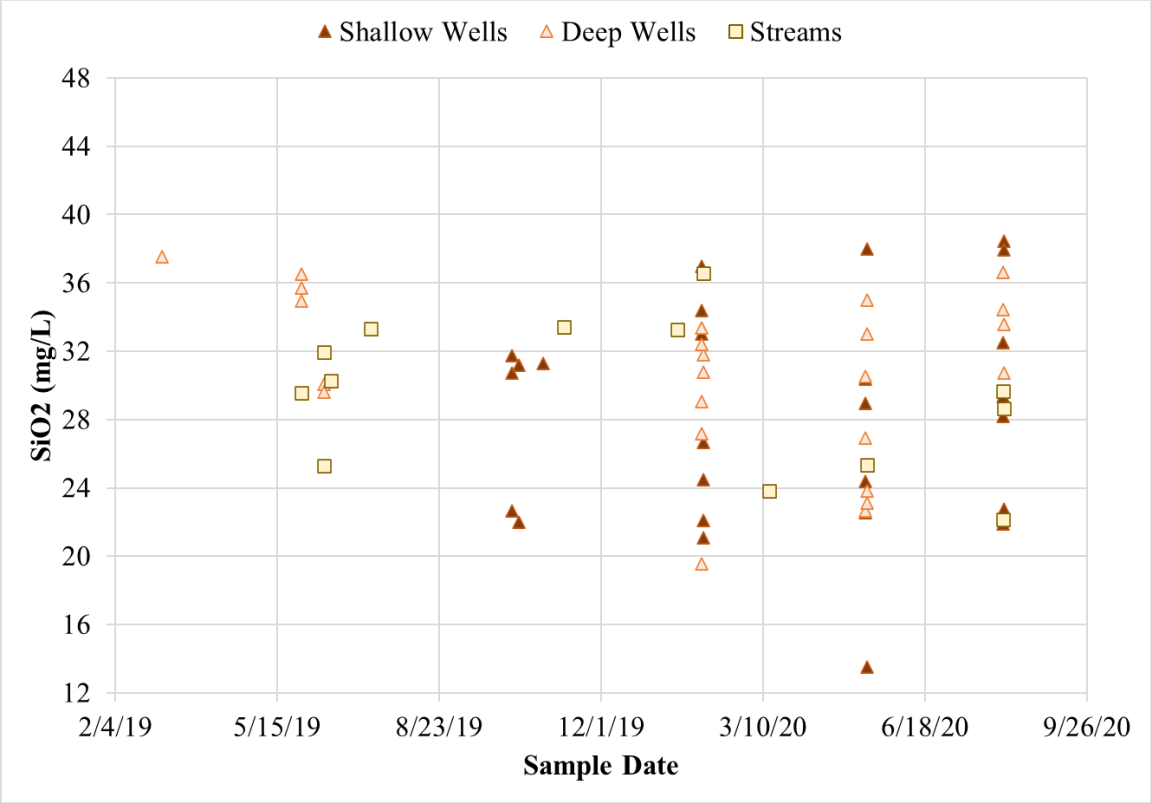

Figure 54. Silica concentrations color-coordinated and plotted per watershed with respective streams (squares). This figure illustrates that the amount of silica in the streams plot roughly intermediate between the shallow wells (dark triangles) and deep wells (light triangles).

Sulfate (SO_4^{2-}) concentrations varied per watershed (Figure 55-56) with time but seemed to be highest during the initial months after well installation. Well installation took place from January-March 2019, and since then, there has been a general decrease in SO_4^{2-} concentrations. For the Duffy watershed, sulfate ranged from 0.9 to 197 mg/L, with 197 mg/L being a significant outlier found in the DU-W1S well. The second highest sulfate concentration at this watershed was 39.3 mg/L, which was from DU-W1M. The average sulfate concentration was 18.9 mg/L. In the Deep watershed, sulfate concentrations ranged from 1.0 to 47.3 mg/L, with an average of 7.9 mg/L. The South Rhyne watershed sulfate concentrations ranged from 1.4 to 30.5 mg/L, with a lower value of 4.5 mg/L on average. The sulfate concentrations from DESR-W1D, which is at the Deep and South Rhyne watershed divide, were incorporated into the statistics for both watersheds individually. The

North Rhyne watershed had sulfate concentrations ranging from 1.6 to 22.1 mg/L with an average of 13.1 mg/L.

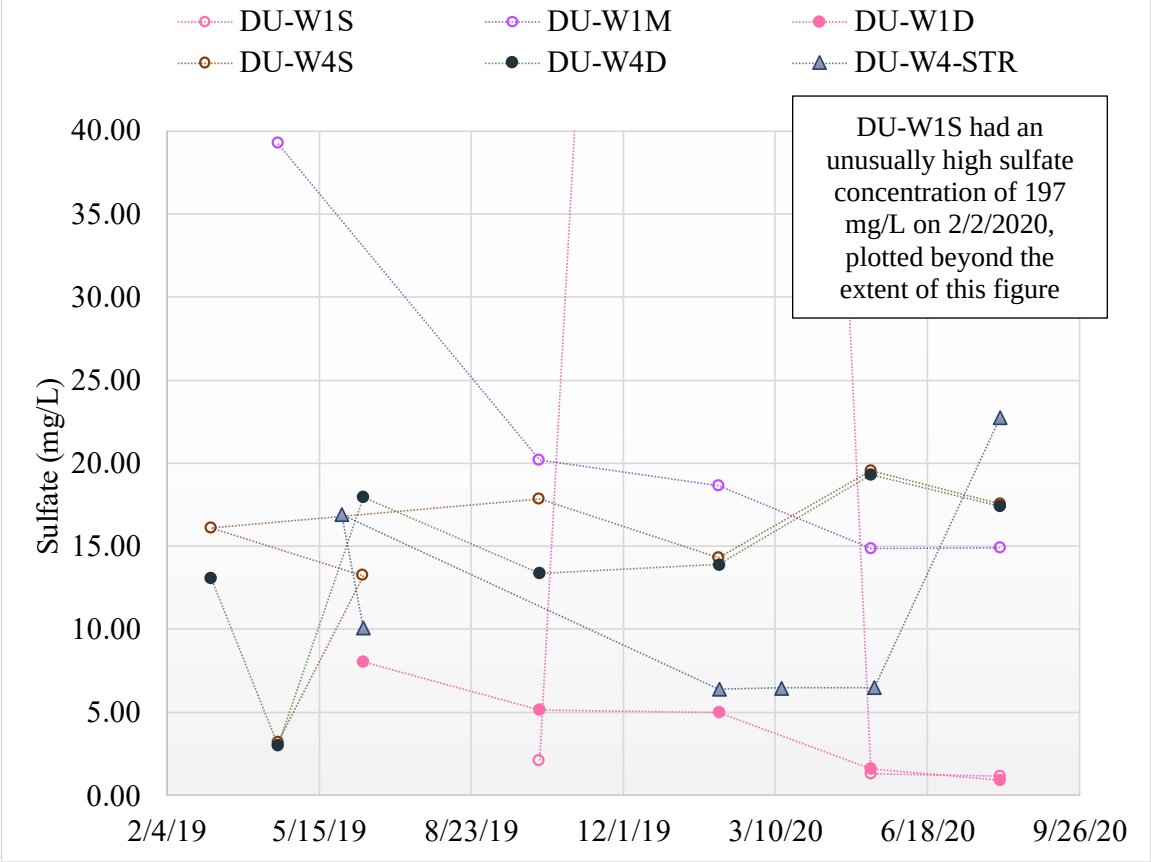

Figure 55. Sulfate (SO_4^{2-}) concentrations of water from the Duffy watershed throughout the duration of the study.

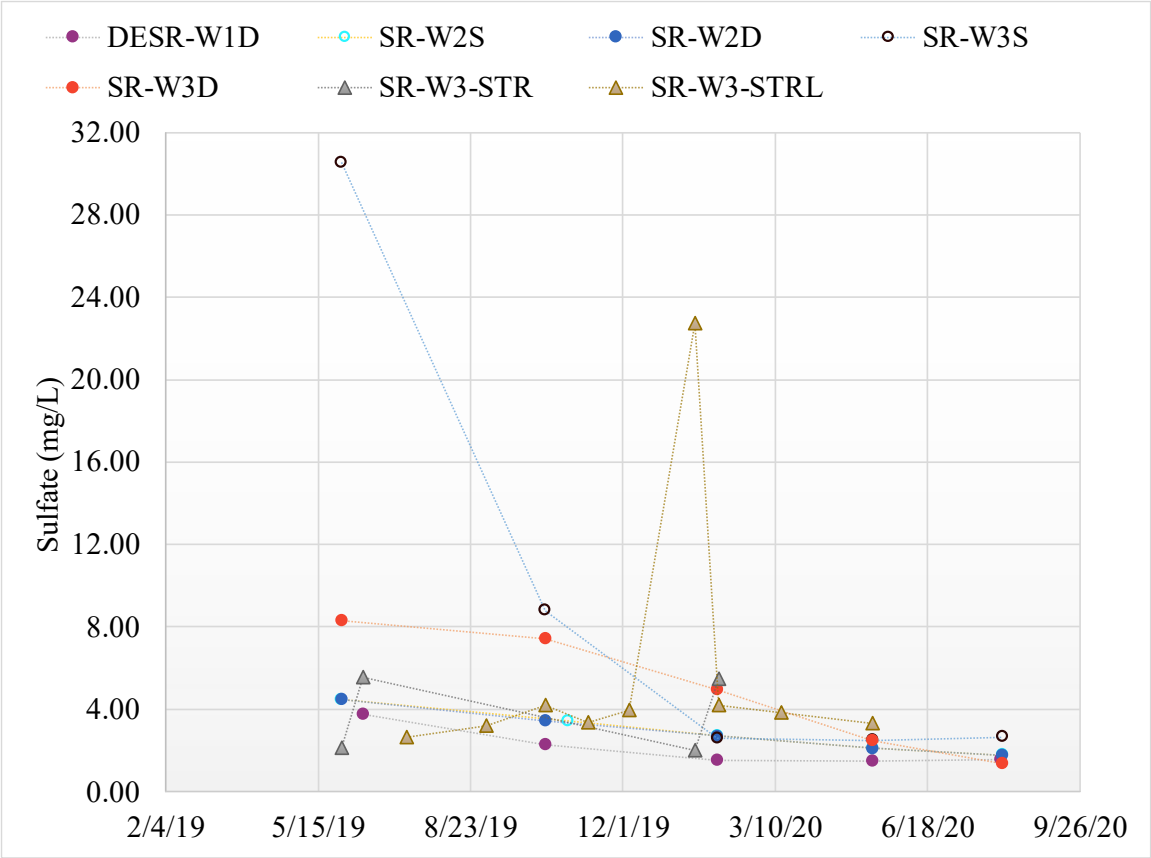

Figure 56. Sulfate concentrations of water from the South Rhyne watershed throughout the duration of the study.

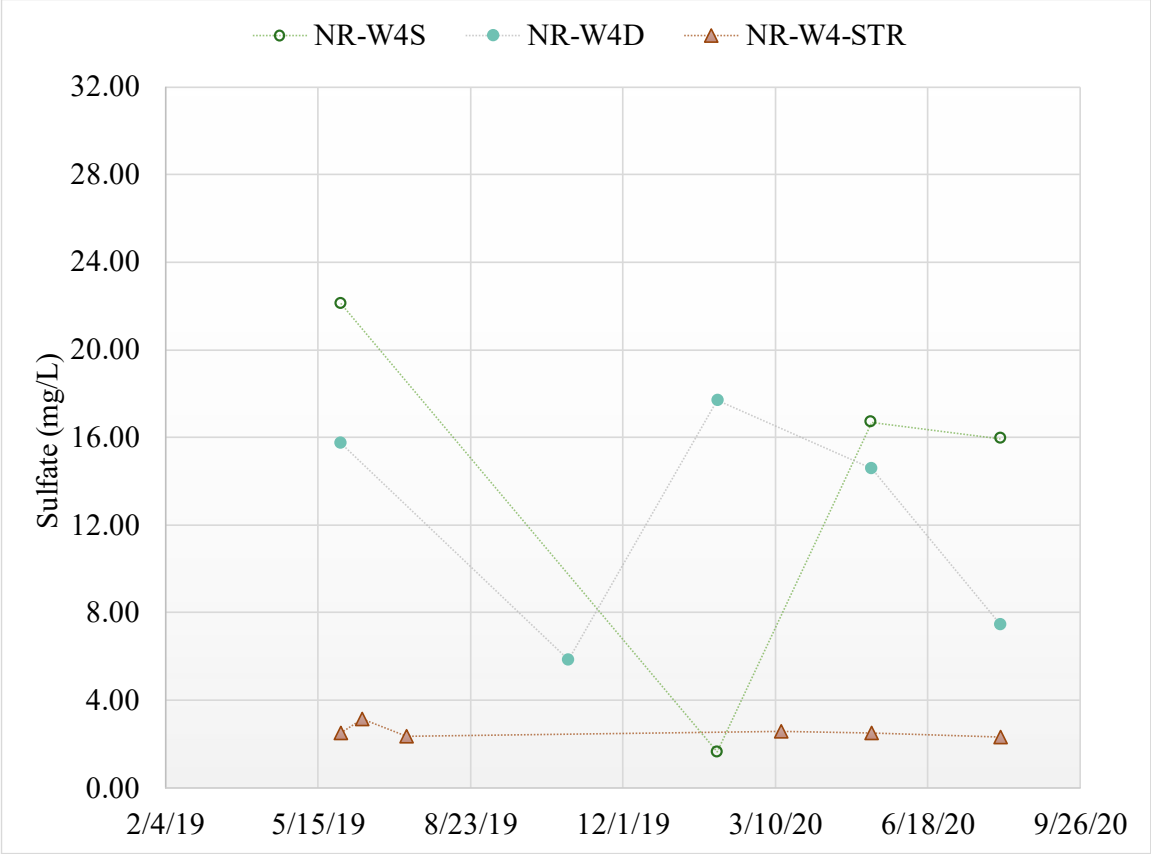

Figure 57. Sulfate concentrations of water from the North Rhyne watershed throughout the duration of the study.

Figure 58 shows the relationship between alkalinity concentrations and pH for the four watersheds. Groundwater pH values ranged from 5.5-7.9, with a few outliers from the South Rhyne and Duffy watersheds reaching a pH of 12.1. Alkalinity concentrations seemed to follow a similar pattern, generally ranging from 0.4-2.6 meq/L. There is no apparent difference in alkalinity or pH between the four watersheds.

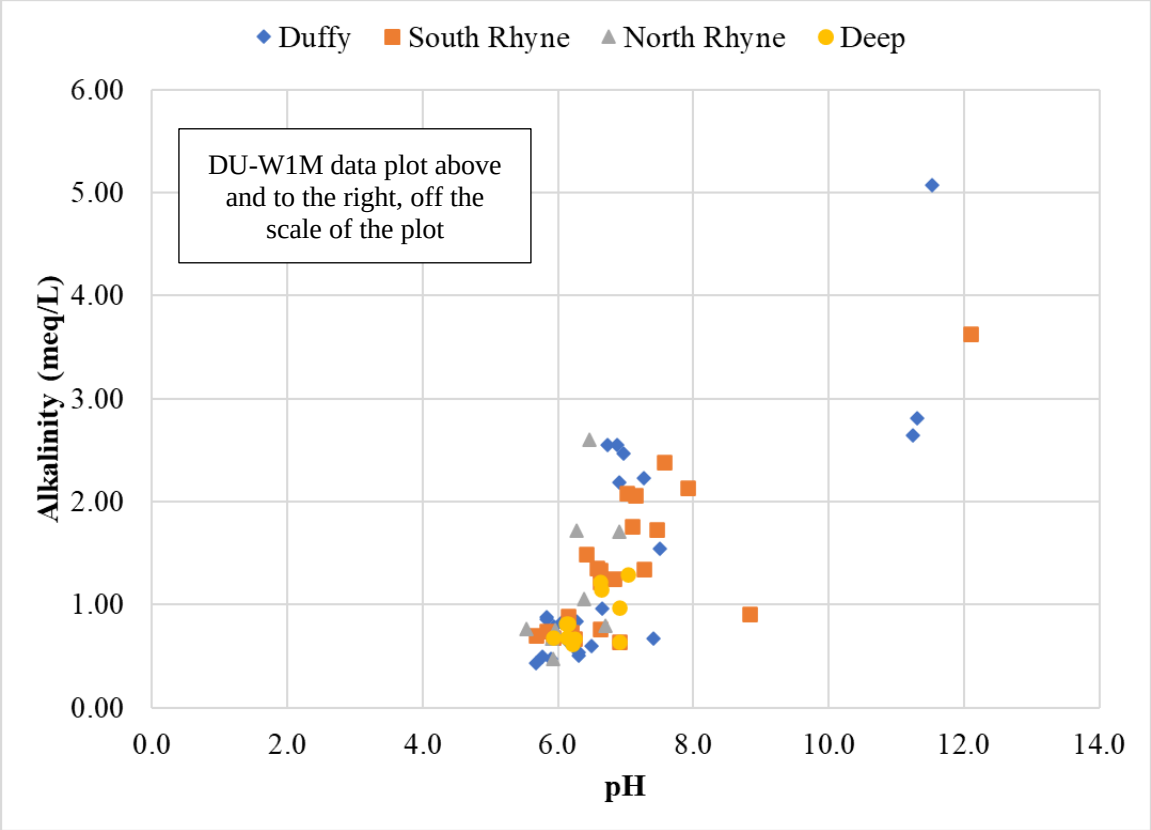

Figure 58. pH versus alkalinity (meq/L) are plotted for the four watersheds at Redlair. Groundwater pH concentrations ranged from 4.0-7.6.

Figure 59 and 60 show calcium and sodium concentrations as a function of absolute well screen elevation (above sea level) acquired from the LiDAR data. Calcium concentrations appeared to be more uniform among the different well screen elevations. Overall, average calcium concentrations are indistinguishable across each box plot (Figure 59). Equally-classified well screen elevations show that sodium concentrations in the mid-elevation wells were lower than those of shallower or deeper wells (Figure 60). There appears to be no evident elevation trend with sodium. Figure 61 shows the Ca/Na molar ratio as a function of absolute well screen elevation (above sea level). There is not much of a trend, but the highest elevation has higher Ca/Na ratios than the lowest elevation.

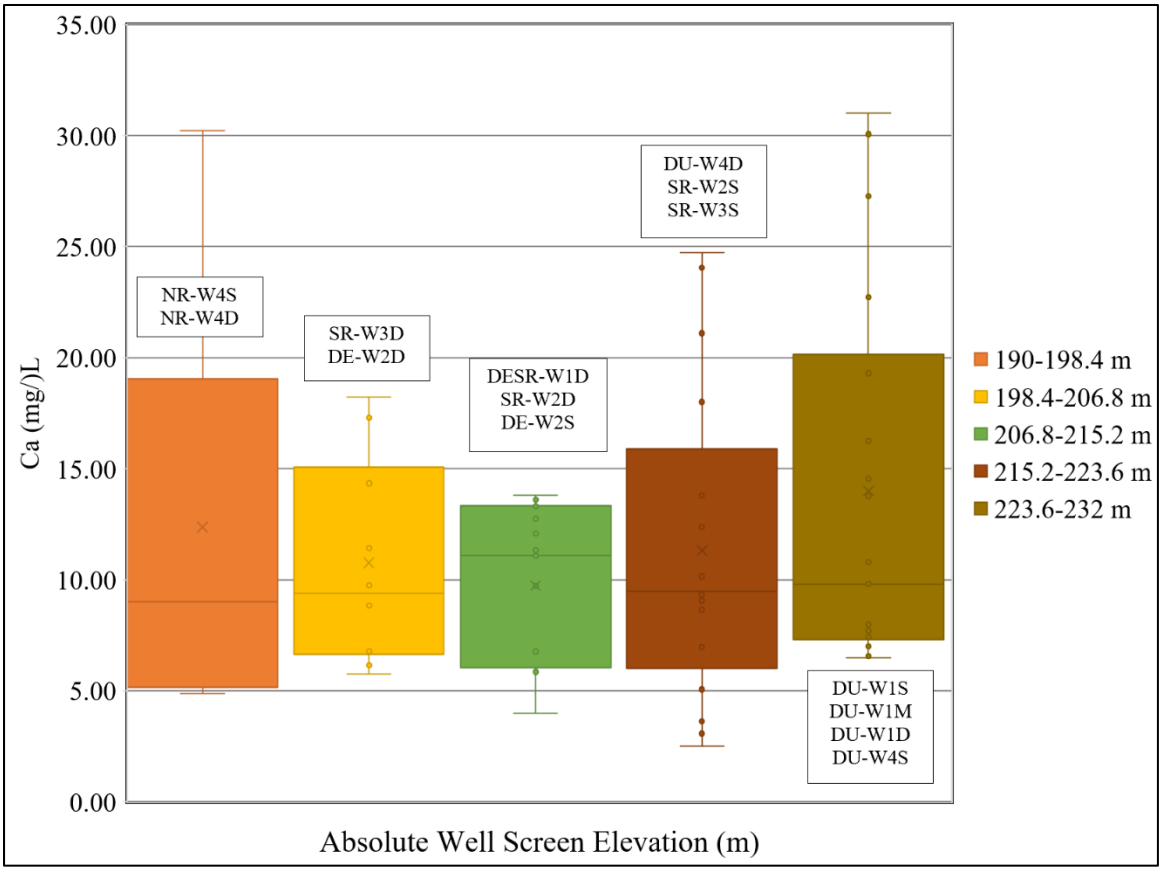

Figure 59. Calcium concentrations based on the absolute elevation of well screens classified into five groups, as indicated in the legend.

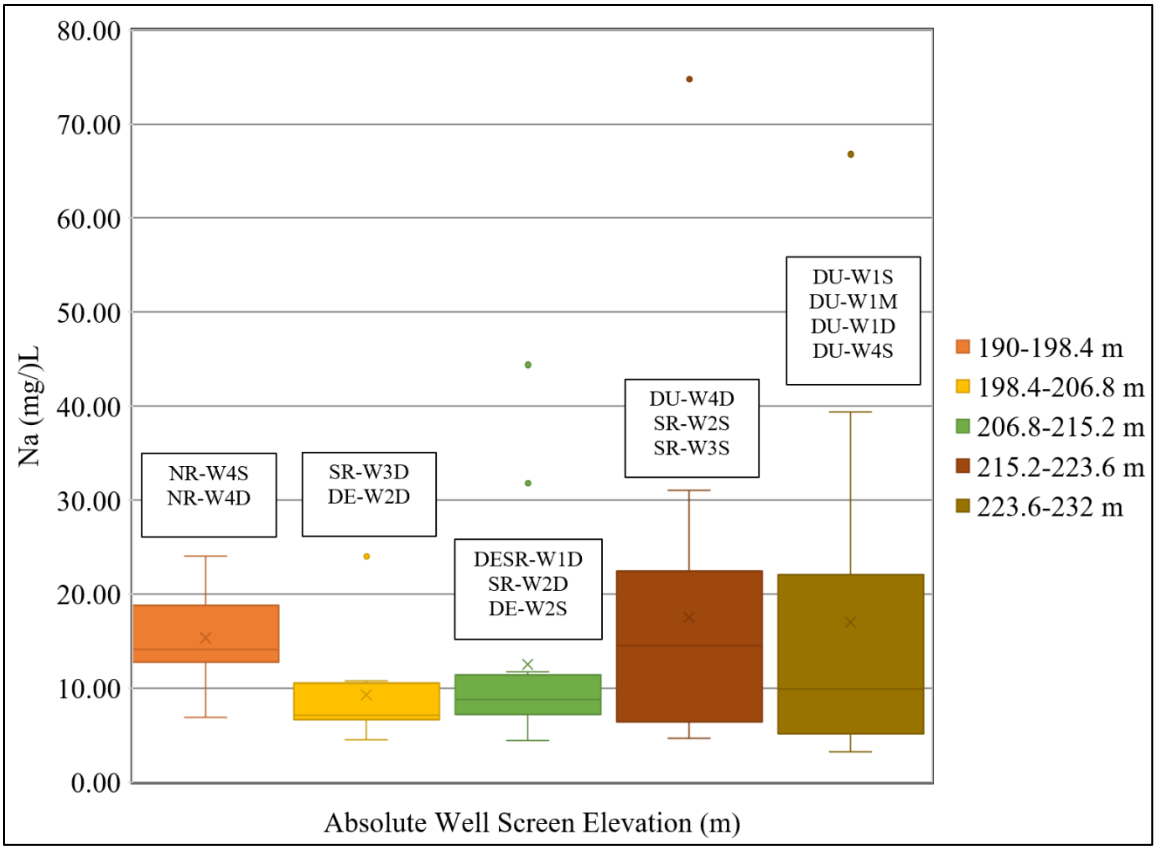

Figure 60. Sodium concentrations based on the absolute elevation of well screens classified into five groups, as indicated in the legend.

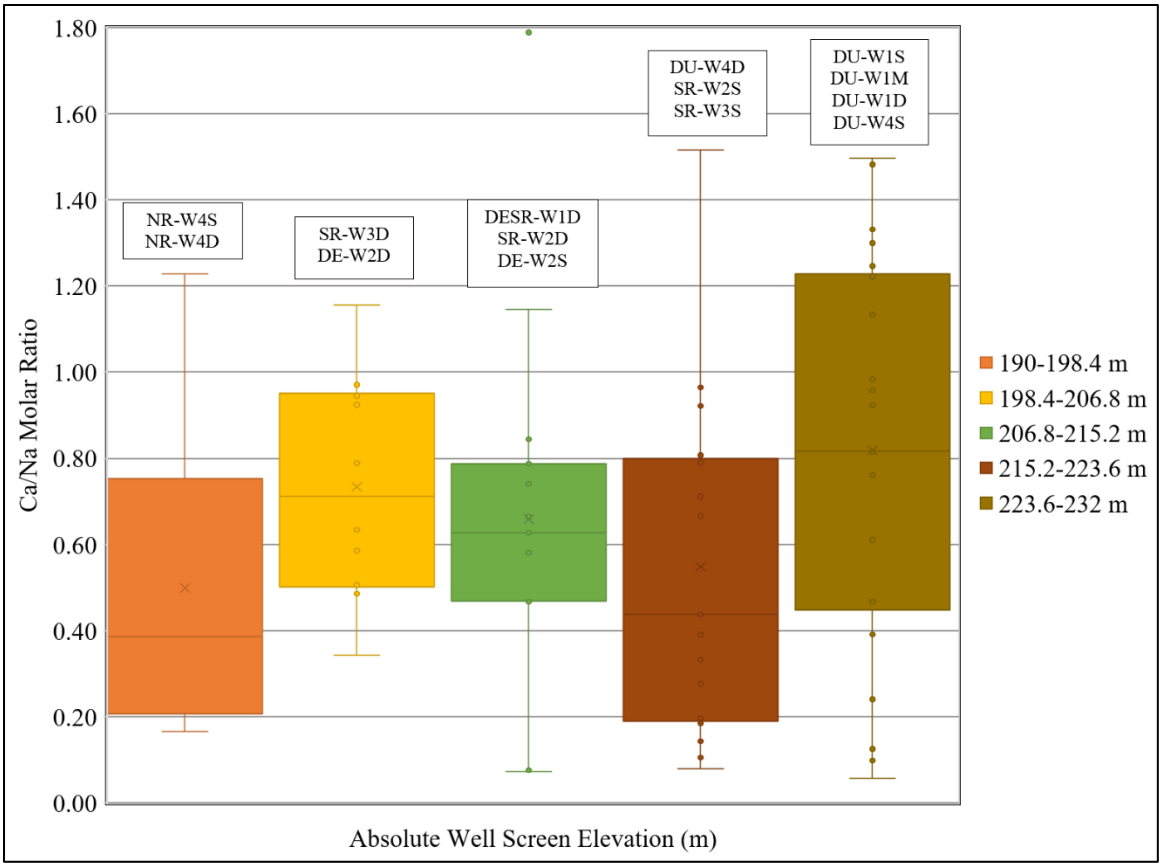

Figure 61. Ca/Na molar ratio based on the absolute elevation of well screens classified into five groups, as indicated in the legend.

5.5 Water isotopes

Like the groundwater chemistry data, the isotopic data also lack an apparent seasonal temporal trend during the period of the study. There is little to no relationship between the water isotopes, δD (deuterium) or $\delta^{18}O$, and time of year. In early spring of 2019, some groundwater samples exhibited an apparently lighter isotopic composition with respect to both δD (

Figure 62) and $\delta^{18}O$ (Figure 63). For the winter months, isotopic compositions were heavier, with δD ranging from -35.8 to -25.4‰ with an average value of -32.1‰; $\delta^{18}O$ composition ranged from -7.9 to -4.6‰ with an average of -6.1‰. There is no clear time trend related to the groundwater isotopes. There also seems to be little to no spatial variation in these isotopic values of $\delta^{18}O$ (Figure 64) and δD (Figure 65). DE-W2D had the lightest δD value of -25.4‰; DU-W1D had the heaviest value of -35.8‰.

Figure 66 shows the relationship between the groundwater and surface water at Redlair compared to local precipitation and the Global Meteoric Water Line (GMWL), which represents the global average precipitation ($\delta D = 8^* \delta^{18}O + 10$) (Craig, 1961). All the surface water and groundwater isotopic compositions plot slightly to the left of the GMWL. There is little to no variability distinguishing groundwater from surface water. Some of the precipitation data plot to the right of the GMWL, but most also plot to the left (Torrellas, 2018). The Redlair data, on average, plot within the domain of the Torrellas (2018) precipitation data; both data sets are slightly left of the GMWL.

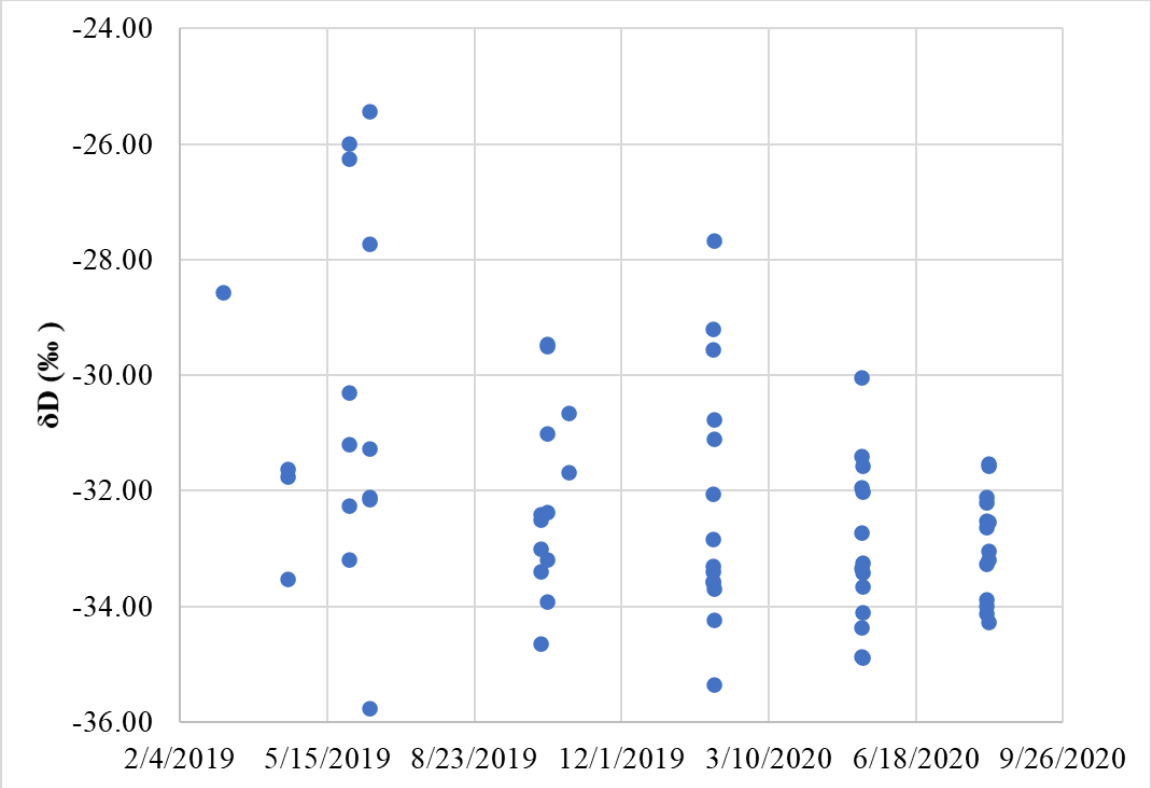

Figure 62. A time series plot of δD values for groundwater samples collected at Redlair Observatory from 2019-2020.

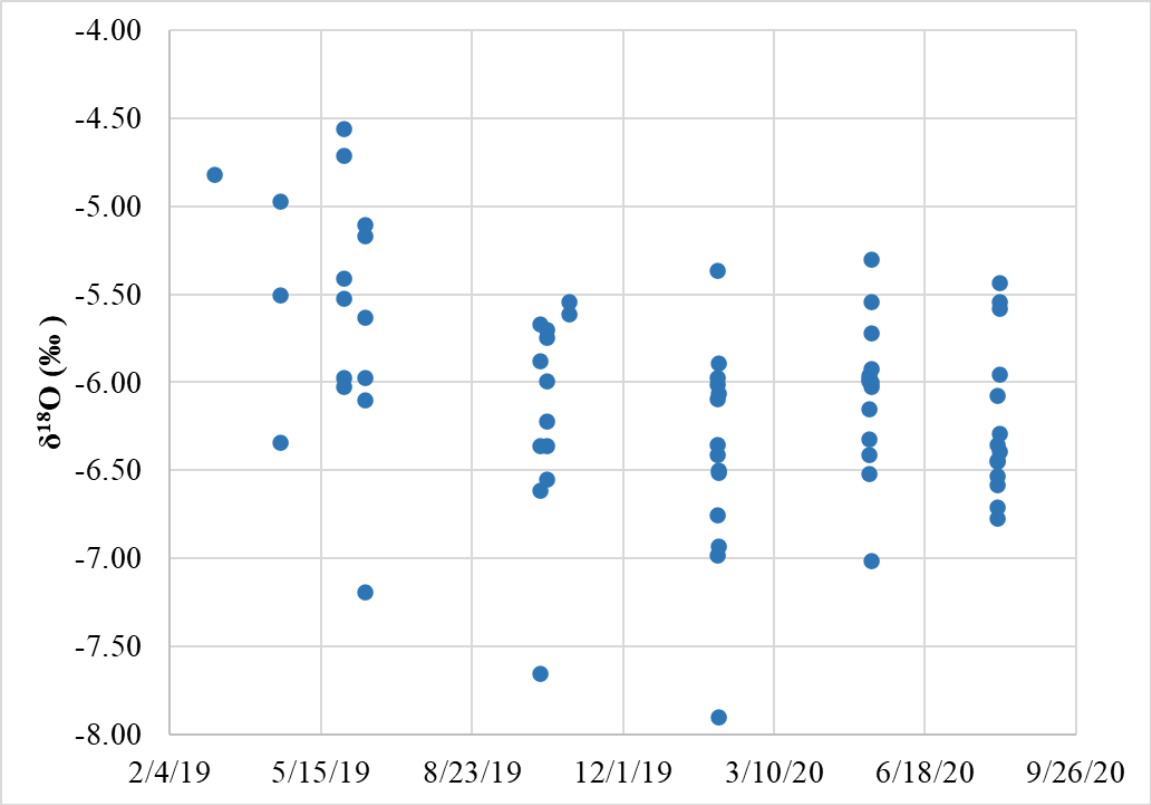

Figure 63. A time series plot of $\delta^{18}O$ values for groundwater samples collected at Redlair Observatory from 2019-2020.

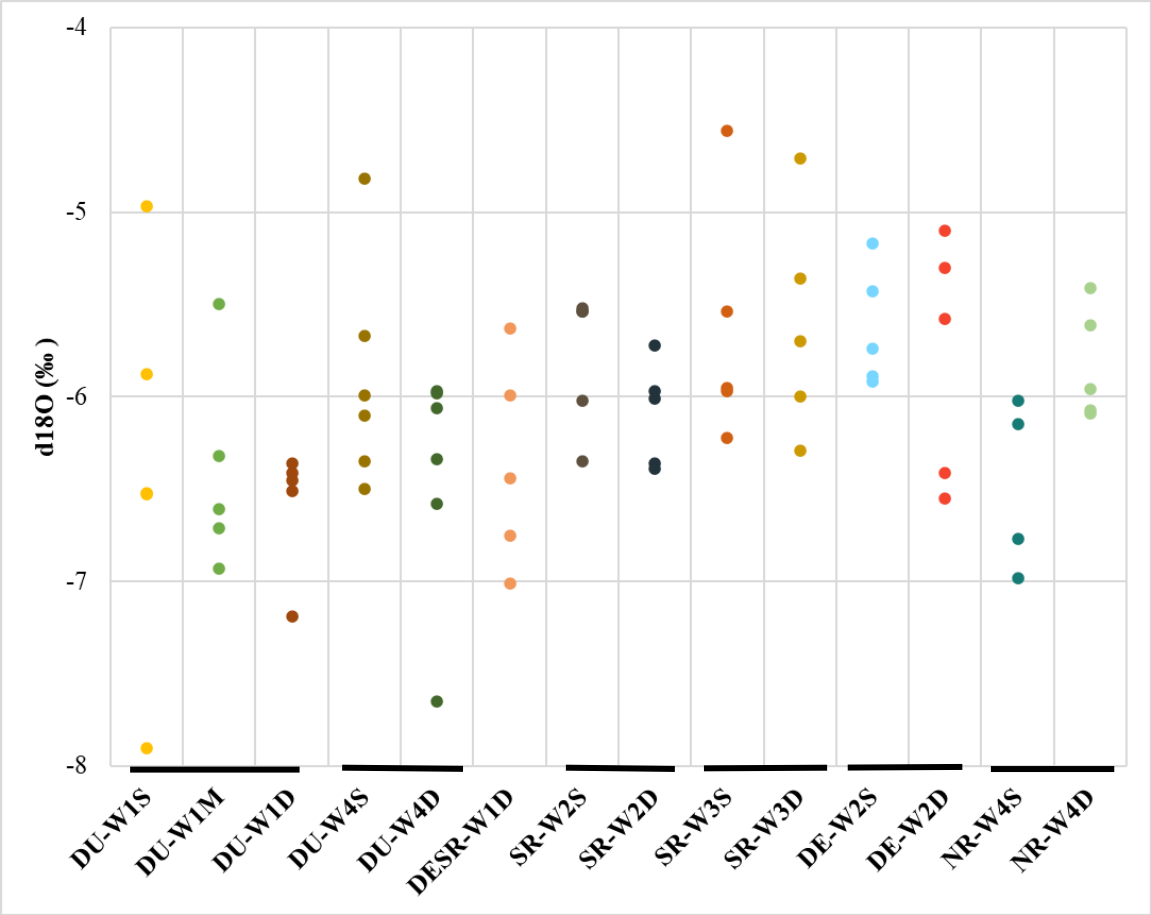

Figure 64. Dot plot of $\delta^{18}O$ groundwater values per well.

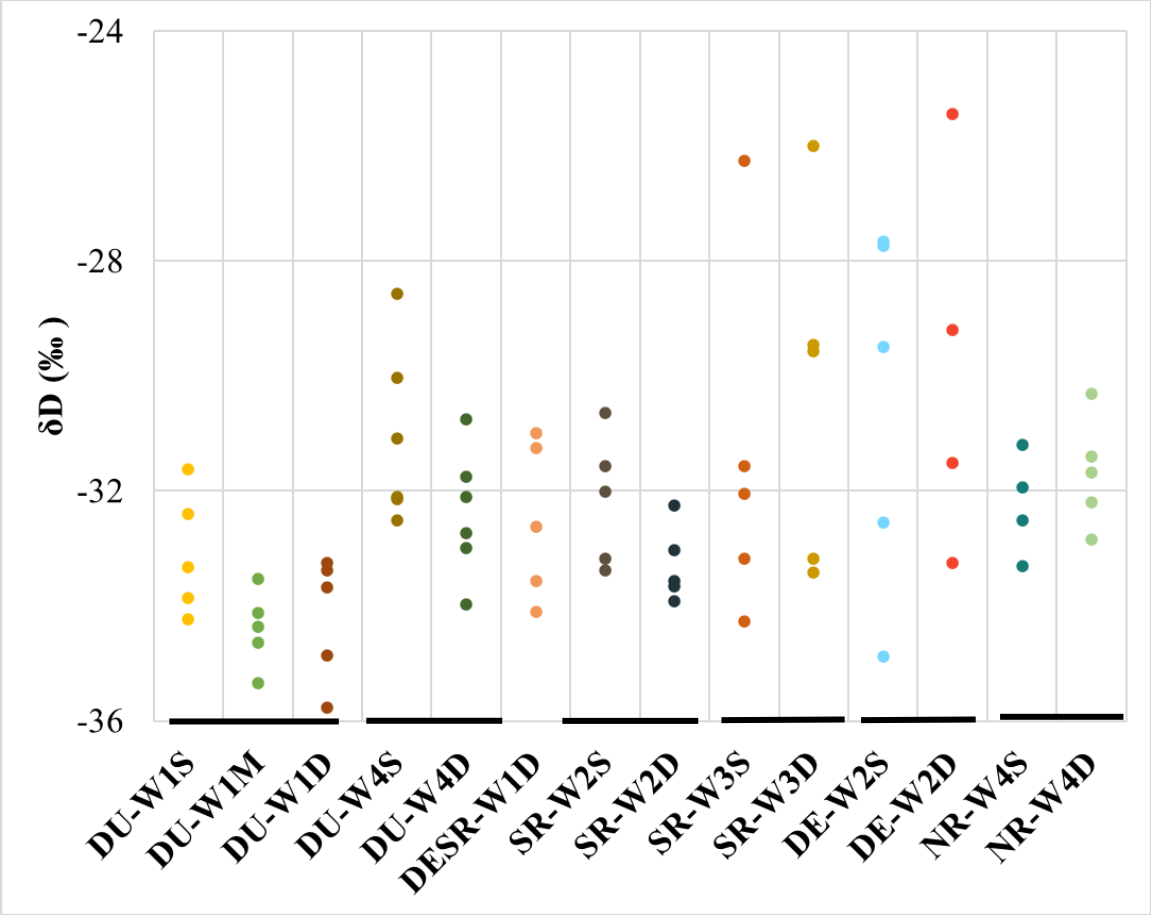

Figure 65. Dot plot of groundwater δD values per well.

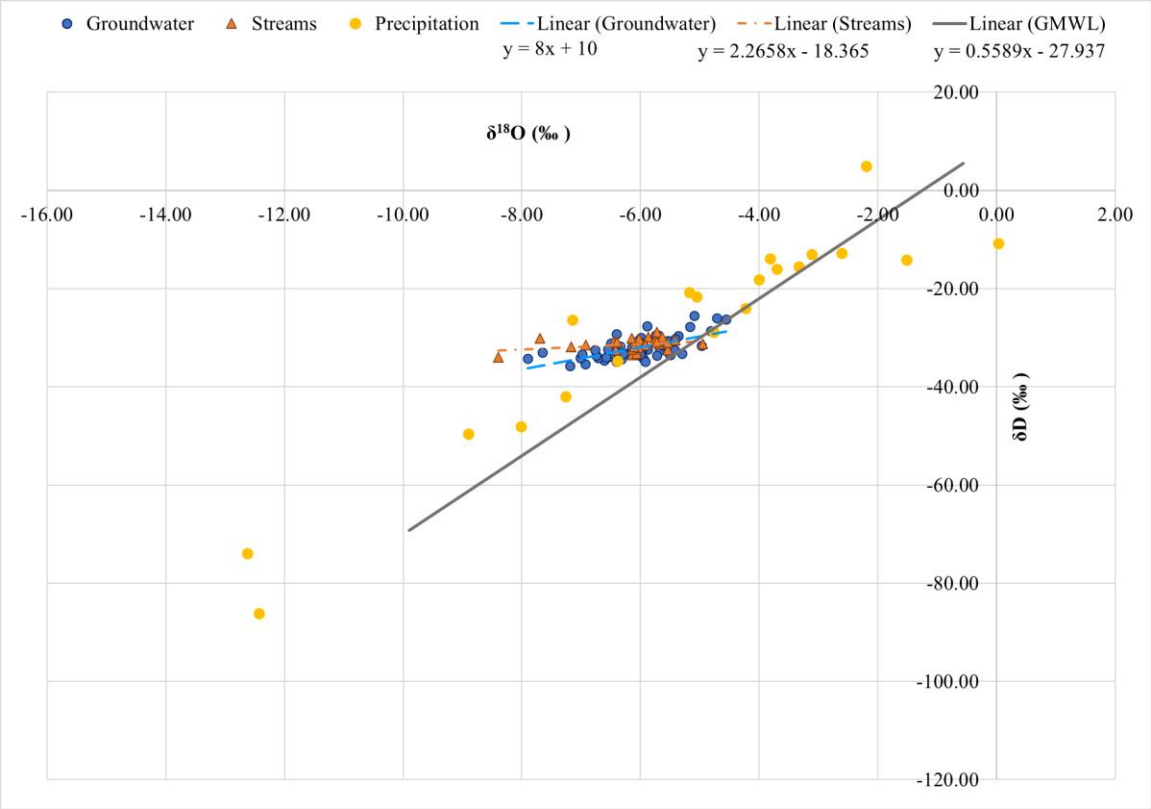

Figure 66. Groundwater and surface water isotopic values are plotted here, along with the Global Meteoric Water Line (GMWL; Craig, 1961). Charlotte precipitation data (Torrellas, 2018) imply that the groundwater and surface water are well-mixed at Redlair. The linear trend was calculated for the groundwater and surface water isotopic data and provided in the legend of the graph.

Limited $\delta^{13}C$ of dissolved inorganic carbon (DIC) analyses were also conducted on Redlair water samples. SR-W3D had the most enriched $\delta^{13}C$-DIC per mil (-8.9‰). The average DIC concentrations for Duffy, Deep, South Rhyne, and North Rhyne watersheds were 2.1 mmol/L, 1.2 mmol/L, 1.4 mmol/L, and 2.1 mmol/L, respectively (Table 9). Results for individual well locations are presented in Figure 67.

Table 9. Summary of the groundwater DIC and $\delta^{13}C$ analysis presented below.

Watershed	Mean DIC (mmol/L)	Mean $\delta^{13}C$-DIC (‰ VSMOW)	*n*
Duffy	2.11	-20.5	5
Deep	1.20	-16.0	4
South Rhyne	1.42	-16.6	5
North Rhyne	2.08	-19.9	2

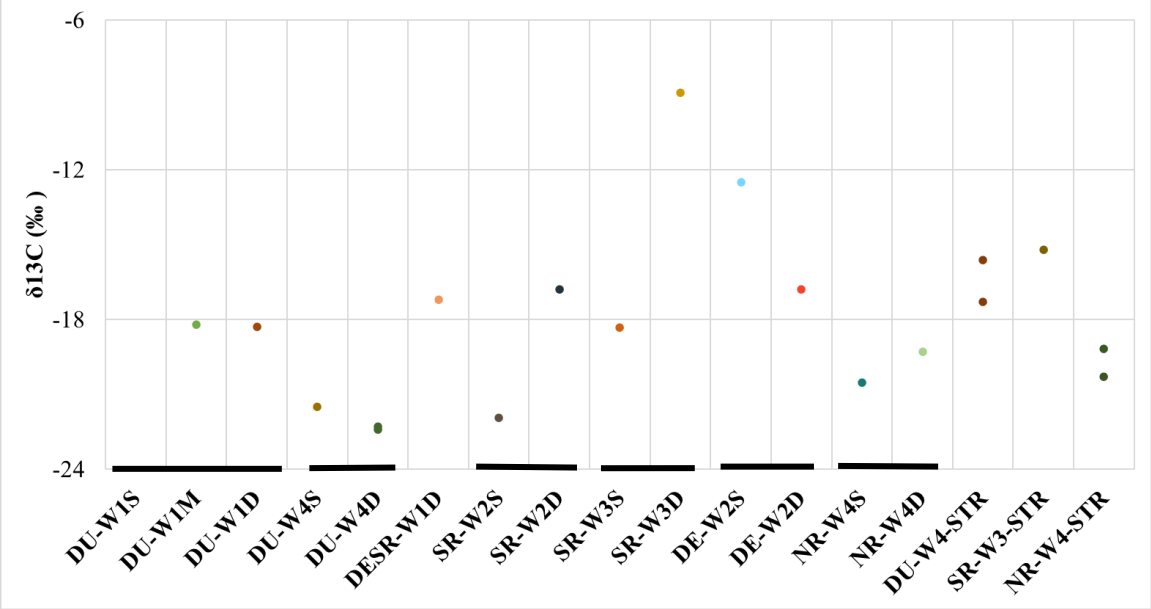

Figure 67. Dot plot showing the $\delta^{13}C$ (‰) concentrations in the groundwater and surface water samples collected from Redlair. Only one sample per location was analyzed.

6 DISCUSSION

6.1 Analysis of watershed geomorphology using LiDAR data – its relationship to watershed hydrology

Geospatial analyses reveal the complexity of the landscape due to legacy land use. The curvature data appear "noisier" in the densely forested areas, but exhibit slight changes (i.e., concave or convex) in the pasture and agricultural areas. Some of these changes may be caused by the contours (i.e., legacy terracing agricultural techniques), incised gullies, and perhaps even fallen trees and leaf litter. These agricultural man-made features likely contribute to the neutral or flat

topography identified by the curvature maps. The maps (Figure 18-21) also reveal more legacy contours than previously evident in the DEM figures, particularly in the North Rhyne watershed. These contours were designed to detain overland flow downslope and increase water residence time (i.e., hydrologic retention). The contours were primarily used to stop gully erosion. It would be worth exploring whether the terraces lengthen hydrologic residence time and gullies shorten hydrologic residence time in zero-order watersheds in future studies. For instance, when looking at groundwater levels in the Deep-South Rhyne watersheds, DESR-W1D (ridgeline/watershed divide) had its summer peak (shallowest groundwater level) before SR-W3 (riparian) but after SR-W2 (mid-slope). This suggests a complex relationship between well depth and landscape position.

In addition to analyzing the profile curvature of the watersheds, channel heads were also identified at three of the four watersheds in the field. Julian et al. described in 2011 that the mid-Atlantic region of the US commonly had recognizable bowl-shaped channel heads. Figure 68, which has photographs of channel heads identified at Redlair, also follow this pattern.

The hypsometric curves analysis allows for a three-dimensional view of each watershed. North Rhyne and Duffy seem less influenced by incision, as they seem to have a more gradual decline in proportional elevation relative to proportional area (Figure 22). This is also apparent in the slope analysis as well (Figure 17). The South Rhyne headwaters start a bit lower, perhaps due to incision (Figure 22).

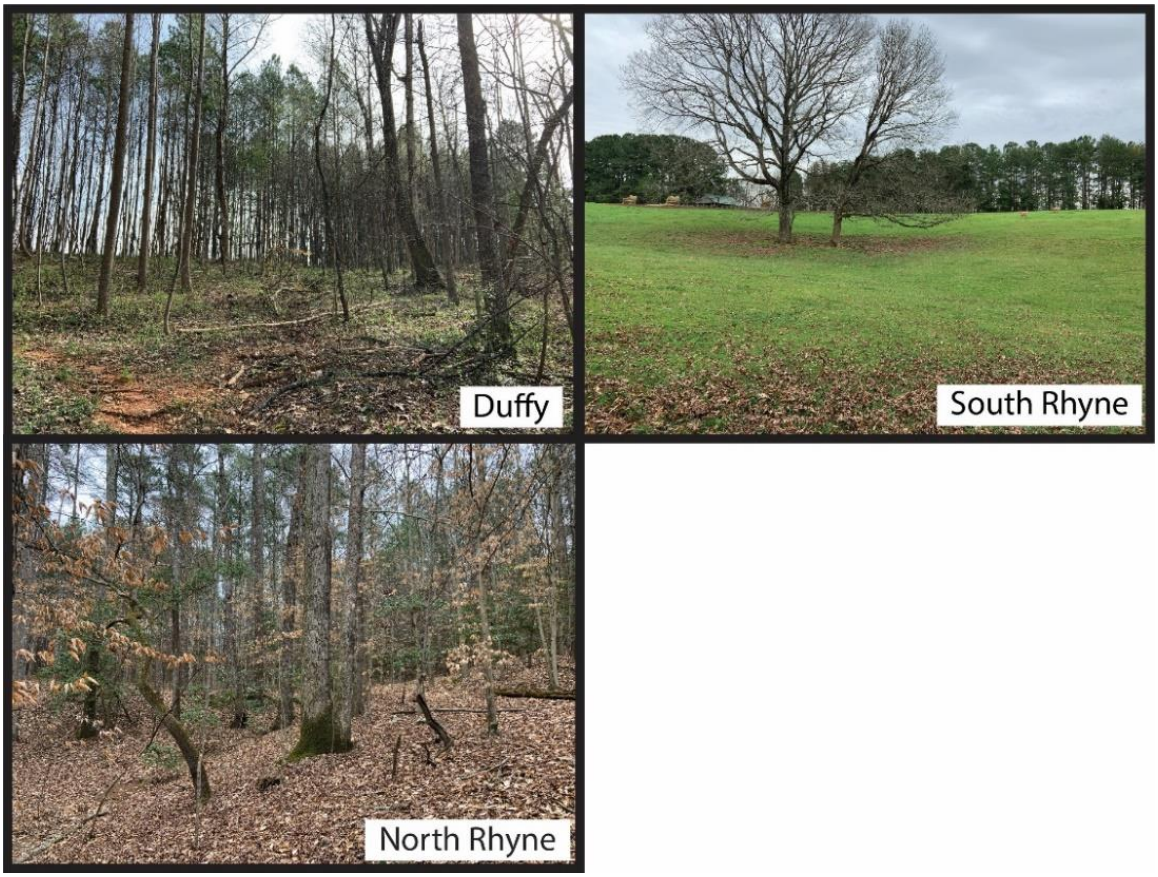

Figure 68. Photographs looking upstream at the channel heads of the three main watersheds of the study.

6.2 Groundwater levels and temperature – apparent relationship to watershed-scale residence time

The HOBO and manual groundwater measurements are useful for assessing the watershed-scale residence time of these zero-order watersheds. The HOBO plots show slight variations in water levels due to evapotranspiration (Figure 32). Figure 32 and Figure 38 also allow for comparison of seasonal peaks and lows of groundwater levels. Even with the gaps in data logging, it is evident that DESR-W1D, a deep well located at the boundary of two watersheds, had its summer peak later than the other wells

The HOBO temperature data also show apparent lag in groundwater temperature changes between summer peaks and winter lows (Figure 38). DESR-W1D temperature data were not

reliable, possibly related to the logger being too deep at almost 25 m below the land surface. For this reason, the temperature data for this well were not added to Figure 38. DU-W4S had its warmest groundwater temperature peak before any of the other wells with loggers. SR-W2D had its warmest temperature peak last of the four wells, lasting from December-March.

When comparing HOBO groundwater levels (GWLs) and temperature for two riparian wells (DU-W4S and DU-W4D versus NR-W4S), there were some differences in response times to these two variables. GWLs lagged slightly in NR-W4S, rising in late February compared to DU-W4S and DU-W4D. Day-to-day fluctuations in GWLs likely caused by evapotranspiration processes. GWL evapotranspiration (daily noisiness in Figure 32) trends in DU-W4S and DU-W4D do not seem as prominent as they appear in NR-W4S. NR-W4S temperature peaks seem like they would have occurred later than DU-W4S and DU-W4D (if data were available for the exact same length of time). The minimum temperature also occurred approximately one month later at NR-W4S than DU-W4S and DU-W4D. Furthermore, groundwater temperatures were not isothermal, and the seasonal samples had temperature variations correlated to the seasons.

Manual groundwater measurements varied well to well based on topographic differences, but at each individual well cluster, there was little variation between the shallow and deep wells. The similarities in groundwater levels at individual well nest clusters indicate vertical connectivity at the watersheds. These results suggest that the main factor that influenced GWLs during this study was the depth of each well (Figure 25-31). The following is a summary of the apparent lag in GWLs decreasing in response to the late summer-early fall peak for the different wells:

- The late summer-early fall peak falls in October at SR-W2 (well nest depth: 8.76-15.24 m), SR-W3 (well nest depth: 7.62-21.04 m), and DU-W4 (well nest depth: 4.27-6.10 m)
- That same peak was delayed one month (until November) at NR-W4 (well nest depth: 4.57-6.40 m)

- That same peak does not fall until December at DE-W2 (well nest depth: 18.29-24.39) and DU-W1 (well nest depth: 16.16-24.39 m)
- The late summer/early fall peak was delayed about three months (not occurring until January) at DESR-W1D (well depth: 21.34 m)

The late summer-early fall GWL peak falls in DESR-W1D last perhaps because it is a ridgeline well that sits at the boundary between two watersheds.

Figure 69 compares GWLs for two deep ridgeline wells, DU-W1D and DESR-W1D. DESR-W1D had its shallowest summer GWL in August 2019. Its winter minimum occurred in January 2020. However, DU-W1D had its summer peak in about June 2019 and winter minimum in December 2019. The amplitude, or vertical variation, in groundwater levels was greater for DU-W1D than DESR-W1D. This may be because DESR-W1D is situated at a watershed divide and DU-W1D is not. Since groundwater levels are closer to the land surface in the Duffy watershed compared to at the Deep-South Rhyne watershed divide, less attenuation is expected in the Duffy watershed. Further comparison to the deep riparian well in the Duffy watershed (DU-W4D) shows shallowest GWLs in June 2019 and a winter minimum in December 2019 (Figure 69).

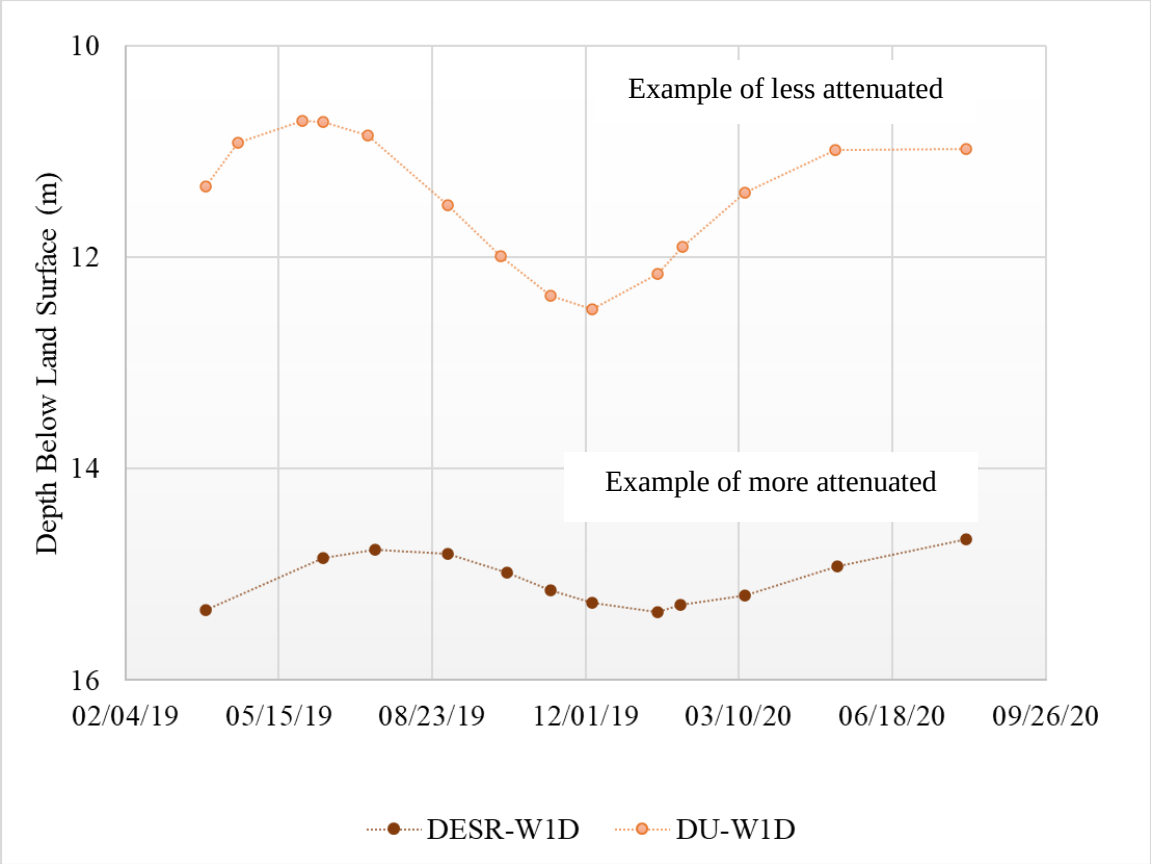

Figure 69. Manual groundwater measurements of two ridgeline wells, DU-W1D in the Duffy watershed and DESR-W1D at the Deep-South Rhyne watershed divide. DU-W1D had its winter low occur before DESR-W1D. These are both ridgeline wells.

6.3 Groundwater chemical evolution – relationship between groundwater chemistry and well depth

The Piper diagram is used to plot major groundwater cations and anions and derive hydrochemical facies based on the water composition (Ryan, 2014). The diamond of the Piper diagram (Figure 70) highlights the variability in Ca^{2+} concentrations, with concentrations being higher for the deep wells and lower for the shallow wells. The Piper diagram also has arrows to help visually pair the shallow and deep wells of each well nest. Figure 70 shows that the deeper well of each pair had higher Ca^{2+} proportion, while the shallow well of each pair had higher Na^{+} proportion. Generally, there was no discernable major dominant cation. All wells seem to have been dominated by bicarbonate (HCO_3^-) as the main anion, representing a carbonate facies (Ryan,

2014). Bicarbonate is the dominant anion in these watersheds since most groundwater had a pH of 8.0 or less (Ryan, 2014). Further, there was no significant shallow versus deep well nest relationship with bicarbonate ($p = 0.55$; Table 10), as some of the well pairs had similar concentrations (DU-W4) and some wells did not (NR-W4). The t-test analyses help to confirm the relationship between groundwater chemistry and well depth, especially related to calcium and sodium. These results will be further discussed (Table 10).

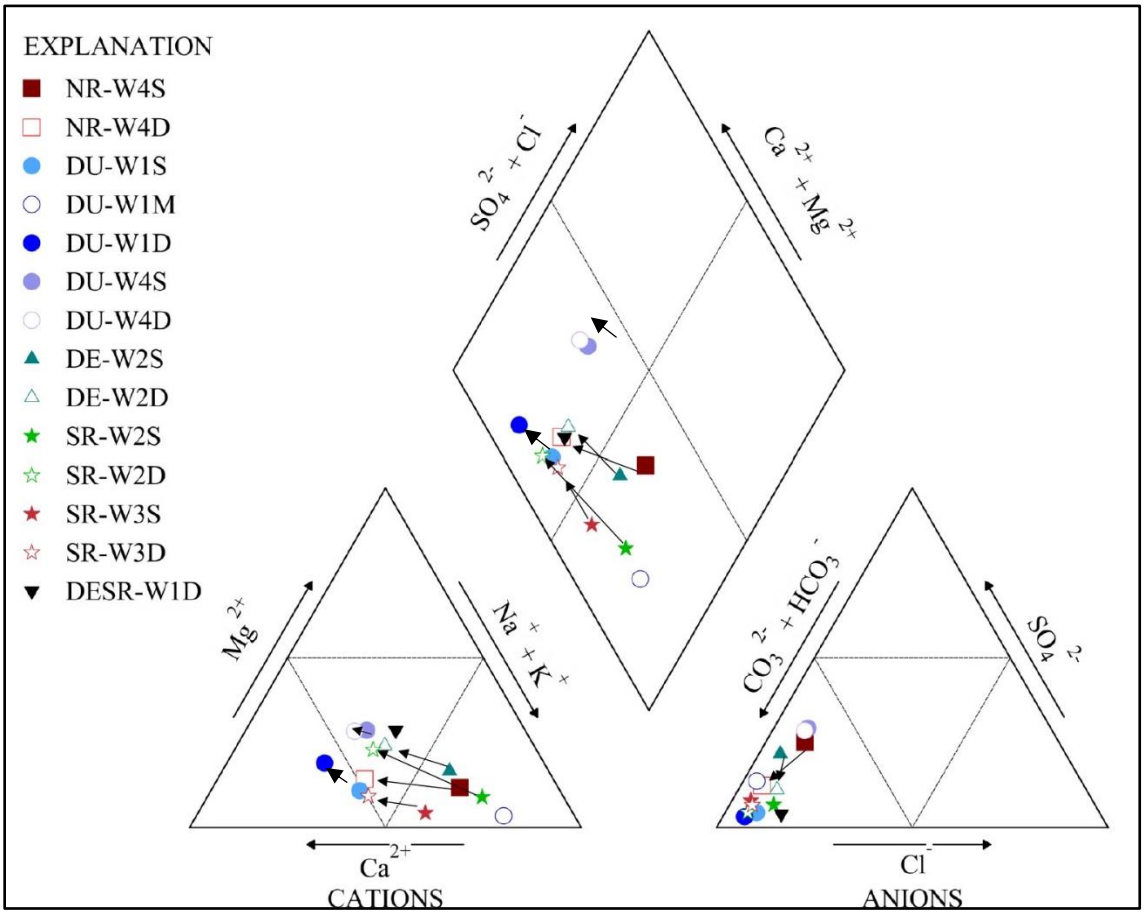

Figure 70. A Piper diagram showing the average major cation and anion proportions. Deep wells are hollow icons, and the shallow wells are filled-in icons. Arrows on the diagrams help to connect shallow and deep well pair trends. Symbols without arrows indicate concentrations at the well nest plotted in proximity. Concentrations are reported in mg/L.

Table 10. Table presenting two-tailed t-tests on two-sample equal variance variables of ion concentrations for shallow versus deep wells. Significant *p*-values were found difference in shallow and deep groundwater for the Ca/Na molar ratio, sodium, potassium, magnesium, and calcium concentrations.

Ion	***p*-Value**	**Significant at $p<0.05$**
Silica	0.122	
alkalinity	0.834	
Ca/Na molar ratio	0.0031	X
Sodium	0.0167	X
Potassium	0.021	X
Magnesium	4.373E-08	X
Calcium	0.0110	X
Fluoride	0.822	
Chloride	0.238	
Bromide	0.251	
Nitrate (as NO_3^-)	0.582	
Phosphate	0.447	
Sulfate	0.115	

Another study with a similar scope to this one was conducted in 1998 by Peters et al. That study took place in Panola Mountain Research Watershed (PMRW) of Georgia, which while in the Piedmont, is comprised of different geology. The bedrock geology of that region is granodiorite, which differs from the more easily weathered metavolcanics of Redlair. Peters et al. (1998) differentiated between "new" and "old" groundwater based on depth. They defined "new" groundwater as groundwater originating from hillslopes at shallow depth, perhaps even running dry throughout the year. They defined "old" groundwater as groundwater sourced from a deeper perennial reservoir in a lower portion of the watershed. Additionally, the screened interval of the wells installed at PMRW was deeper below the water table, therefore providing "older" groundwater. The chemistry of the "old" groundwater at PMRW showed an increase of sodium (~0.7-7 mg/L) and silica (~6-35 mg/L) in groundwater with depth. These concentration ranges are lower than the groundwater data at Redlair show, which varied from ~3-75 mg/L for sodium and ~13-38 mg/L for silica. However, the difference in these two ion concentrations instead shows that

the groundwater sampled in this study, from wells containing water year-round, mostly corresponds to the "old" groundwater from the Peters et al., (1998) study.

At Redlair, few geomorphic influences were seen from the available data of this study. If landscape position influenced waters at Redlair, then the North Rhyne watershed, which is situated at the bottom of the hillslope closest to the South Fork of the Catawba, would have different groundwater chemistry than Duffy, which is farthest away (to the South Fork of the Catawba) closer to a watershed divide. The North Rhyne watershed would have shown well-mixed groundwater chemistry, but instead, concentrations remained somewhat consistent from Duffy watershed to North Rhyne watershed. A study of similar scope found a vertical disconnect between the soil profiles of deep and shallow water tables as well as laterally across the hillslope (Zimmer and McGlynn, 2017). Zimmer and McGlynn (2017) found many pockets of perched water in the study area. Another study conducted by van Meerveld et al. (2015), found rather consistent and robust groundwater levels for the riparian zone and less attenuation in groundwater in the bedrock and upper hillslope regions. However, the van Meerveld et al. (2015) study took place for only a few events during a one-month period, which was a shorter timescale than this study at Redlair. That study found wells in the riparian zone responded to rainfall events sooner than hillslope wells, which is also seen at Redlair. Redlair wells with HOBO data revealed that only the riparian wells noticeably responded to precipitation events (Figure 32). This may have to do with depth and proximity to the watershed outlet and/or shallow subsurface flow. For instance, the shallow riparian well in the Duffy watershed (DU-W4S) responded to a precipitation event (June 9, 2019) that the North Rhyne riparian well (NR-W4S) did not (Figure 32). Lastly, this study found that the mid-slope and lower slope positions have a large influence on hillslope-stream connectivity.

Detty and McGuire (2010) found that surficial topography influenced watershed connectivity between hillslope and riparian zones at the Hubbard Brook Experimental Forest in New Hampshire. The authors even found seasonal signatures in water table dynamics. They inferred that distinct seasonal signatures meant poor connectivity between their studied watershed

and the larger channel network. The opposite is found at Redlair (i.e., no seasonal signatures and strong connectivity). The stream chemistry at Redlair also seem to be intermediate between the shallow and deep wells, implying strong connectivity. However, the geology of this study and the Detty and McGuire (2010) study was different. The geology of that study is a pelitic schist of the Northern Appalachian with glacial till making up most of the surficial geology. The soils were characterized as spodosols, which are rich in aluminum oxides and organic matter and having low fertility.

6.4 Land-use and mineral weathering contributions to groundwater chemistry

The water chemistry from Redlair can help shed light on chemical weathering reactions dominated by silicate weathering (hydrolysis) that converts primary rock-forming minerals into clays, ions, alkalinity, and dissolved silica. Albite and anorthite are feldspar minerals commonly found in volcanic rocks. Figure 72-73 show that these minerals are not chemically stable, and easily weather to kaolinite (and other clay) minerals, which is widespread in the southern Piedmont region. This type of chemical weathering involves the breakdown of minerals, in this case feldspars, in weakly acidic waters. This acidity is due to the carbonic acid found in rainwater and soil waters, which can interact with the silica-bearing feldspar minerals. The metavolcanic and metaigneous rocks at Redlair are comprised of both feldspar members, Ca-rich and Na-rich. Therefore, the breakdown to kaolinite due to silicate hydrolysis is expected. The equations below were acquired from Hiscock and Bense (2014).

Anorthite weathering:

Equation 1. $CaAl_2Si_2O_{8\,(s)} + 2H_2CO_{3\,(aq)} + H_2O \rightarrow Ca^{2+}_{(aq)} + 2HCO_3^-{}_{(aq)} + Al_2Si_2O_5(OH)_{4\,(s)}$

Albite weathering:

Equation 2. $2NaAlSi_3O_{8\,(s)} + 9H_2O + 2H_2CO_{3\,(aq)} \rightarrow Al_2Si_2O_5(OH)_{4\,(s)} + 2Na^+{}_{(aq)} + 2HCO_3^-{}_{(aq)} + 4Si(OH)_{4\,(aq)}$

In the weathering equations above, only albite feldspar weathering yields dissolved silica ($4Si(OH)_{4\,(aq)}$).

Since the watersheds at Redlair are characterized as forested (i.e., non-urban), there is little urban development influence on the groundwater chemistry. Similar studies have also found low major ion concentrations from forested watershed groundwater (Bird et al., 2018). While potassium concentrations were generally low in Redlair groundwater, DU-W1M did have variable and more elevated concentrations.

Potential sources of phosphate may be from biotite and muscovite weathering. Elevated calcium (Ca^{2+}), magnesium (Mg^{2+}), and bicarbonate (HCO_3^-) concentrations typically occur in developed watersheds due to the addition of deicing salts on roads and concrete. Sulfate concentrations, which were also mostly low at these watersheds, are typically influenced by precipitation (Bird et al., 2018).

High levels of chloride are associated with higher amounts of impervious surface cover and are not typically found in forested watersheds (Price and Szymanski, 2012; Khan et al., 2015). The highest chloride concentration was recorded at DU-W1M at 7.0 mg/L. The Duffy watershed, specifically the DU-W1 triple well nest, is located closest to Hickory Grove Road. Much of the chemistry for the DU-W1M well was anomalous throughout the study, including previously mentioned chloride, potassium, and pH. This may be because the well is situated in a poorly connected region within the Duffy watershed or in a pocket of highly weathered clay material.

Sulfate concentrations were elevated at the beginning of this study (Figure 55-57), likely due to the well installation in early 2019. Well installation typically includes setting the wells with concrete, which can be rich in gypsum. Sulfate is often a byproduct of gypsum-rich weathered cement. Moore et al. (2017) found a similar increase in groundwater sulfate concentrations due to concrete weathering. Seasonal increases in phosphate and nitrate (as NO_3^-) (Figure 71) found in the Deep Watershed (DE-W2 shallow and deep) may be because they are in a pasture at RO. Biosolids were spread to the upper parts of the pasture at some point between October 2019 and February

2020 (Haywood Rankin, personal communication). This is the same time in which an increase in sulfate, phosphate, and nitrate were documented in the groundwater chemistry of pasture wells. More specifically, sulfate and nitrate appear to have moved quickly through the watersheds, as the concentrations started to decline to normal values in March 2020. Nitrate and phosphate dropped to ambient levels soon after these biosolid increases occurred, which also supports a fast-moving groundwater system. Based on the movement of these ions throughout the watersheds, water residence time is on the scale of months. A similar pattern was observed when looking at groundwater levels and water isotope values.

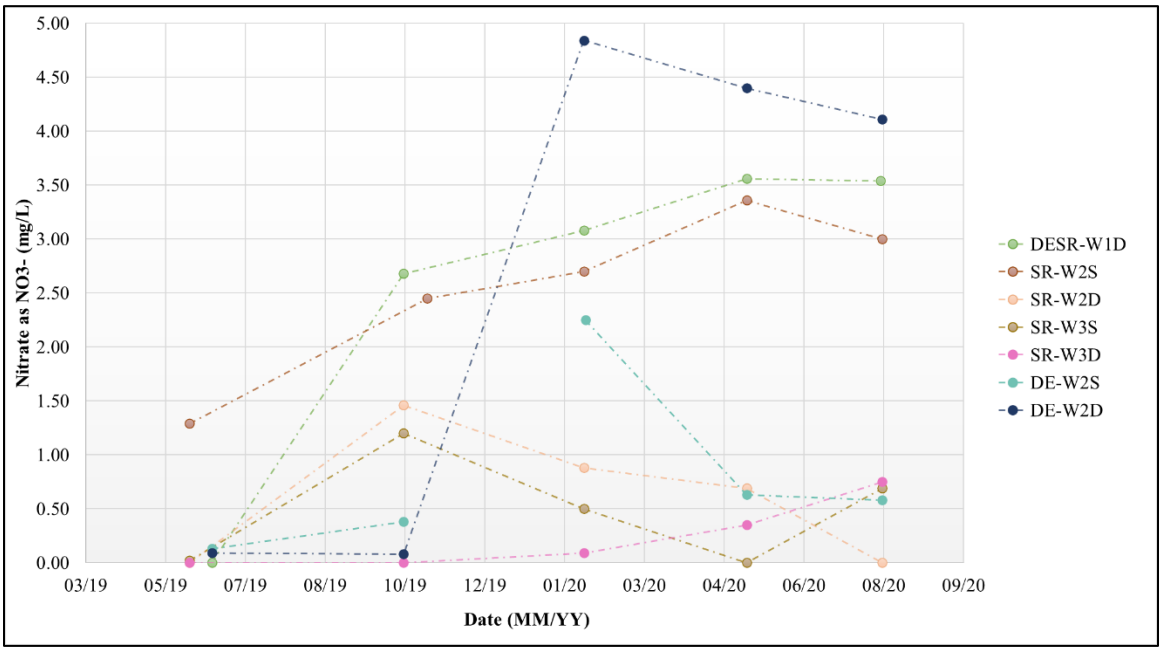

Figure 71. A time series plot showing the nitrate concentrations (as NO_3^-) in groundwater near the pasture. There was an increase in nitrate concentrations during the October 2019-February 2020 period, most evident in DE-W2D, DESR-W1D, and SR-W2S. Note that 4.4 mg/L nitrate as NO_3^- is equivalent to 1 mg/L nitrate as N.

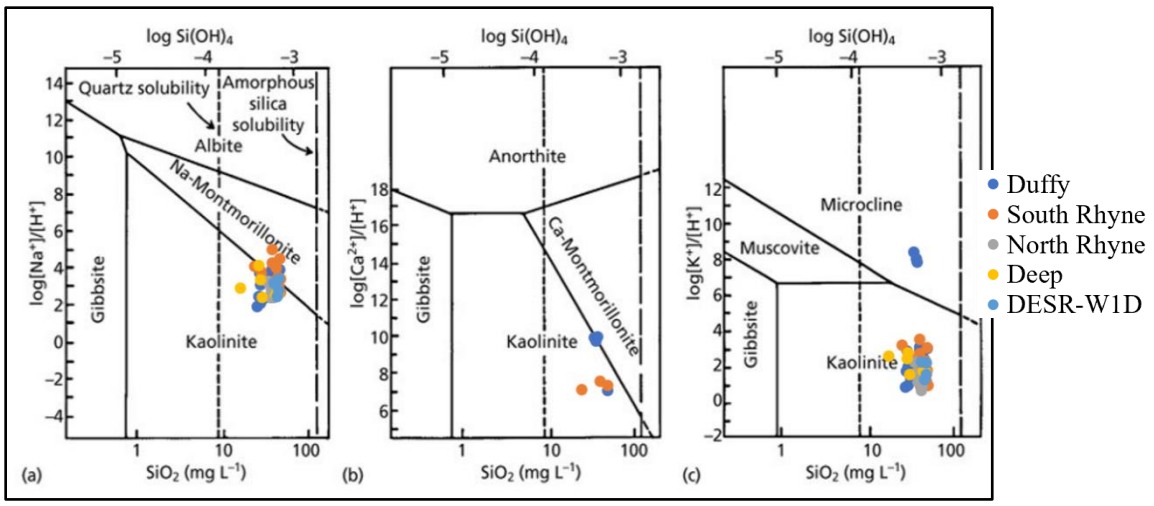

Figure 72. Groundwater samples from Redlair plotted on three different stability diagrams. Samples not shown plotted off scale (modified from Hiscock and Bense, 2014).

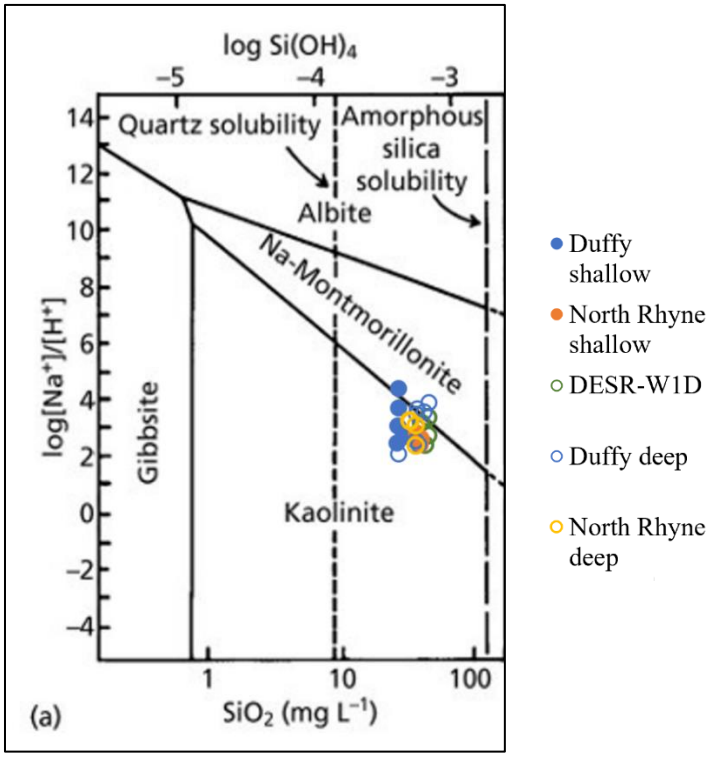

Figure 73. A representative sample of shallow versus deep groundwater samples from Redlair plotted on top of a stability diagram. The deep groundwater is symbolized with hollow circles while the shallow groundwater are solid circles (modified from Hiscock and Bense, 2014).

The variations in calcium and sodium-rich plagioclase between the deep wells and shallow wells imply different degrees of weathered material at depth. Since the Ca/Na ratio is higher in the deeper wells, these wells are more enriched in Ca-rich plagioclase feldspar rather than Na-rich plagioclase feldspar. According to the Goldich weathering sequence, Ca-rich plagioclase is one of the most easily weathered minerals, whereas Na-rich plagioclase is slightly more resistant (Figure 74). This implies that the deeper wells at Redlair, with their higher Ca/Na ratios, are interacting with a less weathered saprolite since the Ca-rich plagioclase feldspars have yet to fully weather out. Conversely, the shallower wells, with lower Ca/Na ratios, are interacting with a more weathered saprolite in which the calcium feldspars have already been weathered out. In this case, the Na-rich plagioclase feldspar undergoes an incongruent reaction that produces Na^+ and HCO_3^- ions (Hiscock and Bense, 2014). Furthermore, silicate weathering reaction rates may have been too slow to record seasonal differences in the available data for this study.

Silica (SiO_2) analysis can also help to better understand water residence times and water-rock interactions within a watershed. The length of time which water interacts with silicate rock material can result in higher silica concentrations in the water sample (Khan et al., 2014). One study found that higher silica concentrations and pH levels corresponded with longer groundwater residence times (Zimmer et al., 2013). However, this study was also conducted at the Hubbard Brook Experimental Forest. The difference from that study and this one may be due to the difference in soil chemistry and overall climate, which leads to different weathering rates.

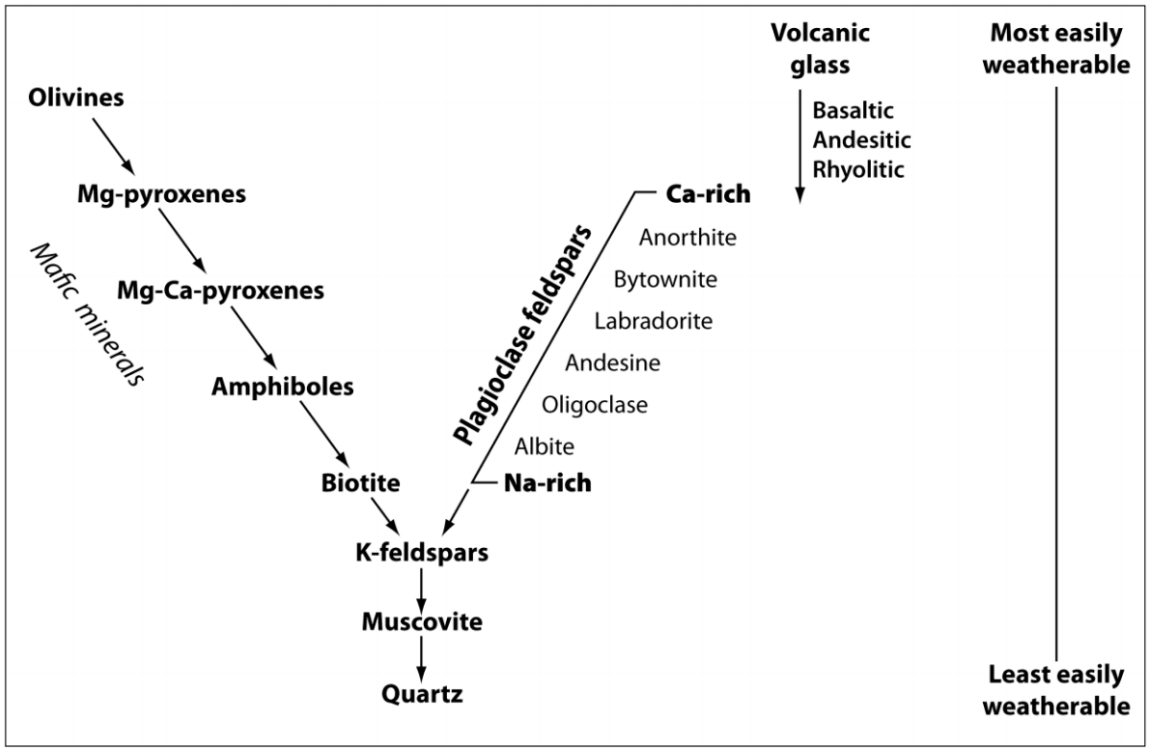

Figure 74. The Goldich weathering sequence shows the resistivity to weathering different minerals may exhibit based on their chemistry. Based on this series, calcium-rich plagioclase would be more easily weathered (broken down) and may transition to its more resistant counterpart, sodium-rich plagioclase (Churchman et al., 2012).

6.5 Relationship between baseflow chemistry and groundwater chemistry

The surface water chemistry at Redlair seems to represent well-mixed waters between the shallow and deep saprolite in the first-order watersheds (Figure 75). Surface water chemistry did not have a discernable seasonal pattern. Furthermore, the surface water samples are generally indistinguishable from the precipitation data from Torrellas, 2018 (Figure 66). However, a limitation of this study is that storm flows were not sampled. Without storm flow data, understanding precipitation flow through the surface and subsurface within the watershed is not fully attainable.

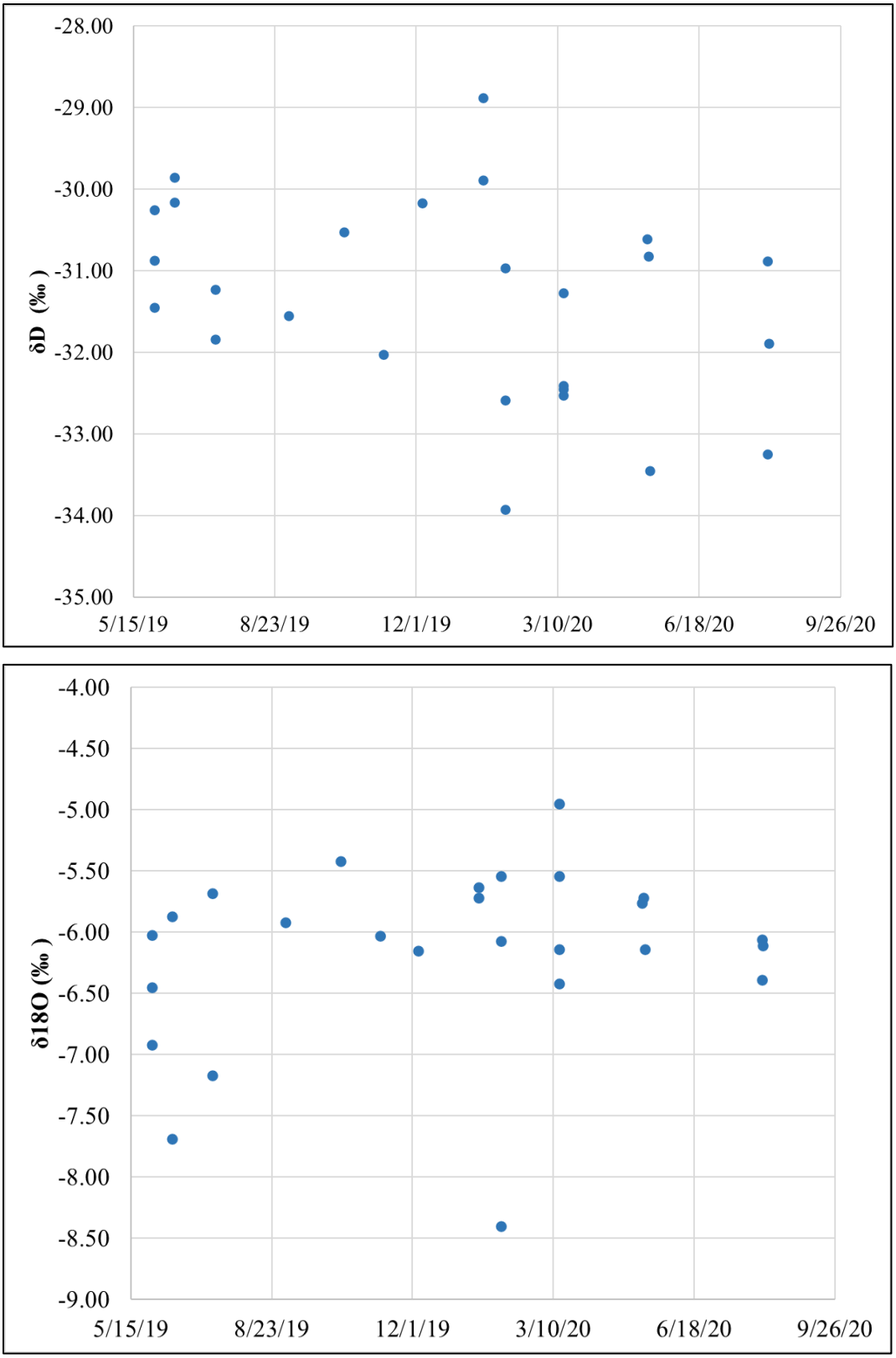

Figure 75. Time series plots of δD and $\delta^{18}O$ for surface water samples collected at Redlair. There is no seasonal pattern distinguishable from these samples.

Other factors can influence groundwater chemistry besides well depth. A study that took place at a 41-hectare headwater catchment at the Hubbard Brook Experimental Forest in New Hampshire found that groundwater and soils can control chemical transformations within the environment. This can further influence groundwater and stream chemistry. That study included higher-resolution chemical analysis of soil horizons and their influences on solutes across the watershed (Zimmer et al., 2013). At map-scale resolution, the soils at Redlair were perceived to be uniform Entisols and Ultisols. Perhaps categorizing them as uniform throughout the study area led to missing microscale variations in watershed chemistry. This study also contradicted the authors' initial hypothesis that the stream chemistry would be consistent within the sub-watersheds but vary between the sub-watersheds. At Redlair, surface water chemistry also stayed consistent between the four watersheds. This could also be scale-dependent; Zimmer et al. (2013) found that the resolution of the sampling event within a watershed, as well as the size of the watershed itself, can affect chemistry results. Furthermore, the groundwater depth may also be important since that study only collected from 40-100 cm deep (subsurface perched waters); these are much shallower depths than the ~6-24 m well depths at Redlair (deep groundwaters).

The water isotopes and chemistry data of the groundwater and surface water appear to be well-mixed on a seasonal timescale and having no robust seasonal effect. This may be because groundwaters reach the stream channel and are already mixed by the time of the sampling event, which is why it was not possible to distinguish between different seasons from the data.

6.6 Groundwater isotopes

Based on the $\delta^{18}O$ and δD isotope analysis, groundwaters at Redlair are well-mixed on a seasonal to annual timescale. There may have been inadequate isotopic variation between average summer and winter precipitation, also resulting in no seasonal effect on the water isotopes. The isotopic data provided during this study may have not been in high enough resolution to show

distinctions in winter and summer recharge events. The precipitation data provided in Figure 66 was from a study conducted by Torrellas in 2018.

The temporal influence on water isotopes in these watersheds seem to be lacking, perhaps because they may also be too small for time to have any significant role.

6.7 Dissolved inorganic carbon (DIC)

δ^{13}C-DIC values are consistent with the expected evolution between shallow and deep groundwater. As water infiltrates through the subsurface and makes its way to a stream outlet, δ^{13}C-DIC evolves from having a soil-influenced signature to a more mineral-influenced signature. Since there are no carbonates that dominate at Redlair, δ^{13}C-DIC ranges are typically around -25‰ in humid regions (Clark and Fritz, 1997). In the waters at Redlair, pH remained relatively neutral throughout, which is also associated with higher (less negative) δ^{13}C-DIC values. Commonly, these values ranged from -21‰ to -18‰ specifically in this region of the Piedmont (Clark and Fritz, 1997).

Another common product that derives from silicate weathering (specifically anorthite feldspar) is bicarbonate (HCO_3^-). In Equation 1, anorthite reacts with carbonic acid and water and dissolves into calcium ions, bicarbonate, and kaolinite. Furthermore, DIC is influenced by pH, and since pH values at Redlair were mostly neutral, it is reasonable to assume all alkalinity concentrations come in the form of bicarbonate (Hiscock and Bense, 2014).

6.8 Future Recommendations

The results of this study have pointed to knowledge gaps in the studied watersheds at Redlair Observatory. This suggests areas for research incorporating:

1. Mineralogical characterization of the saprolite and bedrock.

2. Examining stormflow for a more thorough watershed balance equation and to trace precipitation influences on water chemistry.
3. Collecting precipitation samples for isotope analysis.
4. Elevation survey of groundwater levels relative to sea level.
5. An aquatic invertebrate survey, including biologic diversity index (Bird et al., 2018) paired with a stream quality assessment to evaluate watershed water quality.
6. Exploring the potential effects of legacy contours and incised gullies on groundwater residence time.
7. Additionally, examination of legacy sedimentation would provide a more holistic understanding of anthropogenic influences on the zero-order watershed hydrology and landscape.

7 CONCLUSIONS

The goal of this study was improved understanding of critical zone and hydrological processes in small watersheds in undeveloped areas of the Piedmont. Four small watersheds were examined based on hydrochemical and geomorphological data acquired from field and laboratory work as well as geospatial analysis. The relationships found in this study between water chemistry, watershed geomorphology, and well depth within the saprolite and within critical zone shed light on processes that occur within these small watersheds. Water chemistry collected from fourteen wells among the four watersheds exhibited watershed-scale residence time on the order of a season and evidence of vertical connectivity within each watershed. Sudden increases in nutrients such as nitrate (NO_3^-) and phosphate imply rapid transit times, on the order of a season to about three to four months, within these small watersheds. Additionally, the initial high sulfate concentrations that quickly decrease over time further support ions are easily processed in these watersheds. This study has documented the rapid transport of nutrient ions apparently derived from biosolids

application in the pasture areas of Redlair, providing an example of how groundwater research and monitoring can benefit management of Redlair Preserve.

The strongest influence on groundwater levels and chemistry appeared to be depth of the well screen below the land surface at each well site. In general, the shallower well of each well pair responded to seasonal changes in water levels and temperatures sooner than the deeper well. Overall, groundwater levels at these four watersheds were shallowest in the late spring-early summer months, and deepest in the late fall-early winter months.

The groundwater Ca/Na molar ratio also implies a difference in weathered material at depth. The deep wells, which were drilled at 6-24 m deep, appeared to be situated in less weathered material (i.e., high in Ca-rich feldspar). Conversely, the shallow wells, drilled at 4-21 m, were higher in Na-rich feldspar concentrations, implying a more weathered material at a shallower depth. Further, the stream baseflow Ca/Na ratios were mostly intermediate (ranging from 0.23-1.64), consistent between the shallow wells (ranging from 0.07-1.79) and deep wells (ranging from 0.34-1.52). These results suggest that waters are well-mixed within the watershed.

Results of geospatial analysis show that the topography at Redlair has been influenced by legacy contours and pastures present in the area. Thus, the LiDAR data, while high resolution, exhibit the effects of by legacy contours and agricultural land. This became evident when examining landscape curvature. Instead of curvature varying systematically across the landscape from river valley to river basin divide, the analysis shows an overall more planar landscape with concave-dominant topography in the streambeds, convex topography at the tops of the streambanks, and complex curvature elsewhere.

It is important to understand how these smaller watersheds behave and respond to changes in environment as they play a vital role in the water quality of larger downstream rivers and streams. Further, Gaston County, North Carolina, continues to see an increase in population and development, as it is located near the major city of Charlotte. The data presented in this study will serve as the foundation for future research at RO and will support management of Redlair Preserve.

It is imperative that we understand the natural processes that occur so that managers and researchers may make informed decisions that will help predict the response of small watersheds such as these to the effects of climate change and urbanization.

8 REFERENCES

Alexander, R.B., Boyer, E.W., Smith, R.A., Schwarz, G.E., and Moore, R.B., 2007, The role of headwater streams in downstream water quality: Journal of the American Water Resources Association, v. 43, p. 41-59, doi: 10.1111/j.1752-1688.2007.00005.x.

Aula, I., Braunschweiler, H., and Malin, I., 1995, The watershed flux of mercury examined with indicators in the Tucuruí reservoir in Pará, Brazil: Science of the Total Environment, v. 175, p. 97-107, doi: 10.1016/0048-9697(95)04906-1.

Aust, W.M., and Blinn, C.R., 2004, Forestry best management practices for timber harvesting and site preparation in the eastern United States: An overview of water quality and productivity research during the past 20 years (1982–2002): Water, Air and Soil Pollution: Focus, v. 4, p. 5-36, doi: WAFO.0000012828.33069.f6.

Bajracharya, P., and Jain, S., 2021, Characterization of Drainage Basin Hypsometry: A Generalized Approach: Geomorphology (Amsterdam, Netherlands), v. 381, p. 107645-107660, doi: 10.1016/j.geomorph.2021.107645.

Bastola, S., Dialynas, Y.G., Bras, R.L., Noto, L.V., and Istanbulluoglu, E., 2018, The role of vegetation on gully erosion stabilization at a severely degraded landscape: A case study from Calhoun Experimental Critical Zone Observatory: Geomorphology (Amsterdam, Netherlands), v. 308, p. 25-39, doi: 10.1016/j.geomorph.2017.12.032.

Bird, D.L., Groffman, P.M., Salice, C.J., and Moore, J., 2018, Steady-State land cover but con-steady-state major ion chemistry in urban streams: Environmental Science & Technology, v. 52, p. 13015-13026.

Blaszcynski, J.S., 1997, Landform characterization with geographic information systems: Photogrammetric Engineering and Remote Sensing, v. 63, p. 183-191.

Boggs, J., Sun, G., and McNulty, S., 2016, Effects of timber harvest on water quantity and quality in small watersheds in the Piedmont of North Carolina: Journal of Forestry, v. 114, p. 27-40, doi: 10.5849/jof.14-102.

Booth, D.B., 2011, Urbanization and the natural drainage system - Impacts, Solutions, and Prognoses: v. 7, p. 93-118.

Bracken, L.J., Wainwright, J., Ali, G.A., Tetzlaff, D., Smith, M.W., Reaney, S.M., and Roy, A.G., 2013, Concepts of hydrological connectivity: Research approaches, pathways and future agendas: Earth-Science Reviews, v. 119, p. 17-34, doi: 10.1016/j.earscirev.2013.02.001.

Burns, D.A., Hooper, R.P., McDonnell, J.J., Freer, J.E., Kendall, C., and Beven, K., 1998, Base cation concentrations in subsurface flow from a forested hillslope: The role of flushing frequency: Water Resources Research, v. 34, p. 3535-3544, doi: 10.1029/98WR02450.

Burns, D.A., McDonnell, J.J., Hooper, R.P., Peters, N.E., Freer, J.E., Kendall, C., and Beven, K., 2001, Quantifying contributions to storm runoff through end-member mixing analysis and hydrologic measurements at the Panola Mountain Research Watershed (Georgia, USA): Hydrological Processes, v. 15, p. 1903-1924, doi: 10.1002/hyp.246.

Burt, T.P., and Mcdonnell, J.J., 2015, Whither field hydrology? The need for discovery science and outrageous hydrological hypotheses: Water Resources Research, v. 51, p. 5919.

Buttle, J.M., 1998, Fundamentals of small catchment hydrology, in Kendall, C. and McDonnell, J.J., eds., Isotope Tracers in Catchment Hydrology: Elsevier, p. 1-49.

Catawba Lands Conservancy, 2009: https://catawbalands.org/ (accessed January 2021).

Chorover, J., Troch, P.A., Rasmussen, C., Brooks, P.D., Pelletier, J.D., Breshears, D.D., Huxman, T.E., Kurc, S.A., Lohse, K.A., Mcintosh, J.C., Meixner, T., Schaap, M.G., Litvak, M.E., Perdrial, J., Harpold, A., and Durcik, M., 2011a, How Water, Carbon, and Energy Drive Critical Zone Evolution: The Jemez–Santa Catalina Critical Zone Observatory: Vadose Zone Journal, v. 10, p. 884, doi: 10.2136/vzj2010.0132.

Clark, I. and Fritz, P.F.,1997, Environmental Isotopes in Hydrology. Lewis Publishers. doi:10.1201/9781482242911.

Churchman, J., and Lowe, D., 2012, Alteration, formation, and occurrence of minerals in soils. In: Huang, P.M.; Li, Y; Sumner, M.E. (editors) "Handbook of Soil Sciences. 2nd edition, Vol. 1: Properties and Processes". CRC Press (Taylor & Francis), Boca Raton FL, p.20.1-20.72

Craig, H., 1961, Isotopic Variations in Meteoric Waters: Science, v. 133, p. 1702-1703, doi: 10.1126/science.133.3465.1702.

Dahl, M., Nilsson, B., Langhoff, J.H., and Refsgaard, J.C., 2007, Review of classification systems and new multi-scale typology of groundwater–surface water interaction: Journal of Hydrology (Amsterdam), v. 344, p. 1-16, doi: 10.1016/j.jhydrol.2007.06.027.

Daniel, C.C., and Dahlen, P.R., 2002, Preliminary hydrogeologic assessment and study plan for a regional ground-water resource investigation of the Blue Ridge and Piedmont Provinces of North Carolina: US Geological Survey Water-Resources Investigations Report 2002-4105.

Davis, J., 2020, Hypsometry Tool: Institute for Geographic Information Science, San Francisco State University: https://gis.sfsu.edu/content/hypsometry-tools

Dennis, A.J., and Shervais, J.W., 1996, The Carolina Terrane in northwestern South Carolina: Insights into the development of an evolving island arc, in Nance, R.D. and Thompson, M.D., eds., Avalonian and related peri-Gondwanan terranes of the Circum-North Atlantic: Geological Society of America, p. 237-256.

Detty, J.M., and McGuire, K.J., 2010, Topographic controls on shallow groundwater dynamics: implications of hydrologic connectivity between hillslopes and riparian zones in a till mantled catchment: Hydrological Processes, v. 24, p. 2222-2236, doi: 10.1002/hyp.7656.

Duncan, J.M., Band, L.E., and Groffman, P.M., 2017, Variable nitrate concentration-discharge relationships in a forested watershed: Hydrological Processes, v. 31, p. 1817-1824.

Esri. "Topographic" [basemap]. Scale not given. "World Topographic Map". January 6, 2020.

Farvolden, R.N., 1963, Geologic controls on ground-water storage and base flow: Journal of Hydrology, v. 1, p. 219-249.

Fenneman, N.M., 1938, Physiography of eastern United States: New York, McGraw-Hill, 714 p.

Fetter, C.W., 2001, Applied Hydrogeology: Prentice-Hall, Inc.

Freer, J., McDonnell, J., Beven, K.J., Brammer, D., Burns, D., Hooper, R.P., and Kendal, C., 1997, Topographic controls on subsurface storm flow at the hillslope scale for two hydrologically distinct small catchments: Hydrological Processes, v. 11, p. 1347-1352

Freer, J., McDonnell, J.J., Beven, K.J., Peters, N.E., Burns, D.A., Hooper, R.P., Aulenbach, B., and Kendall, C., 2002, The role of bedrock topography on subsurface storm flow: Water Resources Research, v. 38, p. 1269-16, doi: 10.1029/2001WR000872.

Garrett, K.K., and Wohl, E.E., 2017, Climate-invariant area–slope relations in channel heads initiated by surface runoff: Earth Surface Processes and Landforms, v. 42, p. 1745-1751, doi: 10.1002/esp.4148.

Gieskes, J.M., and Rogers, W.C., 1973, Alkalinity determination in interstitial waters of marine sediments: Journal of Sedimentary Research, v. 43, p. 272-277, doi: 10.1306/74D72743-2B21-11D7-8648000102C1865D.

Goldsmith, R., Milton, D.J., Horton, J.W., 1985. Geologic map of the Charlotte 1-degree x 2-degrees quadrangle, North Carolina and South Carolina, US Geological Survey Investigations I-1251-E.

Hearn E.W., Drane F.P., Brinkley L.L., 1909, Soil Map - North Carolina Gaston County, p. 345-373)

Heidbüchel, I., Troch, P.A., and Lyon, S.W., 2013, Separating physical and meteorological controls of variable transit times in zero-order catchments: Water Resources Research, v. 49, p. 7644-7657, doi: 10.1002/2012WR013149.

Hibbard, J.P., Stoddard, E.F., Secor, D.T., and Dennis, A.J., 2002, The Carolina Zone: overview of Neoproterozoic to Early Paleozoic peri-Gondwanan terranes along the eastern Flank of the

southern Appalachians: Earth-Science Reviews, v. 57, p. 299-339, doi: 10.1016/S0012-8252(01)00079-4.

Hiscock, Kevin M., Bense Victor F., 2014. Hydrogeology Principles and Practice. Wiley Blackwell 2014.

Holbrook, W.S., Marcon, V., Bacon, A.R., Brantley, S.L., Carr, B.J., Flinchum, B.A., Richter, D.D., and Riebe, C.S., 2019, Links between physical and chemical weathering inferred from a 65m-deep borehole through Earth's critical zone: Scientific Reports, v. 9.

Hopp, L., and McDonnell, J.J., 2009, Connectivity at the hillslope scale: Identifying interactions between storm size, bedrock permeability, slope angle and soil depth: Journal of Hydrology (Amsterdam), v. 376, p. 378-391, doi: 10.1016/j.jhydrol.2009.07.047.

Horgan, J., Eppes, M.C., Vinson, D.S., 2021, Groundwater levels and ion concentrations in saprolite wells at Redlair Observatory, North Carolina, 2019-2020, HydroShare, (http://www.hydroshare.org/resource/8083b54faab344fc8336121a2a9093df).

International Atomic Energy Agency, 2009, Laser spectroscopic analysis of liquid water samples for stable hydrogen and oxygen isotopes. IAEA training course series 35. International Atomic Energy Agency, Vienna, p. 35.

Jacques C. Finlay, 2003, Controls of streamwater dissolved inorganic carbon dynamics in a forested watershed: Biogeochemistry, v. 62, p. 231-252, doi: 10.1023/A:1021183023963.

James, L.A., Watson, D.G., and Hansen, W.F., 2007, Using LiDAR data to map gullies and headwater streams under forest canopy: South Carolina, USA: Catena, v. 71, p. 132-144, doi: 10.1016/j.catena.2006.10.010.

Jefferson, A.J., and Mcgee, R.W., 2012, Channel network extent in the context of historical land use, flow generation processes, and landscape evolution in the North Carolina Piedmont: Earth Surface Processes and Landforms, v. 38, p. 601.

Julian, J.P., Elmore, A.J., and Guinn, S.M., 2012, Channel head locations in forested watersheds across the mid-Atlantic United States: A physiographic analysis: Geomorphology (Amsterdam, Netherlands), v. 177-178, p. 194-203, doi: 10.1016/j.geomorph.2012.07.029.

Kendall, C. and Doctor, D.H., 2003, Environmental isotope applications in hydrologic studies, in Drever, J.I. ed., Surface and Groundwater, Weathering and Soils, Oxford, Elsevier, Treatise on Geochemistry, v. 5, p. 319-364.

Khan, A., Umar, R., and Khan, H., 2015, Significance of silica in identifying the processes affecting groundwater chemistry in parts of Kali watershed, Central Ganga Plain, India: Applied Water Science, v. 5, p. 65-72, doi: 10.1007/s13201-014-0164-z.

Klaus, J., McDonnell, J.J., Jackson, C.R., Du, E., and Griffiths, N.A., 2015, Where does streamwater come from in low-relief forested watersheds? A dual-isotope approach: Hydrology and Earth System Sciences, v. 19, p. 125-135, doi: 10.5194/hess-19-125-2015.

Luo, W., Gao, X., and Zhang, X., 2018, Geochemical processes controlling the groundwater chemistry and fluoride contamination in the Yuncheng Basin, China—An area with complex hydrogeochemical conditions: PloS One, v. 13, p. e0199082, doi: 10.1371/journal.pone.0199082.

MacDonald, L.H., and Coe, D., 2006, Influence of headwater streams on downstream reaches in forested areas: Forest Science, v. 53, p. 148-168.

Maher, K., 2010, The dependence of chemical weathering rates on fluid residence time: Earth and Planetary Science Letters, v. 294, p. 101-110, doi: 10.1016/j.epsl.2010.03.010.

Matsuura, T., and Suzuki, W., 2013, Analysis of topography and vegetation distribution using a digital elevation model: case study of a snowy mountain basin in northeastern Japan: Landscape and Ecological Engineering, v. 9, p. 143-155, doi: 10.1007/s11355-012-0187-2.

McGlynn, B.L., McDonnel, J.J., 2003, Quantifying the relative contributions of riparian and hillslope zones to catchment runoff: Water Resources Research, v. 39, doi: 10.1029/2003WR002091.

McDonnell, J.J., 2009, Hewlett, J.D. and Hibbert, A.R. 1967: Factors affecting the response of small watersheds to precipitation in humid areas. In Sopper, W.E. and Lull, H.W., ed., Forest hydrology, New York: Pergamon Press, 275—90: Progress in Physical Geography, v. 33, p. 288-293, doi: 10.1177/0309133309338118.

Meredith, K.T., Han, L.F., Cendón, D.I., Crawford, J., Hankin, S., Peterson, M., and Hollins, S.E., 2018, Evolution of dissolved inorganic carbon in groundwater recharged by cyclones and groundwater age estimations using the 14C statistical approach: Geochimica Et Cosmochimica Acta, v. 220, p. 483-498, doi: 10.1016/j.gca.2017.09.011.

Meshgi, A., Schmitter, P., Babovic, V., and Chui, T.F.M., 2014, An empirical method for approximating stream baseflow time series using groundwater table fluctuations: Journal of Hydrology, v. 519, p. 1031-1041, doi: 10.1016/j.jhydrol.2014.08.033.

North Carolina Department of Commerce, 1999, 1998 State population projections by county: http://demog.state.nc.us/demog/. (accessed January 2019).

North Carolina Floodplain Mapping Program, “Welcome to North Carolina's Spatial Data Download.” North Carolina Spatial Data Download, https://sdd.nc.gov/DataDownload.aspx#. (accessed March 2021).

North Carolina Geological Survey, 1985, Geologic Map of North Carolina: Raleigh, North Carolina Department of Natural Resources and Community Development, Geological Survey Section, scale 1:500,000, in color.

North Carolina Office of State Budget and Management, 2019 Standard Population Estimates, Vintage 2019: https://files.nc.gov/ncosbm/demog/countygrowth_cert_2019.html (accessed March 2021)

NOAA National Centers for Environmental information, Climate at a Glance: Divisional Time Series, published May 2019, retrieved on May 17, 2019, https://www.ncdc.noaa.gov/cag/

O'Driscoll, M., Clinton, S., Jefferson, A., Manda, A., and McMillan, S., 2010b, Urbanization Effects on Watershed Hydrology and In-Stream Processes in the Southern United States: Water (Basel), v. 2, p. 605-648, doi: 10.3390/w2030605.

Ohnuki, Y., Kimhean, C., Shinomiya, Y., and Toriyama, J., 2008, Distribution and characteristics of soil thickness and effects upon water storage in forested areas of Cambodia: Hydrological Processes, v. 22, p. 1272-1280, doi: 10.1002/hyp.6937.

Peters, N., Ratcliffe, E., and Tranter, M.,1998, Tracing solute mobility at the Panola Mountain Research Watershed, Georgia, USA: Variations in Na^+, Cl^-, and H_4SiO_4 concentrations. IAHS-AISH Publication, v. 248, p. 483-490.

Peters, N.E., Shanley, J.B., Aulenbach, B.T., Webb, R.M., Campbell, D.H., Hunt, R., Larsen, M.C., Stallard, R.F., Troester, J., and Walker, J.F., 2006, Water and solute mass balance of five small, relatively undisturbed watersheds in the U.S: The Science of the Total Environment, v. 358, p. 221-242, doi: 10.1016/j.scitotenv.2005.04.044.

Pippin, C.G., Chapman, M.J., Huffman, B.A., Heller, M.J., and Schelgel, M.E., 2008, Hydrogeologic setting, ground-water flow, and ground-water quality at the Langtree Peninsula research station, Iredell County, North Carolina, 2000–2005: U.S. Geological Survey Scientific Investigations Report 2008–5055, 89 p. (available online at http://pubs.water.usgs.gov/sir2008–5055)

Price, J. and Szymanski, D., 2014, The effects of road salt on stream water chemistry in two small, forested watersheds, Catoctin Mountain, Maryland, USA: Aquatic Geochemistry, v. 20, p. 243-265, doi: 10.1007/s10498-013-9193-8.

Price, K., 2011, Effects of watershed topography, soils, land use, and climate on baseflow hydrology in humid regions: A review: Progress in Physical Geography: Earth and Environment, v. 35, p. 465.

Richter, Daniel D., and Markewitz, D., 2001, Understanding Soil Change: Soil Sustainability over Millennia, Centuries, and Decades. Cambridge University Press, New York, 255.

Richter, D.D., Markewitz, D., Trumbore, S.E., and Wells, C.G., 1999, Rapid accumulation and turnover of soil carbon in a re-establishing forest: Nature, v. 400, p. 56-58, doi: 10.1038/21867.

Ryan, P., 2014, Environmental and low temperature geochemistry: Hoboken, Wiley, p. 143-145.

Sklash, M.G., and Farvolden, R.N., 1979, The role of groundwater in storm runoff: Journal of Hydrology, v. 43, p. 45-65, doi: 10.1016/0022-1694(79)90164-1.

Trimble, S.W., Man-induced soil erosion on the southern Piedmont, 1700-1970: Ankeny, Iowa, Soil and Water Conservation Society, p. 1-66.

U.S. Geological Survey, 2016, The StreamStats program, online at http://streamstats.usgs.gov, accessed 2020.

Van Meerveld, H.J., Seibert, J., and Peters, N.E., 2015, Hillslope-riparian-stream connectivity and flow directions at the Panola Mountain Research Watershed: Hydrological Processes, v. 29, p. 3556.

Vivoni, E.R., Entekhabi, D., Bras, R.L., and Ivanov, V.Y., 2007, Hydrology and Earth System Sciences Controls on runoff generation and scale-dependence in a distributed hydrologic model: Hydrol. Earth Syst. Sci, v. 11, p. 1683-1701.

Wang, Y., Chen, Y., and Li, W., 2014, Temporal and spatial variation of water stable isotopes (^{18}O and ^{2}H) in the Kaidu River basin, Northwestern China: Hydrological Processes, v. 28, p. 653-661.

West, N., Kirby, E., Bierman, P., Clarke, B.A., 2014, Aspect-dependent variations in regolith creep revealed by meteoric ^{10}Be: Geology, v. 6, p. 507-510, doi: https://doi.org/10.1130/G35357.1

Wymore, A.S., Brereton, R.L., Ibarra, D.E., Maher, K., and McDowell, W.H., 2017, Critical zone structure controls concentration-discharge relationships and solute generation in forested

tropical montane watersheds: Water Resources Research, v. 53, p. 6279-6295, doi: 10.1002/2016WR020016.

Wymore, A.S., West, N.R., Maher, K., Sullivan, P.L., Harpold, A., Karwan, D., Marshall, J.A., Perdrial, J., Rempe, D.M., and Ma, L., 2017, Growing new generations of critical zone scientists: Earth Surface Processes and Landforms, v. 42, p. 2498-2502, doi: 10.1002/esp.4196.

Zhang, B., Tang, J.L., Gao, C., and Zepp, H., 2011, Subsurface lateral flow from hillslope and its contribution to nitrate loading in streams through an agricultural catchment during subtropical rainstorm events: Hydrology and Earth System Sciences, v. 15, p. 3153-3170, doi: 10.5194/hess-15-3153-2011.

Zimmer, M.A., Bailey, S.W., McGuire, K.J., and Bullen, T.D., 2013, Fine scale variations of surface water chemistry in an ephemeral to perennial drainage network: Hydrological Processes, v. 27, p. 3438-3451.

Zimmer M.A, McGlynn B.L., 2017a, Bidirectional stream–groundwater flow in response to ephemeral and intermittent streamflow and groundwater seasonality: Hydrological Processes, v. 31, doi: 10.1002/hyp.1130.

Zimmer, M.A., and McGlynn, B.L., 2017b, Ephemeral and intermittent runoff generation processes in a low relief, highly weathered catchment: Water Resources Research, v. 53, p. 7055-7078, doi:10.1002/2016WR019742.